Part III

Further developments

10
Time-dependent current-DFT

The first half of this book was concerned with the foundations and applications of TDDFT in real time (Part I) and in linear response (Part II). The cornerstones of TDDFT are the two basic existence theorems given by Runge and Gross (1984) and by van Leeuwen (1999), which guarantee a one-to-one correspondence between time-dependent densities and potentials, for fixed initial states. From this, we were able to access a wide variety of physical observables which characterize the dynamics of finite electronic systems acted upon by weak or strong external potentials, and we found efficient and accurate ways to calculate excitation energies of molecules.

In the second half of this book, we will go beyond the TDDFT formalism presented so far and introduce new formal developments and applications. Part III will be concerned with questions of great practical importance, such as these: How can we find approximate time-dependent xc functionals beyond the adiabatic approximation, and how can the TDDFT formalism be generalized to extended systems and to the treatment of electromagnetic fields? These questions are the subject of much ongoing research, and, as we will see, they are closely related.

In this chapter, our focus will be on the basics and applications of time-dependent current-density-functional theory (TDCDFT). We will first explain the motivation for switching from the particle density to the current density as the basic variable, and then go over the formal basis of TDCDFT. As we shall see, TDCDFT is a natural framework in which to construct nonadiabatic local approximations to the xc potential, and we shall discuss this in some detail.

10.1   The adiabatic approximation and beyond

The vast majority of applications of TDDFT are carried out using the adiabatic approximation to the xc potential, defined in eqn (4.13). In linear-response theory, the adiabatic xc kernel is given by eqn (8.31). Let us now review the evidence collected so far and ask under what circumstances the adiabatic approximation works well, and when it becomes necessary to go beyond it.

As we said in Section 4.3, the adiabatic approximation to $v_{xc}(\mathbf{r}, t)$ becomes exact in the limit of slow variations such that the system remains close to the instantaneous ground state. In practice this is hardly ever the case for systems driven by nontrivial time-dependent external potentials or carrying out free oscillations after some initial excitation process. In spite of this, the adiabatic approximation often works surprisingly well if one avoids situations in which the system is forced to undergo extremely rapid changes, and we illustrated this with numerical examples in Figs. 4.1 and 4.2.

But can we be a bit more precise as to when the adiabatic approximation is valid and when it isn't? As we shall now explain, the question shouldn't be whether the electron dynamics is "fast" or "slow" in absolute terms, but what part of the system's excitation spectrum is involved in the electron dynamics: this will provide us with the appropriate time or frequency scales to assess the degree of adiabaticity of the electronic dynamics.

In Chapter 9, we gave an overview of the performance of linear-response TDDFT for the calculation of excitation energies in atoms and molecules. We found that, in general, TDDFT gives very good results for "simple" excitations, but it also turned out that it is necessary to go beyond the adiabatic approximation for double excitations and certain types of charge-transfer excitations and to use an xc kernel with a frequency dependence.

For the case of double (and multiple) excitations, the explanation is relatively simple. The Kohn–Sham excitation spectrum consists of single excitations, and with a frequency-independent f_{xc} the Casida equation only gives solutions which correspond to single excitations in the interacting system. Multiple excitations are associated with poles in the interacting response function which do not have a counterpart in the Kohn–Sham noninteracting spectrum, and to access these poles the xc kernel must depend on the frequency; the Casida equation can then have additional solutions.

However, a more basic paradox remains. Formally, the adiabatic approximation is justified only in the limit of infinitely slow electron dynamics, close to the instantaneous ground state. But excitations in atoms and molecules do occur at finite frequencies, and in spite of this, linear-response TDDFT with adiabatic (frequency-independent) xc kernels gives excellent results! The question is therefore this: what is the characteristic time (or frequency) scale on which the adiabatic approximation is valid? The answer depends on the system under study, but we can identify the following general features:

- As we have seen in many examples, the adiabatic approximation is successful for those excitations of the physical system for which a correspondence to a single excitation in the Kohn–Sham system exists. The Casida formalism then shifts the Kohn–Sham excitation towards the correct value for the physical system.

- The frequency dependence of f_{xc} must kick in whenever one wants to describe those excitations of the physical system which are *missing* in the Kohn–Sham spectrum, namely, double or multiple excitations. In small systems such as isolated atoms, these excitations lie at much higher energies than single excitations, and the adiabatic approximation thus remains valid over a wide frequency range. This resolves the paradox above.

- In larger systems such as the biological molecules we considered in Section 9.4, certain types of charge-transfer excitations between open-shell fragments involve low-lying doubly excited states. In these cases, the adiabatic approximation breaks down even at very low frequencies.

These arguments also carry over to the time domain and beyond linear response: as long as the electron dynamics is dominated by single excitations, the adiabatic approximation should work well. If not, one needs to find suitable nonadiabatic approximations.
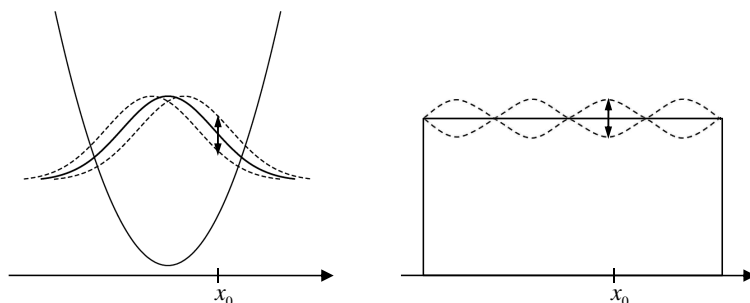
Fig. 10.1 Locally, the charge-density fluctuations at x_0 are the same in a harmonically confined system and in a bulk system. There is no damping in the harmonic system, whereas bulk plasmons are damped. A local density functional cannot distinguish between the two cases.

10.2   The failure of nonadiabatic local approximations in TDDFT

10.2.1   The Gross–Kohn approximation

The exact xc potential of static DFT is a nonlocal functional of the density, i.e., $v_{xc}^0(\mathbf{r})$ at position $\mathbf{r}$ depends on the particle density $n_0(\mathbf{r}')$ at all values of $\mathbf{r}'$ in space. The LDA (2.81), without doubt the most important xc functional, is a local approximation which depends only on the density at the very same position $\mathbf{r}$. Many approximations beyond the LDA, such as the GGAs and meta-GGAs, are functionals that are also based on local quantities (the density itself, gradients of the density, or the kinetic-energy density), all evaluated at position $\mathbf{r}$. In the limit of slow density variation these (semi)local approximations for $v_{xc}^0(\mathbf{r})$ become *exact*.

Now let us see what happens in TDDFT. As long as we restrict ourselves to the adiabatic approximation and ignore all memory dependence, constructing a local approximation to $v_{xc}^A[n](\mathbf{r}, t)$ works just the same way as in DFT: we start from the ALDA, and, if desired, include local density gradients or other local quantities at time t.

It would be extremely nice if we were able to construct an xc potential beyond the adiabatic approximation which depends only on local quantities. The first such attempt was made by Gross and Kohn (GK) (1985), who introduced the following approximation:

$$f_{xc}^{GK}(\mathbf{r}, \mathbf{r}', \omega) = f_{xc}^L(\omega)\delta(\mathbf{r} - \mathbf{r}') \,, \tag{10.1}$$

where $f_{xc}^L(\omega)$ [to be evaluated at the local ground-state density $n_0(\mathbf{r})$] is the zero-wave-vector limit $f_{xc}^L(q = 0, \omega)$ of the longitudinal xc kernel of the homogeneous electron liquid, which was discussed in Section 8.3. This approximation should be valid as long as the ground-state density $n_0(\mathbf{r})$ is slowly varying in space (weakly inhomogeneous).

It was first pointed out by Dobson (1994) that there is a problem with the GK approximation (10.1), namely, it violates the harmonic potential theorem (see Section 6.3.2). To see why, consider Fig. 10.1, which compares the charge-density fluctuations in a harmonically confined system and in a uniform bulk system. Recall that we proved in Section 6.3.2 that there exist solutions of the time-dependent Schrödinger equation
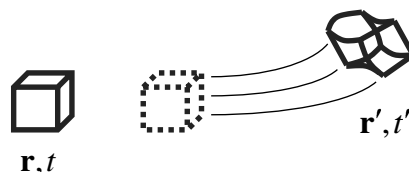
Fig. 10.2 During time evolution, the electron liquid in an initial volume element moves to a different position, and the volume element itself undergoes a deformation. This illustrates how memory and spatial nonlocality are inextricably connected.

in a harmonically confined interacting system where the ground state is rigidly translated. The charge-density oscillations on the left in Fig. 10.1 are therefore undamped, and the xc potential simply rides along with the density.

By contrast, the charge-density oscillations in the bulk system on the right-hand side of Fig. 10.1 involve periodic compression and rarefaction, and are subject to damping via the xc potential (we'll say more about plasmons and plasmon damping in metallic systems in Section 12.2).

At position x_0, the local charge-density fluctuations due to the sloshing motion of the harmonic system and due to the plasmon oscillations in the bulk are the same. A local xc functional which sees only the density at point x_0 can therefore not distinguish between the two very different types of global motion. The Gross–Kohn xc functional (10.1) therefore causes damping both of the bulk plasmon (which is physically correct) *and* of the oscillator in the harmonically confined system (which is unphysical). The damping is due to the imaginary part of $f_{\text{xc}}^L(\omega)$ at finite frequencies.

10.2.2   The ultranonlocality problem

As we have seen, a straightforward attempt to construct a local nonadiabatic approximation in TDDFT leads to a violation of basic theorems. To make progress, let us try to gain some deeper insight into the meaning of nonlocality in space and time.

Figure 10.2 shows a small spatial volume element (assumed to be part of some larger system), located at position $\mathbf{r}$ at the initial time t. As the system evolves in time, its density distribution changes, and, owing to the continuity equation (3.25), this implies a flow of currents. The electron liquid associated with the initial volume element will be displaced to position $\mathbf{r}'$ at a later time t', and the volume element itself can become deformed.[1] One can also turn this around and say that the density at a space–time point $(\mathbf{r}', t')$ came from a different position $\mathbf{r}$ at an earlier time t. Either way, it is clear that history dependence and spatial nonlocality are inextricably linked.

The concept of a local-density approximation in TDDFT breaks down as soon as we try to include retardation: this is known as the *ultranonlocality problem*. We have already shown this formally in Section 8.1.2, where we proved that the frequency-dependent xc kernel, $f_{\text{xc}}(\mathbf{r}, \mathbf{r}', \omega)$, has a long spatial range and therefore the integral

[1]The idea of introducing memory into TDDFT via the motion of infinitesimal fluid elements and their initial-position dependence was first proposed by Dobson *et al.* (1997). In Appendix L we discuss a formulation of TDCDFT in a Lagrangian frame which puts these concepts on a rigorous foundation.
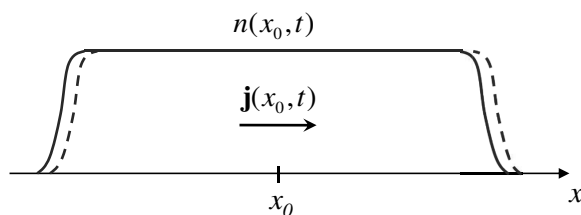
Fig. 10.3 From the local density at position x_0 alone, it is impossible to tell that the slab with constant electron density shown here is moving to the right. A better local indicator is the current density.

$\int d^3 r f_{\mathrm{xc}}(\mathbf{r}, \mathbf{r}', \omega)$ diverges. The Gross–Kohn approximation (10.1) was originally assumed to be valid if the density is slowly varying in space; but the length scale of spatial variation is set by the range of $f_{\mathrm{xc}}(\mathbf{r}, \mathbf{r}', \omega)$, which is infinitely long. Therefore, a memory-dependent local-density approximation *does not exist.*[2]

Further illustration is provided by the example of Fig. 10.3, which shows a long slab of uniform electron density moving to the right. For an extremely nearsighted observer at position x_0 who can only see the local density $n(x_0, t)$, it is impossible to tell that the slab is moving at all, since the density remains unchanged as long as the edges are still far away. It is obvious that this would have severe consequences if one were to attempt to construct a memory-dependent xc potential based on the local density alone: such a potential would behave in an identical way whether or not the slab was moving, which of course is inconsistent with the history of the system. To detect the motion of the slab, the observer would need to notice density changes far away at the edges of the slab—a drastic example of the ultranonlocality problem in TDDFT.

By contrast, if the observer looks at the local current density $\mathbf{j}(x_0, t)$ at position x_0, it becomes very easy to tell whether the slab is moving or standing still. This is a strong indication that it may be possible to construct a local nonadiabatic approximation by replacing the density with the current density as the fundamental variable.

As we have seen, a nonadiabatic $v_{\mathrm{xc}}(\mathbf{r}, t)$ depends on the density in a nonlocal fashion. The current density $\mathbf{j}(\mathbf{r}, t)$ is related to $n(\mathbf{r}, t)$ through the nonlocal continuity equation; correspondingly, we define an xc vector potential $\mathbf{A}_{\mathrm{xc}}(\mathbf{r}, t)$, which is connected to the xc scalar potential via a nonlocal relation. Thus, nonlocality is an automatic side effect of replacing the density with the current density as the basic variable, and we have good reason to expect that the relation between $\mathbf{j}(\mathbf{r}, t)$ and $\mathbf{A}_{\mathrm{xc}}(\mathbf{r}, t)$ should be essentially local in nature.[3] This strategy is also illustrated in Fig. 10.4.

---

[2]The question of the validity of the Gross–Kohn approximation has some subtleties (Giuliani and Vignale, 2005). It turns out that the range of the xc kernel of the homogeneous electron liquid is finite, but becomes infinite as soon as translational symmetry is broken and inhomogeneities appear. The Gross–Kohn approximation is qualitatively correct if the degree of inhomogeneity (measured by a wave vector q) is much smaller than the wave vector k of the induced perturbation. This is, for instance, the case for the bulk plasmon of Fig. 10.1, but not for the harmonic-potential sloshing motion.

[3]Strictly speaking, the connection between density and current density and between xc scalar and vector potentials determines only the longitudinal components of $\mathbf{j}$ and $\mathbf{A}_{\mathrm{xc}}$; however, we will soon see that the local relation between $\mathbf{j}$ and $\mathbf{A}_{\mathrm{xc}}$ also holds for the transverse components.

$$n(\mathbf{r},t) \xleftrightarrow{\text{Nonlocal}} v_{\text{xc}}(\mathbf{r},t)$$

Nonlocal $\qquad\qquad\qquad$ Nonlocal

$$\nabla \cdot \mathbf{j} = -\frac{\partial n}{\partial t} \qquad\qquad \nabla v_{\text{xc}} = \frac{\partial \mathbf{A}_{\text{xc}}}{\partial t}$$

$$\mathbf{j}(\mathbf{r},t) \xleftrightarrow{\text{Local}} \mathbf{A}_{\text{xc}}(\mathbf{r},t)$$
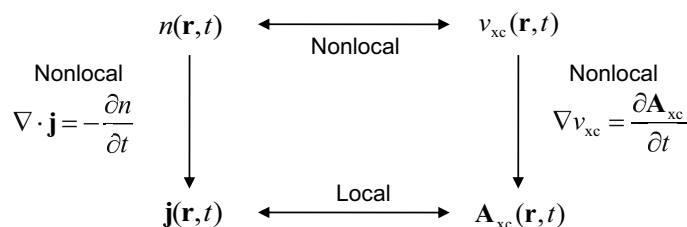
Fig. 10.4 The dependence of a nonadiabatic $v_{\text{xc}}(\mathbf{r},t)$ on the density is intrinsically nonlocal. Instead, it is possible to construct an adiabatic approximation to the xc vector potential in terms of the local current density.

Let us now summarize what we've learned so far:

- The adiabatic approximation in TDDFT works as long as the electron dynamics is governed by excitations that have a counterpart in the Kohn–Sham excitation spectrum.
- The scale of the frequency dependence of f_{xc} is determined by those excitations which are missing in the Kohn–Sham spectrum.
- For practical convenience, a nonadiabatic approximation that is still local in space would be desirable; however, such an approximation in terms of the local, time-dependent density does not exist, since nonlocality in space and time are inseparably linked.
- The current density seems to be a much more promising quantity with which to construct a local, nonadiabatic approximation.

In the following, we will first discuss some fundamental aspects of TDCDFT and then show how a local, current-dependent nonadiabatic xc functional can be constructed (Vignale and Kohn, 1996; Vignale *et al.*, 1997; Ullrich and Vignale, 2002; Vignale, 2006; van Faassen, 2006).

10.3 The formal framework of TDCDFT

10.3.1 Upgrading from densities to currents

Let us begin by discussing the reasons why and under what circumstances one should consider an "upgrade" from densities to currents as basic variables.

Electromagnetic waves. TDDFT, as discussed so far, is restricted to systems under the influence of time-dependent scalar potentials, and in general does not apply to situations involving vector potentials. This means that an important class of problems is not accessible with TDDFT, namely those involving time-dependent magnetic fields or the interaction of electromagnetic waves with matter. So far, we have treated the latter case in the dipole approximation (see Appendix H), which holds in the limit of large wavelengths; however, the more general situation of time- *and* space-dependent external vector potentials is not covered in TDDFT. This was recognized soon after

the Runge–Gross theorem had been established, and stimulated early work (Xu and Rajagopal, 1985; Dhara and Ghosh, 1987; Ghosh and Dhara, 1988) to develop TD-CDFT. The conjugate variables are now the time-dependent vector potential and the current density:

$$\text{TDDFT:}\quad v(\mathbf{r},t) \longleftrightarrow n(\mathbf{r},t)\,, \qquad\qquad \text{TDCDFT:}\quad \mathbf{A}(\mathbf{r},t) \longleftrightarrow \mathbf{j}(\mathbf{r},t)\,. \qquad (10.2)$$

We will discuss the formal framework of TDCDFT in Section 10.3.2.

v-representability of current densities. The current density $\mathbf{j}(\mathbf{r},t)$ is also of interest in itself: it can often be viewed as a more "natural" quantity to describe dynamical phenomena in electronic systems than the time-dependent density $n(\mathbf{r},t)$. Furthermore, as discussed in Section 10.2, we suspect that a local nonadiabatic approximation can be more easily constructed in terms of the current density than the particle density.

But why should we go through all the trouble of constructing a new theoretical framework—isn't TDDFT by itself already enough to get the current density? Our first impulse might be to say yes: first of all, we saw in Chapter 3 that all observables obtainable from the many-body wave function $\Psi(t)$ are, at least formally, a functional of the density, and that should clearly include the current density. Secondly, we have shown in the first step of the proof of the Runge–Gross theorem that the time-dependent current density uniquely determines the external scalar potential. However, this is not the whole story.

Let us recall the fact that any arbitrary vector field $\mathbf{V}(\mathbf{r},t)$ can be decomposed as

$$\mathbf{V}(\mathbf{r},t) = \mathbf{V}_L(\mathbf{r},t) + \mathbf{V}_T(\mathbf{r},t)\,. \qquad (10.3)$$

Assuming differentiability and ignoring surface contributions for simplicity, the longitudinal (curl-free) and transverse (divergence-free) components of the vector field are given by

$$\mathbf{V}_L(\mathbf{r},t) = -\frac{1}{4\pi}\nabla \int d^3r'\, \frac{\nabla'\cdot\mathbf{V}(\mathbf{r}',t)}{|\mathbf{r}-\mathbf{r}'|}\,, \qquad (10.4)$$

$$\mathbf{V}_T(\mathbf{r},t) = \frac{1}{4\pi}\nabla\times\nabla\times \int d^3r'\, \frac{\mathbf{V}(\mathbf{r}',t)}{|\mathbf{r}-\mathbf{r}'|}\,. \qquad (10.5)$$

Likewise, an arbitrary current density in general has both longitudinal and transverse parts, $\mathbf{j}(\mathbf{r},t) = \mathbf{j}_L(\mathbf{r},t) + \mathbf{j}_T(\mathbf{r},t)$, but the continuity equation (3.25) determines only the longitudinal part:

$$\frac{\partial}{\partial t}n(\mathbf{r},t) = -\nabla\cdot\mathbf{j}_L(\mathbf{r},t) \qquad (10.6)$$

(the divergence of a transverse current density vanishes). The density $n(\mathbf{r},t)$ thus says nothing about the transverse component $\mathbf{j}_T$ of the current density. This, of course, was not an issue in the proof of the Runge–Gross theorem, but it points to a deep-rooted problem in the relation between scalar potentials and current densities: in general, it is impossible to find a scalar potential $v(\mathbf{r},t)$ that generates an arbitrary current density $\mathbf{j}(\mathbf{r},t)$. In other words, time-dependent current densities are non-v-representable except in special cases (D'Agosta and Vignale, 2005).

The proof is straightforward: assume that a current density $\mathbf{j}(\mathbf{r}, t) = \mathbf{j}_L(\mathbf{r}, t) + \mathbf{j}_T(\mathbf{r}, t)$ comes from a potential $v(\mathbf{r}, t)$. Now consider another current density $\mathbf{j}'(\mathbf{r}, t) = \mathbf{j}_L(\mathbf{r}, t) + \mathbf{j}'_T(\mathbf{r}, t)$ which differs from $\mathbf{j}(\mathbf{r}, t)$ only in the transverse part. $\mathbf{j}'(\mathbf{r}, t)$ cannot come from a scalar potential $v'(\mathbf{r}, t)$. If it did, the Runge–Gross theorem would be violated, since both currents have the same density $n(\mathbf{r}, t)$ via the continuity equation (10.6). This shows that current densities are, in general, not v-representable.[4]

This result intuitively makes sense: current densities are vector fields with three components, whereas the potential is a scalar field with only one component, and hence it is not surprising that the mapping $v(\mathbf{r}, t)$–$\mathbf{j}(\mathbf{r}, t)$ is incomplete. By this argument, the mapping $\mathbf{A}(\mathbf{r}, t)$–$\mathbf{j}(\mathbf{r}, t)$ is much more appropriate (even though, in practice, $\mathbf{A}$-representability of current densities has not been proved and remains an assumption, although a highly plausible one).

Extended systems.   There's a third reason why we would want to upgrade from densities to currents. In contrast to the situation for finite systems, the Runge–Gross theorem is not always valid for extended systems: it fails for uniform fields. However, a rigorous existence proof can be given within TDCDFT. We will postpone this discussion to Section 12.4.

10.3.2   Existence theorems of TDCDFT

Let us now discuss the fundamental existence theorem of TDCDFT, following Vignale (2004). Consider a many-body system governed by the time-dependent Hamiltonian

$$\hat{H}(t) = \sum_{j=1}^{N} \left\{ \frac{1}{2} \left[\frac{\nabla_j}{i} + \mathbf{A}(\mathbf{r}_j, t) \right]^2 + v(\mathbf{r}_j, t) \right\} + \frac{1}{2} \sum_{i,j \neq i}^{N} w(\mathbf{r}_i - \mathbf{r}_j). \tag{10.7}$$

Here, $v(\mathbf{r}, t)$ and $\mathbf{A}(\mathbf{r}, t)$ are external scalar and vector potentials which possess a Taylor expansion in the time coordinate in the neighborhood of $t = 0$, and w is a given particle–particle interaction.

Now consider a second many-particle system featuring a different particle–particle interaction w' and different external scalar and vector potentials $v'(\mathbf{r}, t)$ and $\mathbf{A}'(\mathbf{r}, t)$:

$$\hat{H}'(t) = \sum_{j=1}^{N} \left\{ \frac{1}{2} \left[\frac{\nabla_j}{i} + \mathbf{A}'(\mathbf{r}_j, t) \right]^2 + v'(\mathbf{r}_j, t) \right\} + \frac{1}{2} \sum_{i,j \neq i}^{N} w'(\mathbf{r}_i - \mathbf{r}_j). \tag{10.8}$$

The initial state of this system, $\Psi'(0)$, is such that it produces the same particle density $n(\mathbf{r}, 0)$ and current density $\mathbf{j}(\mathbf{r}, 0)$ as in the unprimed system with initial state $\Psi(0)$.

Under reasonable assumptions about the convergence radius of a Taylor series expansion of $\mathbf{A}'$ about $t = 0$, one can prove that the primed system (10.8) produces the same time-dependent particle and current densities $n(\mathbf{r}, t)$ and $\mathbf{j}(\mathbf{r}, t)$ as in the unprimed system (10.7). The potentials $v'(\mathbf{r}, t)$ and $\mathbf{A}'(\mathbf{r}, t)$ are then uniquely determined by $v(\mathbf{r}, t)$, $\mathbf{A}(\mathbf{r}, t)$, $\Psi(0)$, and $\Psi'(0)$ up to gauge transformations of the form

---

[4]Furthermore, a current density that is v-representable in an interacting system is, in general, not v-representable in a noninteracting system. On the other hand, the error in the transverse Kohn–Sham current calculated with TDDFT tends to be relatively small (D'Agosta and Vignale, 2005).

$$v'(\mathbf{r}, t) \rightarrow v'(\mathbf{r}, t) - \frac{\partial \Lambda(\mathbf{r}, t)}{\partial t} \, , \tag{10.9}$$

$$\mathbf{A}'(\mathbf{r}, t) \rightarrow \mathbf{A}'(\mathbf{r}, t) + \nabla \Lambda(\mathbf{r}, t) \, . \tag{10.10}$$

Here, $\Lambda(\mathbf{r}, t)$ is an arbitrary scalar function with the initial condition $\Lambda(\mathbf{r}, 0) = 0$.

This basic theorem of TDCDFT can be viewed as a generalization of van Leeuwen's theorem for TDDFT (see Chapter 3). There are two special cases of particular interest:

1. If the primed and the unprimed system are chosen to coincide, i.e., $w = w'$ and $\Psi(0) = \Psi'(0)$, then it follows that the external scalar and vector potentials that produce a given pair of particle and current densities are *unique*, up to a gauge transformation. This establishes a one-to-one mapping between the pair of scalar and vector potentials and the pair of particle and current densities:

$$\{v(\mathbf{r}, t), \mathbf{A}(\mathbf{r}, t)\} \Longleftrightarrow \{n(\mathbf{r}, t), \mathbf{j}(\mathbf{r}, t)\} \, . \tag{10.11}$$

This is the generalization of the Runge–Gross theorem to time-dependent vector potentials and current densities, which was proved earlier by Ghosh and Dhara (1988) in a different manner.

2. If the particle–particle interaction in the primed system is chosen to vanish, i.e., $w' = 0$, then the theorem proves that the particle and current densities of an interacting system can also be obtained in a noninteracting system governed by the Hamiltonian

$$\hat{H}_s(t) = \sum_{j=1}^{N} \left\{ \frac{1}{2} \left[\frac{\nabla_j}{i} + \mathbf{A}_s(\mathbf{r}_j, t) \right]^2 + v_s(\mathbf{r}_j, t) \right\} \, . \tag{10.12}$$

This provides a rigorous basis for the TDKS approach in the presence of vector potentials. It also solves the noninteracting $\mathbf{A}$-representability problem, just as the noninteracting v-representability problem in TDDFT was solved by the van Leeuwen theorem.

The TDKS equation in TDCDFT reads

$$i \frac{\partial}{\partial t} \varphi_j(\mathbf{r}, t) = \left(\frac{1}{2} \left[\frac{\nabla}{i} + \mathbf{A}_s(\mathbf{r}, t) \right]^2 + v_s(\mathbf{r}, t) \right) \varphi_j(\mathbf{r}, t). \tag{10.13}$$

The density $n(\mathbf{r}, t)$ is obtained, as before, via eqn (4.6), and the gauge-invariant physical current density,

$$\mathbf{j}(\mathbf{r}, t) = n(\mathbf{r}, t) \mathbf{A}_s(\mathbf{r}, t) + \frac{1}{2i} \sum_{j=1}^{N} \left[\varphi_j^*(\mathbf{r}, t) \nabla \varphi_j(\mathbf{r}, t) - \varphi_j(\mathbf{r}, t) \nabla \varphi_j^*(\mathbf{r}, t) \right]$$

$$= \mathbf{j}_d(\mathbf{r}, t) + \mathbf{j}_p(\mathbf{r}, t) \, , \tag{10.14}$$

is given by the sum of the diamagnetic and the paramagnetic current density. Thus, in contrast with TDDFT, the full physical current density of the interacting system is reproduced by the current density of the Kohn–Sham system.

A possible choice to fix the gauge freedom of the potentials in eqn (10.13) is

$$v_s(\mathbf{r}, t) = v(\mathbf{r}, t) + v_\mathrm{H}(\mathbf{r}, t) + v_\mathrm{xc}(\mathbf{r}, t) \,, \tag{10.15}$$

$$\mathbf{A}_s(\mathbf{r}, t) = \mathbf{A}(\mathbf{r}, t) + \mathbf{A}_\mathrm{xc}(\mathbf{r}, t) \,, \tag{10.16}$$

i.e., we admit both external and xc scalar and vector potentials. Notice that in this choice of gauge there is only a scalar Hartree potential and no Hartree vector potential. In other words, we neglect induced currents as sources of additional magnetic fields. Such effects are of higher order in $1/c$ and would be present in a fully relativistic treatment, but that is beyond the scope of this book.

Very recently, a rigorous formulation of TDCDFT on lattice systems was presented by Tokatly (2011). In this case, the density-to-potential mapping problem and the **A**-representability problem can both be reduced to proving the existence of unique solutions of a system of nonlinear ordinary differential equations.

10.3.3   The zero-force and zero-torque theorems

One of the exact properties of the xc potential was the zero-force theorem discussed in Section 6.2.2, which states that $v_\mathrm{xc}(\mathbf{r}, t)$ causes only internal forces and no net force on the system [see eqn (6.9)]. This theorem involves only longitudinal forces and is therefore completely captured by TDDFT, since the proof relies only on the fact that the density $n(\mathbf{r}, t)$ is the same in the interacting and in the Kohn–Sham system.

The situation is different for the total angular momentum $\mathbf{L}(t)$ [eqn (3.33)]. In TDDFT, the current densities of the interacting and the Kohn–Sham system are in general not identical: as we have seen above, they can differ by a transverse current contribution. The net torque due to the xc potential can therefore turn out to be nonvanishing (van Leeuwen, 2001), which is a somewhat unsatisfactory state of affairs.

Fortunately, this problem disappears in TDCDFT. It is convenient to introduce the force in the Kohn–Sham system, $\mathbf{F}_s(\mathbf{r}, t) = \mathbf{F}(\mathbf{r}, t) + \mathbf{F}_\mathrm{H}(\mathbf{r}, t) + \mathbf{F}_\mathrm{xc}(\mathbf{r}, t)$, where the external, Hartree, and xc forces are given by

$$\mathbf{F}(\mathbf{r}, t) = -\nabla v(\mathbf{r}, t) - \frac{\partial}{\partial t}\mathbf{A}(\mathbf{r}, t) + \mathbf{u} \times [\nabla \times \mathbf{A}(\mathbf{r}, t)] \,, \tag{10.17}$$

$$\mathbf{F}_\mathrm{H}(\mathbf{r}, t) = -\nabla v_\mathrm{H}(\mathbf{r}, t) \,, \tag{10.18}$$

$$\mathbf{F}_\mathrm{xc}(\mathbf{r}, t) = -\nabla v_\mathrm{xc}(\mathbf{r}, t) - \frac{\partial}{\partial t}\mathbf{A}_\mathrm{xc}(\mathbf{r}, t) + \mathbf{u} \times [\nabla \times \mathbf{A}_\mathrm{xc}(\mathbf{r}, t)] \,, \tag{10.19}$$

and the velocity is defined as $\mathbf{u}(\mathbf{r}, t) = \mathbf{j}(\mathbf{r}, t)/n(\mathbf{r}, t)$. Remember that in TDCDFT (as opposed to TDDFT) the physical density $n(\mathbf{r}, t)$ *and* the current density $\mathbf{j}(\mathbf{r}, t)$ are exactly reproduced by the Kohn–Sham system. The zero-force theorem of TDCDFT thus follows via straightforward generalization of eqns (6.7)–(6.9):

$$\int d^3r \, n(\mathbf{r}, t)\mathbf{F}_\mathrm{xc}(\mathbf{r}, t) = 0 \,. \tag{10.20}$$

Since the current densities are identical, the total angular momenta in the interacting and in the Kohn–Sham system are the same [see eqn (3.33)], so that

$$0 = \frac{\partial}{\partial t}\mathbf{L}(t) - \frac{\partial}{\partial t}\mathbf{L}_s(t) = \int d^3r\, n(\mathbf{r},t)\mathbf{r} \times [\mathbf{F}(\mathbf{r},t) - \mathbf{F}_s(\mathbf{r},t)]$$

$$= -\int d^3r\, n(\mathbf{r},t)\mathbf{r} \times [\mathbf{F}_{\mathrm{H}}(\mathbf{r},t) + \mathbf{F}_{\mathrm{xc}}(\mathbf{r},t)]\ . \quad (10.21)$$

The net torque due to the Hartree force can be shown to vanish (Exercise 10.1), and we end up with the zero-torque theorem of TDCDFT:

$$\int d^3r\, n(\mathbf{r},t)\mathbf{r} \times \mathbf{F}_{\mathrm{xc}}(\mathbf{r},t) = 0\ . \quad (10.22)$$

From a higher point of view, the zero-force and zero-torque theorems arise naturally from the fact that the xc force can be written as the divergence of a stress tensor, $nF_{\mathrm{xc},\mu} = \sum_\nu \nabla_\nu P_{\mathrm{xc},\mu\nu}$. This will be further discussed below and in Appendix L.

10.3.4   TDCDFT in linear response

The linear current-density response $\mathbf{j}_1(\mathbf{r},\omega)$ to an external, frequency-dependent vector potential $\mathbf{A}_1(\mathbf{r},\omega)$ is given by

$$j_{1,\mu}(\mathbf{r},\omega) = \sum_\nu \int d^3r'\chi_{s,\mu\nu}(\mathbf{r},\mathbf{r}',\omega)\left[A_{1,\nu}(\mathbf{r}',\omega) + A_{\mathrm{H1},\nu}(\mathbf{r}',\omega) + A_{\mathrm{xc1},\nu}(\mathbf{r}',\omega)\right]\ ,$$

$$(10.23)$$

where μ and ν denote Cartesian coordinates. Equation (10.23) features the noninteracting (Kohn–Sham) current–current response tensor $\chi_{s,\mu\nu}$, defined as

$$\chi_{s,\mu\nu}(\mathbf{r},\mathbf{r}',\omega) = n_0(\mathbf{r})\delta(\mathbf{r} - \mathbf{r}')\delta_{\mu\nu} + \frac{1}{2}\sum_{j,k}^{\infty}\frac{f_k - f_j}{\varepsilon_k - \varepsilon_j + \omega + i\eta}$$

$$\times\left[\varphi_k^{0*}(\mathbf{r})\nabla_\mu\varphi_j^0(\mathbf{r}) - \varphi_j^0(\mathbf{r})\nabla_\mu\varphi_k^{0*}(\mathbf{r})\right]$$

$$\times\left[\varphi_j^{0*}(\mathbf{r}')\nabla'_\nu\varphi_k^0(\mathbf{r}') - \varphi_k^0(\mathbf{r}')\nabla'_\nu\varphi_j^{0*}(\mathbf{r}')\right].\quad (10.24)$$

The noninteracting density–density response function $\chi_s(\mathbf{r},\mathbf{r}',\omega)$ [eqn (7.69)], is related to $\chi_{s,\mu\nu}$ as follows:

$$\chi_s(\mathbf{r},\mathbf{r}',\omega) = \frac{1}{\omega^2}\sum_{\mu\nu}\nabla_\mu\nabla'_\nu\chi_{s,\mu\nu}(\mathbf{r},\mathbf{r}',\omega)\ . \quad (10.25)$$

$j_{1,\mu}$ is calculated in eqn (10.23) as the current-density response of a noninteracting system to an effective vector potential. The many-body effects enter through the linearized Hartree vector potential

$$\mathbf{A}_{\mathrm{H1}}(\mathbf{r},\omega) = \frac{\nabla}{(i\omega)^2}\int d^3r'\,\frac{\nabla'\cdot\mathbf{j}_1(\mathbf{r}',\omega)}{|\mathbf{r} - \mathbf{r}'|} \quad (10.26)$$

and the xc vector potential

$$A_{\text{xc}1,\mu}(\mathbf{r},\omega) = \sum_\nu \int d^3r' f_{\text{xc},\mu\nu}(\mathbf{r},\mathbf{r}',\omega) j_{1,\nu}(\mathbf{r}',\omega), \tag{10.27}$$

where $f_{\text{xc},\mu\nu}$ is the tensor xc kernel in linear-response TDCDFT. The simplest approximation to $\mathbf{A}_{\text{xc}1}$ is the ALDA, which is given by

$$\mathbf{A}_{\text{xc}1}^{\text{ALDA}}(\mathbf{r},\omega) = \frac{\nabla}{(i\omega)^2} \int d^3r' \, f_{\text{xc}}^{\text{ALDA}}(\mathbf{r},\mathbf{r}') \nabla' \cdot \mathbf{j}_1(\mathbf{r}',\omega) \,, \tag{10.28}$$

where $f_{\text{xc}}^{\text{ALDA}}(\mathbf{r},\mathbf{r}')$ is the ALDA xc kernel of TDDFT.

The properties of the tensor xc kernel were investigated by Vignale and Kohn (1998), and we briefly list three of them here without proof:

Onsager reciprocity relation. The following symmetry property holds if the unperturbed system is invariant under time reversal:

$$f_{\text{xc},\mu\nu}(\mathbf{r},\mathbf{r}',\omega) = f_{\text{xc},\nu\mu}(\mathbf{r}',\mathbf{r},\omega) \,. \tag{10.29}$$

Zero-force theorem. In analogy with eqns (8.10) and (8.11), one obtains

$$\int d^3r \, n_0(\mathbf{r}) f_{\text{xc},\mu\nu}(\mathbf{r},\mathbf{r}',\omega) = \frac{1}{(i\omega)^2} \nabla'_\mu \nabla'_\nu v_{\text{xc}}^0(\mathbf{r}') \tag{10.30}$$

$$\int d^3r' \, n_0(\mathbf{r}') f_{\text{xc},\mu\nu}(\mathbf{r},\mathbf{r}',\omega) = \frac{1}{(i\omega)^2} \nabla_\mu \nabla_\nu v_{\text{xc}}^0(\mathbf{r}) \,. \tag{10.31}$$

Zero-torque theorem.

$$\sum_{\nu\kappa} \int d^3r' \, \epsilon_{\lambda\nu\kappa} f_{\text{xc},\mu\nu}(\mathbf{r},\mathbf{r}',\omega) n_0(\mathbf{r}')(r'_\kappa - r_\kappa) = \frac{1}{(i\omega)^2} \sum_\nu \epsilon_{\lambda\nu\mu} \nabla_\nu v_{\text{xc}}^0(\mathbf{r}) \,, \tag{10.32}$$

where $\epsilon_{\lambda\nu\kappa}$ is the Levi–Civita symbol ($+1$ or -1 if the indices are cyclic or anticyclic, respectively, and 0 if an index is repeated).

Circular dichroism. Let us now discuss an example of a spectroscopic observable that is accessible from linear-response TDCDFT. Circular-dichroism spectra are experimentally obtained by taking the difference between the absorption of left- and right-circularly polarized light. In chemistry, this is an important method to study the properties of chiral molecules (Crawford, 2006).

The characteristic quantity for circular dichroism is the rotatory strength,

$$R_n = \Im[\mathbf{p}_1(\Omega_n) \cdot \mathbf{m}_1^*(\Omega_n)] \,, \tag{10.33}$$

where $\mathbf{p}_1$ is the electric dipole response (7.41) for a particular excitation energy Ω_n, and $\mathbf{m}_1$ is the magnetic dipole response, given by

$$\mathbf{m}_1(\omega) = \frac{1}{2} \int d^3r \, \mathbf{r} \times \mathbf{j}_1(\mathbf{r},\omega) \,. \tag{10.34}$$

In practice, circular-dichroism spectra are often calculated using the eigenvectors of the Casida equation (Furche *et al.*, 2000; Diedrich and Grimme, 2003) or with real-time TDDFT schemes (Yabana and Bertsch, 1999*a*; Varsano *et al.*, 2009). However, this is formally not quite correct: the exact current density is only produced in TDCDFT.

10.3.5   Relation to static CDFT

Let us conclude this overview of the formal framework of TDCDFT by saying a few words about the corresponding theory of static current-DFT (CDFT). The most widely used form of CDFT in the presence of static magnetic fields was developed by Vignale and Rasolt (1987, 1988). In their formulation, the basic variables are the particle density and the *paramagnetic* current density, and the static xc scalar and vector potentials are functionals of both $n_0(\mathbf{r})$ and $\mathbf{j}_{0p}(\mathbf{r})$. Static CDFT à la Vignale and Rasolt is therefore not compatible with our TDCDFT, where the basic variables are the density and the *full* current density (10.14).[5] An alternative CDFT formalism (Diener, 1991), based on the full $\mathbf{j}_0(\mathbf{r})$, provides the appropriate initial conditions for TDCDFT.

In practice, however, most applications of TDCDFT are for situations where the initial state or the unperturbed reference state is the ground state without a magnetic field. In that case, ordinary static DFT is sufficient.

10.4   The VK functional

A local, frequency-dependent approximation for the linearized xc vector potential was first derived by Vignale and Kohn (1996). Soon afterwards it was realized that the rather complicated expression of Vignale and Kohn (VK) can be recast in a much more elegant hydrodynamic form (Vignale *et al.*, 1997; Ullrich and Vignale, 2002; Vignale, 2006). We shall derive and discuss this latter form in the following.

10.4.1   The xc vector potential in a weakly perturbed uniform system

We start by considering the linearized xc vector potential $\mathbf{A}_{\mathrm{xc1}}(\mathbf{r},\omega)$ for situations where the unperturbed system is a homogeneous electron liquid of uniform density $\bar{n}$. The tensor xc kernel $f_{\mathrm{xc},\mu\nu}(\mathbf{r},\mathbf{r}',\omega)$ then becomes a function of $\mathbf{r}-\mathbf{r}'$, and we can Fourier transform eqn (10.27) into

$$A_{\mathrm{xc1},\mu}(\mathbf{q},\omega) = f_{\mathrm{xc},\mu\nu}(\mathbf{q},\omega)j_{1,\nu}(\mathbf{q},\omega) \,. \tag{10.35}$$

This expression can be further simplified, since the homogeneous electron liquid is an isotropic medium. We decompose the current into longitudinal and transverse components, $\mathbf{j}_1 = \mathbf{j}_{1,L} + \mathbf{j}_{1,T}$, and obtain

$$\mathbf{A}_{\mathrm{xc1}}(\mathbf{q},\omega) = \frac{q^2}{\omega^2} f_{\mathrm{xc}}^L(q,\omega)\mathbf{j}_{1,L}(\mathbf{q},\omega) + \frac{q^2}{\omega^2} f_{\mathrm{xc}}^T(q,\omega)\mathbf{j}_{1,T}(\mathbf{q},\omega) \,. \tag{10.36}$$

The action of the tensor xc kernel thus reduces to a simple multiplication of the longitudinal and transverse current components, for any direction of the wave vector $\mathbf{q}$. Here, we define the longitudinal and transverse components of the xc tensor, f_{xc}^L and f_{xc}^T, in such a way that a factor q^2/ω^2 remains explicitly present in eqn (10.36). At this stage this seems just a matter of convenience, since it ensures that $f_{\mathrm{xc}}^L(q,\omega)$ and the density xc kernel $f_{\mathrm{xc}}(q,\omega)$ are identical [see eqn (8.38)]; however, we will soon discover that the factor q^2 plays a very important role.

---

[5]In other words, for static external scalar and vector potentials, our time-dependent v_{xc} and $\mathbf{A}_{\mathrm{xc}}$ functionals do not reduce to the static Vignale–Rasolt v_{xc} and $\mathbf{A}_{\mathrm{xc}}$ functionals.

So far, everything is still exact. Let us now assume that the periodic perturbation we are considering is slowly varying in space $(q \to 0)$ but still has a finite frequency ω. The approximation now consists in replacing the xc kernels at finite q with their zero-q limits:

$$f_{\rm xc}^{L,T}(q,\omega) \approx f_{\rm xc}^{L,T}(q=0,\omega) \,. \tag{10.37}$$

The properties of $f_{\rm xc}^{L,T}(0,\omega) \equiv f_{\rm xc}^{L,T}(\omega)$ were studied in Section 8.3, where we found that they are complex functions with finite real and imaginary parts and known large- and small-frequency behavior. Several analytic parametrizations of $f_{\rm xc}^{L,T}(\omega)$ were given.

With this approximation, we obtain the linearized xc vector potential of a homogeneous system as follows:

$$\mathbf{A}_{\rm xc1}(\mathbf{q},\omega) = \frac{q^2}{\omega^2} f_{\rm xc}^L(\omega) \mathbf{j}_{1,L}(\mathbf{q},\omega) + \frac{q^2}{\omega^2} f_{\rm xc}^T(\omega) \mathbf{j}_{1,T}(\mathbf{q},\omega) \tag{10.38}$$

$$= \mathbf{A}_{\rm xc1}^{\rm ALDA}(\mathbf{q},\omega) + \frac{q^2}{\omega^2}\left[f_{\rm xc}^L(\omega) - \frac{d^2 e_{\rm xc}^h(\bar{n})}{d\bar{n}^2} \right] \mathbf{j}_{1,L}(\mathbf{q},\omega) + \frac{q^2}{\omega^2} f_{\rm xc}^T(\omega) \mathbf{j}_{1,T}(\mathbf{q},\omega) \,. \tag{10.39}$$

In the second equation, we have simply added and subtracted the (purely longitudinal) ALDA xc vector potential of a homogeneous system. We now transform eqn (10.39) back into real space,[6] using the shorthand notation $e_{\rm xc}^{h}{}''$ for the second derivative of the homogeneous xc energy density:

$$\mathbf{A}_{\rm xc1}(\mathbf{r},\omega) = \mathbf{A}_{\rm xc1}^{\rm ALDA}(\mathbf{r},\omega)$$
$$+ \frac{1}{(i\omega)^2}\left\{ \left[f_{\rm xc}^L(\omega) - e_{\rm xc}^{h}{}'' \right] \nabla^2 \mathbf{j}_{1,L}(\mathbf{r},\omega) + f_{\rm xc}^T(\omega)\nabla^2 \mathbf{j}_{1,T}(\mathbf{r},\omega) \right\} \,. \tag{10.40}$$

Using the identity $\nabla^2 \mathbf{V} = \nabla(\nabla \cdot \mathbf{V}) - \nabla \times (\nabla \times \mathbf{V})$ for arbitrary vector fields $\mathbf{V}$ and the fact that longitudinal and transverse vector fields are curl- and divergence-free, respectively, we obtain

$$\mathbf{A}_{\rm xc1}(\mathbf{r},\omega) = \mathbf{A}_{\rm xc1}^{\rm ALDA}(\mathbf{r},\omega)$$
$$+ \frac{\bar{n}}{(i\omega)^2}\left\{ \left[f_{\rm xc}^L(\omega) - e_{\rm xc}^{h}{}'' \right] \nabla(\nabla \cdot \mathbf{u}_1) - f_{\rm xc}^T(\omega)\nabla \times (\nabla \times \mathbf{u}_1) \right\} \,, \tag{10.41}$$

where the velocity field is defined as

$$\mathbf{u}_1(\mathbf{r},\omega) = \frac{\mathbf{j}_1(\mathbf{r},\omega)}{\bar{n}} \,. \tag{10.42}$$

Equation (10.41) can be recast into

$$\mathbf{A}_{\rm xc1}(\mathbf{r},\omega) = \mathbf{A}_{\rm xc1}^{\rm ALDA}(\mathbf{r},\omega)$$
$$+ \frac{\bar{n}}{(i\omega)^2}\left\{ \left[f_{\rm xc}^L(\omega) - f_{\rm xc}^T(\omega) - e_{\rm xc}^{h}{}'' \right] \nabla(\nabla \cdot \mathbf{u}_1) - f_{\rm xc}^T(\omega)\nabla^2 \mathbf{u}_1 \right\} \,, \tag{10.43}$$

and with a few simple manipulations (which will be left as an exercise), one arrives at the following expression for the μth component of the linearized xc vector potential:

---

[6]This is where the factor q^2 in eqn (10.36) becomes important, as it turns into a $(\nabla/i)^2$ operator.

$$A_{\text{xc1},\mu}(\mathbf{r},\omega) = A_{\text{xc1},\mu}^{\text{ALDA}}(\mathbf{r},\omega) + \frac{\bar{n}}{(i\omega)^2} \sum_\nu \nabla_\nu \left\{ f_{\text{xc}}^T(\omega)\left(\nabla_\nu u_{1,\mu} + \nabla_\mu u_{1,\nu} - \frac{2}{3}\nabla\cdot\mathbf{u}_1\delta_{\mu\nu} \right) \right.$$

$$\left. + \left(f_{\text{xc}}^L(\omega) - \frac{4}{3}f_{\text{xc}}^T(\omega) - e_{\text{xc}}^{h}{}'' \right)\nabla\cdot\mathbf{u}_1\delta_{\mu\nu} \right\}. \tag{10.44}$$

It seems like all we've done in the last few steps is to take the nice, compact expression (10.38) and convert it into something more complicated—but all of this has happened for very good reasons: namely, we can now recast eqn (10.44) in the following manner:

$$A_{\text{xc1},\mu}(\mathbf{r},\omega) = A_{\text{xc1},\mu}^{\text{ALDA}}(\mathbf{r},\omega) - \frac{1}{i\omega\bar{n}} \sum_\nu \nabla_\nu \sigma_{\text{xc},\mu\nu}, \tag{10.45}$$

where

$$\sigma_{\text{xc},\mu\nu}(\omega) = \eta_{\text{xc}}(\omega)\left(\nabla_\nu u_{1,\mu} + \nabla_\mu u_{1,\nu} - \frac{2}{3}\nabla\cdot\mathbf{u}_1\delta_{\mu\nu} \right) + \zeta_{\text{xc}}(\omega)\nabla\cdot\mathbf{u}_1\delta_{\mu\nu} \tag{10.46}$$

and

$$\eta_{\text{xc}}(\omega) = -\frac{\bar{n}^2}{i\omega}f_{\text{xc}}^T(\omega), \tag{10.47}$$

$$\zeta_{\text{xc}}(\omega) = -\frac{\bar{n}^2}{i\omega}\left(f_{\text{xc}}^L(\omega) - \frac{4}{3}f_{\text{xc}}^T(\omega) - e_{\text{xc}}^{h}{}'' \right). \tag{10.48}$$

A comparison with classical fluid dynamics (see Appendix I) immediately reveals that $\sigma_{\text{xc},\mu\nu}$, defined in eqn (10.46), has the form of a viscoelastic stress tensor, which plays a key role in the derivation of the equation of motion for viscous fluids. In turn, η_{xc} and ζ_{xc} can be interpreted as viscoelastic coefficients. In many applications of classical hydrodynamics, the viscoelastic coefficients are taken as real viscosity constants; in our case, they are frequency-dependent and complex and thus account for both viscous and elastic behavior of the electron liquid.

We thus have come to a point where we can talk about xc effects using the language of hydrodynamics and elasticity theory, which seems the natural thing to do in TDCDFT. Clearly, the most important object is the xc stress tensor $\mathfrak{o}_{\text{xc}}$, featuring the viscoelastic coefficients η_{xc} and ζ_{xc}, and we shall now discuss their properties.

10.4.2   Discussion: viscoelastic stresses in the electron liquid

In eqn (10.45), we wrote the nonadiabatic contributions to the xc vector potential as the divergence of a stress tensor. In doing so, we immediately ensure that Newton's third law is satisfied, since xc effects are due to internal electron–electron interactions and therefore cannot affect the total momentum of the system (the ALDA already satisfies the zero-force theorem).

The xc viscoelastic stress tensor $\mathfrak{o}_{\text{xc}}$ appears here as the final outcome of a (moderately lengthy) derivation that started out with the general definition of the linearized xc vector potential (10.35) in a homogeneous medium and assumed perturbations that are slowly varying in space. However, the form of the xc stress tensor is in fact quite generic and could have been anticipated based on some very general physical principles. These principles are the same as in classical fluid dynamics (see Appendix I):

- $\mathfrak{o}_{\mathrm{xc}}$ describes memory and retardation effects beyond the adiabatic approximation. One of the main consequences of these effects is the appearance of internal "friction" processes that can lead to dissipation. However, such friction processes require that neighboring fluid elements move with different velocities. Therefore, $\mathfrak{o}_{\mathrm{xc}}$ can depend only on spatial derivatives of the velocity field, and not on $\mathbf{u}_1$ itself.
- For small velocity gradients, it can be expected that $\mathfrak{o}_{\mathrm{xc}}$ is a linear function of only the first derivatives of the velocity field.
- $\mathfrak{o}_{\mathrm{xc}}$ must vanish when $\mathbf{u}_1$ is constant or when the whole system is uniformly rotating; in those cases, there can be no internal friction processes in the fluid.

In other words, in hindsight it is not at all surprising that the xc vector potential (10.45) looks the way it does, namely, the ALDA plus the divergence of a viscoelastic stress tensor to account for nonadiabatic (post-ALDA) effects.

The *real parts* of the coefficients η_{xc} and ζ_{xc} (which are related to the imaginary parts of $f_{\mathrm{xc}}^{L,T}$) play the role of shear and bulk viscosities, respectively, and thus give rise to dissipative behavior in the electron dynamics. We will soon encounter applications where we shall take advantage of this effect.

A comparison with Section 8.3 shows that the *imaginary parts* of η_{xc} and ζ_{xc} (which are related to the real parts of $f_{\mathrm{xc}}^{L,T}$) can be interpreted as frequency-dependent xc bulk and shear moduli K_{xc} and μ_{xc}:

$$\Im\eta_{\mathrm{xc}}(\omega) = -\frac{1}{i\omega}\,\mu_{\mathrm{xc}}(\omega)\,, \tag{10.49}$$

$$\Im\zeta_{\mathrm{xc}}(\omega) = -\frac{1}{i\omega}\left(K_{\mathrm{xc}}(\omega) - \bar{n}^2 e_{\mathrm{xc}}^{h}{}''\right)\,. \tag{10.50}$$

10.4.3   Local approximation

Definition of the VK functional.   We now make the local approximation $\bar{n} \to n_0(\mathbf{r})$ in eqn (10.45), i.e., we replace the density of the uniform system by the local ground-state density of an inhomogeneous system. This substitution defines the VK functional for the linearized xc vector potential (Vignale *et al.*, 1997; Ullrich and Vignale, 2002),

$$A_{\mathrm{xc}1,\mu}^{\mathrm{VK}}(\mathbf{r},\omega) = A_{\mathrm{xc}1,\mu}^{\mathrm{ALDA}}(\mathbf{r},\omega) - \frac{1}{i\omega n_0(\mathbf{r})}\sum_{\nu}\nabla_{\nu}\sigma_{\mathrm{xc},\mu\nu}(\mathbf{r},\omega)\,, \tag{10.51}$$

where the xc viscoelastic stress tensor is still given by eqn (10.46), but the viscosity coefficients are now defined as local quantities:

$$\eta_{\mathrm{xc}}(\mathbf{r},\omega) = -\frac{n_0(\mathbf{r})^2}{i\omega}f_{\mathrm{xc}}^{T}(\mathbf{r},\omega)\,, \tag{10.52}$$

$$\zeta_{\mathrm{xc}}(\mathbf{r},\omega) = -\frac{n_0(\mathbf{r})^2}{i\omega}\left(f_{\mathrm{xc}}^{L}(\mathbf{r},\omega) - \frac{4}{3}f_{\mathrm{xc}}^{T}(\mathbf{r},\omega) - e_{\mathrm{xc}}^{h}{}''\Big|_{n_0(\mathbf{r})}\right)\,, \tag{10.53}$$

where the $f_{\mathrm{xc}}^{L,T}(\mathbf{r},\omega)$ represent the frequency-dependent xc kernels of a homogeneous electron liquid evaluated at the local ground-state density $n_0(\mathbf{r})$ of the system. As in any local approximation, it is implied here that the system is "slowly varying" in some
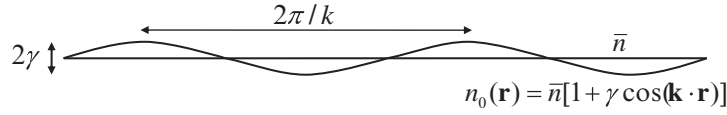
$$2\pi / k$$

$$2\gamma$$

$$\bar{n}$$

$$n_0(\mathbf{r}) = \bar{n}[1 + \gamma \cos(\mathbf{k} \cdot \mathbf{r})]$$

Fig. 10.5 A weakly nonuniform electron liquid modulated by a static perturbation with amplitude γ and wave vector $\mathbf{k}$.

sense; we'll leave it at that for the time being. Below, we give a more precise discussion of the criteria for validity of the local approximation (10.51).

It is interesting to compare the VK functional (10.51), which is a local, frequency-dependent approximation to the xc *vector* potential, with the GK functional

$$v_{\mathrm{xc1}}^{\mathrm{GK}}(\mathbf{r}, \omega) = f_{\mathrm{xc}}^L(\mathbf{r}, \omega) n_1(\mathbf{r}, \omega) , \qquad (10.54)$$

which is a local, frequency-dependent approximation to the xc *scalar* potential. As we discussed in Section 10.2.1, the GK approximation is problematic in the sense that it violates the harmonic potential theorem, and we traced the root of this problem to the ultranonlocality inherent in TDDFT.

By contrast, it is immediately obvious that the VK functional obeys the harmonic potential theorem, since it depends only on *gradients* of the velocity field: the sloshing motion of the charge density in a harmonic confining potential is precisely characterized by a spatially constant velocity field $\mathbf{u}_1(\mathbf{r}, \omega)$ (see also Exercise 10.4).

Discussion: validity of the VK functional.   Our derivation of the VK functional for homogeneous systems, eqn (10.45), was inspired by basic physical principles and conservation laws. However, the crucial step leading to the local VK functional (10.51) seems somewhat ad hoc, in the sense that we made the substitution $\bar{n} \to n_0(\mathbf{r})$ at the very end of our derivation. Had we made the substitution at an earlier stage, say in eqn (10.40), the outcome would have been different. Of course, the final result (10.45) is what we intuitively expect to be correct, but it would be nice to have further supporting evidence.

Fortunately, it turns out that there is an alternative way of arriving at the local approximation (10.51), which in fact is how it was originally derived by Vignale and Kohn (1996, 1998). The idea is to calculate the frequency-dependent xc tensor kernel $f_{\mathrm{xc}, \mu\nu}$ directly for a weakly inhomogeneous electron liquid (see Fig. 10.5), where the ground-state system is characterized by the density

$$n_0(\mathbf{r}) = \bar{n}[1 + \gamma \cos(\mathbf{k} \cdot \mathbf{r})] . \qquad (10.55)$$

This introduces two extra parameters, namely the wave vector $\mathbf{k}$ and the amplitude γ of this static modulation, in addition to the wave vector $\mathbf{q}$ and frequency ω of the time-dependent perturbation acting on this weakly inhomogeneous system. These parameters are subject to the following constraints:

$$k \ll k_F , \qquad q \ll k_F , \qquad (10.56)$$

i.e., both the ground-state density and the frequency-dependent perturbation are slowly varying in space on a scale set by the Fermi wave vector k_F (which is determined by the average density $\bar{n}$), and

$$k \ll \frac{\omega}{v_F} \,, \qquad q \ll \frac{\omega}{v_F} \,, \tag{10.57}$$

where v_F is the Fermi velocity. Notice that v_F/ω is of the same order as the distance traveled back and forth by an electron during one period of the dynamic perturbation. The conditions (10.57) thus mean that the perturbation is "high-frequency," in the sense that the perturbing field rapidly changes sign so that the electrons do not get much opportunity to probe the spatial inhomogeneities of the system. This also implies that the phase velocity of the density disturbance is fast compared with the Fermi velocity so that no form of static screening can occur.

Under these circumstances, an expression can be derived[7] for the off-diagonal elements of the xc tensor kernel $f_{\mathrm{xc},\mu\nu}(\mathbf{q} + \mathbf{k}, \mathbf{q}, \omega)$ to first order in γ, which can be Fourier transformed into a real-space expression for $A_{\mathrm{xc},1}(\mathbf{r}, \omega)$ and rearranged (Vignale *et al.*, 1997) such that one ends up precisely and unambiguously with eqn (10.51). This proves that our physical intuition was indeed correct!

In addition to gaining independent confirmation of the VK functional (10.51), we also obtain a set of local conditions for its validity:

$$\frac{|\nabla n_0(\mathbf{r})|}{n_0(\mathbf{r})} \ll k_F(\mathbf{r}) \,, \qquad \frac{|\nabla n_0(\mathbf{r})|}{n_0(\mathbf{r})} \ll \frac{\omega}{v_F(\mathbf{r})} \,, \tag{10.58}$$

which correspond to the conditions (10.56) and (10.57) for the wave vector k, and

$$\frac{|\nabla j_{1,\mu}(\mathbf{r})|}{j_{1,\mu}(\mathbf{r})} \ll k_F(\mathbf{r}) \,, \qquad \frac{|\nabla j_{1,\mu}(\mathbf{r})|}{j_{1,\mu}(\mathbf{r})} \ll \frac{\omega}{v_F(\mathbf{r})} \,, \tag{10.59}$$

which correspond to the conditions (10.56) and (10.57) for the wave vector q. Both the ground-state density $n_0(\mathbf{r})$ and the current response $\mathbf{j}_1(\mathbf{r}, \omega)$ must be slowly varying on the scale of the local Fermi wave vector and the local value of $\omega/v_F(\mathbf{r})$. Since $\mathbf{u}_1 = n_0 \mathbf{j}_1$, we also have a similar condition for the velocity field of the perturbation,

$$\frac{|\nabla u_{1,\mu}(\mathbf{r})|}{u_{1,\mu}(\mathbf{r})} \ll k_F(\mathbf{r}) \,, \qquad \frac{|\nabla u_{1,\mu}(\mathbf{r})|}{u_{1,\mu}(\mathbf{r})} \ll \frac{\omega}{v_F(\mathbf{r})} \,. \tag{10.60}$$

These conditions provide valuable tools which will help us to analyze the performance of the VK functional in various applications. It will turn out that they can often be violated in practice, which may lead to unphysical results. On the other hand, a mild violation of the conditions (10.58)–(10.60) can usually be tolerated. In the next section, we will look at a variety of examples illustrating both situations.

---

[7]The derivation is quite laborious and not for the faint of heart, and will not be reproduced here. The curious reader is encouraged to consult the original work of Vignale and Kohn (1996, 1998).

10.4.4   Spin-dependent generalization

A spin-dependent generalization of linear-response TDCDFT can be written down in analogy to the spin-dependent formulation of linear-response TDDFT (see Section 7.3.3). The key quantity is the linearized xc vector potential $\mathbf{A}_{\mathrm{xc}1\sigma}(\mathbf{r},\omega)$, and we would like to have a nonadiabatic local approximation for it. Naively, one might think that this is straightforward: all one needs to do is put additional spin indices everywhere in the VK functional (10.51), and we're done. But not quite!

The spin-dependent VK functional was first derived by Qian *et al.* (2003). It can be written as follows:

$$A_{\mathrm{xc}1\sigma,\mu}^{\mathrm{VK}}(\mathbf{r},\omega) = A_{\mathrm{xc}1\sigma,\mu}^{\mathrm{ALDA}}(\mathbf{r},\omega) - \frac{1}{i\omega n_{0\sigma}(\mathbf{r})} \sum_{\sigma'} \sum_{\nu} \nabla_{\nu} \sigma_{\mu\nu,\sigma\sigma'}^{\mathrm{xc}}(\mathbf{r},\omega)$$

$$- \frac{\delta_{\sigma\uparrow} - \delta_{\sigma\downarrow}}{i\omega n_{0\sigma}(\mathbf{r})} \, n_{0\uparrow}(\mathbf{r}) n_{0\downarrow}(\mathbf{r}) \rho_{\uparrow\downarrow}(\mathbf{r},\omega) \left[u_{1\uparrow,\mu}(\mathbf{r},\omega) - u_{1\downarrow,\mu}(\mathbf{r},\omega) \right]. \quad (10.61)$$

Indeed, the first two terms are just what we expected, namely, the ALDA plus a spin-dependent generalization of the viscoelastic xc term, featuring the stress tensor

$$\sigma_{\mu\nu,\sigma\sigma'}^{\mathrm{xc}}(\omega) = \eta_{\sigma\sigma'}^{\mathrm{xc}}(\omega) \left(\nabla_{\nu} u_{1\sigma',\mu} + \nabla_{\mu} u_{1\sigma',\nu} - \frac{2}{3} \nabla \cdot \mathbf{u}_{1\sigma'} \delta_{\mu\nu} \right) + \zeta_{\sigma\sigma'}^{\mathrm{xc}}(\omega) \nabla \cdot \mathbf{u}_{1\sigma'} \delta_{\mu\nu} \,,$$
$$(10.62)$$

with a spin-dependent velocity field $\mathbf{u}_{1\sigma}(\mathbf{r},\omega) = \mathbf{j}_{1\sigma}(\mathbf{r},\omega)/n_{0\sigma}(\mathbf{r})$. The spin-dependent viscosity coefficients $\eta_{\sigma\sigma'}^{\mathrm{xc}}$ and $\zeta_{\sigma\sigma'}^{\mathrm{xc}}$ are defined similarly to eqns (10.52) and (10.53) in terms of a spin-dependent generalization of the longitudinal and transverse xc kernels of the homogeneous electron liquid. Explicit parametrizations of these have been given by Qian and Vignale (2003).

The last term in eqn (10.61) is new and particular to the spin-dependent case; it is easy to see that it vanishes when the spin-up and spin-down velocities are equal. Unlike the case of the viscoelastic stress tensor, this term depends on the velocities themselves and not on the velocity gradients; it therefore persists in the limit where the induced currents are uniform.

$\rho_{\uparrow\downarrow}$ is called the spin-transresistivity and is related to the spin Coulomb drag effect (D'Amico and Vignale, 2000). The spin Coulomb drag is an intrinsic dissipation mechanism caused by exchange of momentum between spin-up and spin-down electrons of different velocities, leading to a drag force exerted by one spin population on the other. The total momentum remains conserved (since only internal Coulomb forces are present), but the momenta of the spin-up and the spin-down electron populations are not separately conserved. We will not pursue the spin Coulomb drag effect any further here; for a recent overview of applications in spintronics and other areas, see D'Amico and Ullrich (2010).

10.5   Applications of TDCDFT in the linear-response regime

In this section, we review the applications of TDCDFT using the VK functional. We will distinguish between applications that take place in the quasi-static ($\omega \to 0$) limit and applications at finite frequencies.
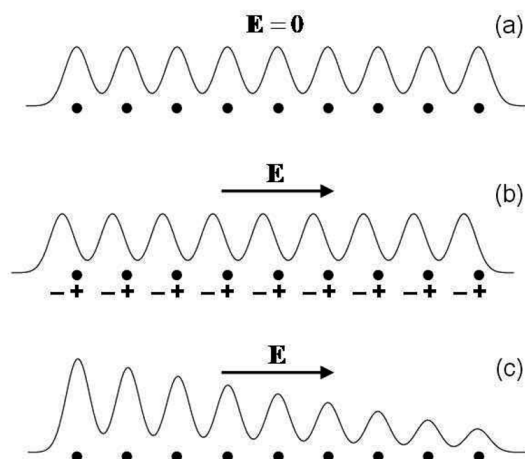
Fig. 10.6 Schematic illustration of the polarization of a long-chain molecule in a static electric field. (a) Field-free ground state; (b) correct polarized state; (c) incorrect polarized state as predicted by the LDA or any other (semi)local xc functional.

10.5.1   Applications in the quasi-static limit

Polarizabilities of π-conjugated molecular chains.   The static dielectric polarizabilities of π-conjugated polymers and molecular chains typically come out much too high with the LDA or other semilocal approximations. If such systems are subject to an electric field along the molecular chain, there is a resulting rearrangement of the electronic charge density, schematically illustrated in Fig. 10.6. The main effect is that each unit cell of the polymer becomes roughly equally polarized, as shown in panel (b). By contrast, the LDA or any other (semi)local xc functional predicts a state in which a large linear charge imbalance occurs along the chain, which indicates a lack of screening of the external field and leads to a significant overestimation of the polarizability.

To prevent this linear charge imbalance, the exact xc potential must have a component that counteracts the external field and is roughly linear in space. But for this to happen, the xc functional must be sufficiently long-ranged to pick up charge-density fluctuations at the ends of the long chain. This is a manifestation of the ultranonlocality problem of static DFT! A partial cure is provided by incorporating exact exchange (van Gisbergen *et al.*, 1999; Mori-Sánchez *et al.*, 2003; Kümmel *et al.*, 2004), which will be discussed in detail in Chapter 11.

TDCDFT provides an alternative approach to curing the polarizability problem of the LDA (van Faassen *et al.*, 2002, 2003). Figure 10.7 shows two examples, for polyacetylene and a chain of hydrogen atoms, comparing results for the polarizability versus number of oligomers obtained from the ALDA and the HF methods, and several high-level wave function methods such as MP2, MP4, CCSD(T), and VK.

Let us first consider polyacetylene. In the static limit of the ALDA, the polarizability increases linearly with the number of oligomers, whereas in all other approaches a saturation sets in. The VK results show an impressive agreement with MP2; similar
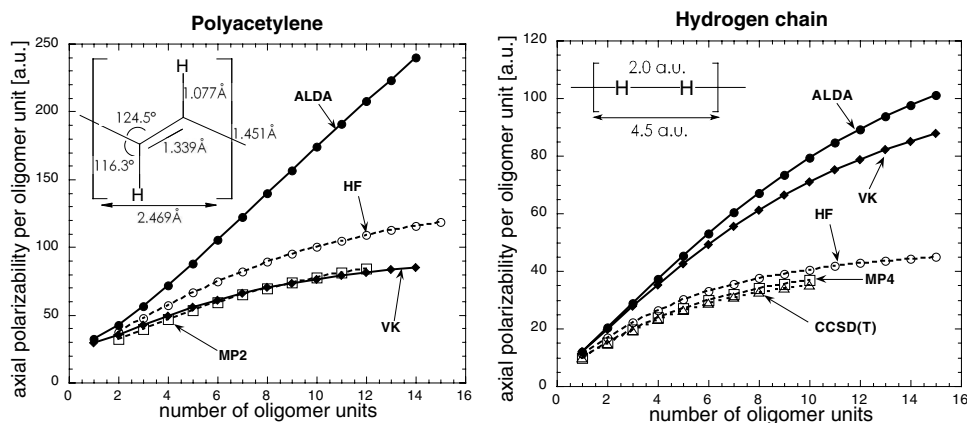
Fig. 10.7 Static axial polarizability of polyacetylene and hydrogen chains as a function of the number of oligomer units. [Reproduced with permission from APS from van Faassen *et al.* (2002), ©2002.]

results are observed for a broad variety of π-conjugated polymer systems.

The success of the VK functional for the static polarizabilities of π-conjugated molecules is due to the fact that it does not reduce to the ALDA in the limit $\omega \to 0$. The reasons for this were discussed in Section 8.3, where we showed that the xc shear modulus μ_{xc} does not vanish in the static limit: in other words, the system remains "dynamical" all the way down to $\omega \to 0$. These xc shear stresses are precisely what opposes the buildup of induced charges shown in Fig. 10.6(c).

By contrast, in the case of the hydrogen chain, only a marginal improvement is achieved by the VK functional. The bonding in H chains is of σ type, and the dominant contribution to the polarization of the chain arises from polarizations within those σ bonds, in contrast to conjugated polymers, with their delocalized π bonds. The criteria for the validity of the VK functional are therefore less well satisfied for these systems.

Stopping power in metals.   If one shoots a beam of ionic projectiles into a material, the projectiles are slowed down owing to collisions with the electrons and ionic cores of the material. Let us consider in particular the frictional forces due to the valence and conduction electrons, and define the resulting *stopping power dE/dx* as the loss of kinetic energy per unit length. As long as the speed of the ion is slow, one has

$$\frac{dE}{dx} = Qu_{\mathrm{ion}}, \tag{10.63}$$

where Q is the friction coefficient of the material under consideration. We restrict the discussion here to metals in which the valence electrons are sufficiently delocalized that they can be treated as an electron liquid.

The friction coefficient describes the interactions of the electron liquid with the ion, including single-particle and many-body effects (Nazarov *et al.*, 2005). The total friction coefficient $Q = Q_{\mathrm{single}} + Q_{\mathrm{xc}}^{\mathrm{dyn}}$ turns out to be a simple sum of (adiabatic) single-particle and (nonadiabatic) many-body contributions. The single-particle contribution
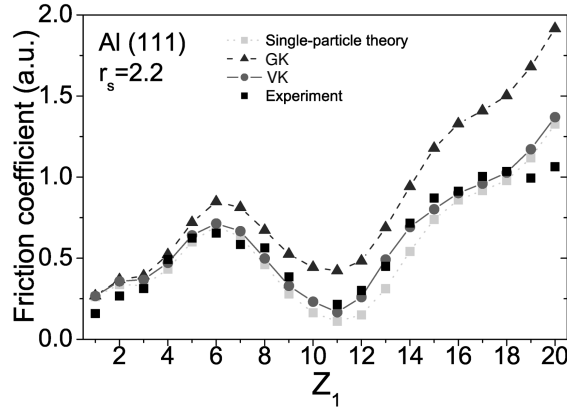
Fig. 10.8 Friction coefficients Q of slow ions of charge Z_1 moving in aluminum. [Adapted with permission from APS from Nazarov *et al.* (2007), ©2007.]

Q_{single} arises from elastic scattering of electrons at the Fermi level by the instantaneous effective Kohn–Sham potential of the moving ion. The many-body contribution $Q_{\text{xc}}^{\text{dyn}}$ is due to dynamical xc effects beyond the adiabatic approximation, and one finds

$$Q_{\text{xc}}^{\text{dyn}} = - \int d^3 r \int d^3 r' \left[\nabla_r n_0(\mathbf{r}) \cdot \hat{\mathbf{u}}_{\text{ion}} \right] \left[\nabla_{r'} n_0(\mathbf{r}') \cdot \hat{\mathbf{u}}_{\text{ion}} \right] \left. \frac{\partial \Im f_{\text{xc}}(\mathbf{r}, \mathbf{r}', \omega)}{\partial \omega} \right|_{\omega=0}, \quad (10.64)$$

where $\hat{\mathbf{u}}_{\text{ion}}$ is the unit vector along the direction of the ion velocity, and $f_{\text{xc}}(\mathbf{r}, \mathbf{r}', \omega)$ is the scalar xc kernel of an inhomogeneous system consisting of the ion at rest in the electron liquid. The imaginary part of $f_{\text{xc}}(\mathbf{r}, \mathbf{r}', \omega)$ leads to dissipation.

   Figure 10.8 shows the total friction coefficients Q of ions of charge up to $Z_1 = 20$ moving in bulk aluminum. Experimental data is compared with calculations using the single-particle theory only, and including nonadiabatic xc contributions using the GK and VK approximations. The friction coefficient increases for small ion charges, has a local maximum around $Z_1 = 6$, and then decreases again; the local minimum around $Z_1 = 11$ occurs because the electrons form a closed-shell bound state around the ion. The single-particle friction coefficient, by itself, is too small compared with the experimental data, as expected. But the GK functional (8.56) overcorrects, giving a value for the friction that is much too large. This is another manifestation of the fact that a local frequency-dependent xc kernel in TDDFT violates basic physical constraints; in this case, it produces a finite friction even in the absence of a surrounding electron liquid.

   The VK functional gives an excellent description of the experimental data. There is a technical complication, namely, that eqn (10.64) requires the scalar xc kernel of TDDFT as an input, whereas the VK theory gives the tensor xc kernel of TDCDFT [see eqn (10.51)]. Expressing $f_{\text{xc}}(\mathbf{r}, \mathbf{r}', \omega)$ in terms of $f_{\text{xc},\mu\nu}(\mathbf{r}, \mathbf{r}', \omega)$ is a bit involved (Nazarov *et al.*, 2007, 2008). Details can be found in Appendix J.

Nanoscale transport. The VK functional has also been applied to nanoscale transport, where it gives a contribution to the resistance in molecular junctions. We will discuss this application in Section 15.2.

Table 10.1 Lowest singlet excitation energies of Be and Mg atoms (in eV), calculated with the ALDA and the VK functional (using the NCT and QV parametrizations for $f_{xc}^{L,T}$) (van Faassen, 2006).

	Experiment	ALDA	VK_{NCT}	VK_{QV}
Be $2s \to 2p$	5.28	4.83	6.03	6.14
Be $2s \to 3s$	6.78	6.53	6.55	6.58
Mg $3s \to 3p$	4.35	4.50	7.17	7.08
Mg $3s \to 4s$	5.39	7.23	7.23	7.25

10.5.2 Applications at finite frequency: excitations and linewidths

As we have seen, the VK functional can be quite successful in the static limit, profiting from the fact that it has a finite xc shear modulus for $\omega \to 0$, i.e., it does not reduce to the ALDA. The question now is, what happens in the truly dynamical regime, when we want to describe excitations at finite frequencies? The VK formalism has been tested for atoms, molecules, bulk solids, and semiconductor quantum wells, with mixed results—some situations are well described, but it fails badly for others. In hindsight, the failures occur precisely in such cases where the VK functional is not meant to be used. In the following we shall explain when the VK functional works and when it doesn't. This will then lead into an in-depth discussion of dissipation in TD(C)DFT.

Atomic and molecular excitation energies. As a case in point, let us consider excitation energies in closed-shell atoms (Ullrich and Burke, 2004; van Faassen, 2006). Table 10.1 shows the lowest two singlet excitation energies of Be and Mg, calculated in the ALDA and using the VK functional (with the NCT and QV parametrizations for $f_{xc}^{L,T}$; see Section 8.3.3). For the $s \to s$-type excitations, the VK functional gives only a marginal correction to the ALDA, but for the $s \to p$ excitations, the VK functional significantly overshoots.

This can be understood by checking the criteria of validity (10.58)–(10.60) for the particular excitation processes under consideration. Figure 10.9 compares the radial component of $|\nabla j/j|$ and the local k_F for the two types of excitations.[8] It can be clearly seen that the condition $|\nabla j/j| \ll k_F$ is strongly violated for the $s \to p$ excitations.

This example is typical of the performance of the VK functional for excitation energies in finite systems; similar observations were made by van Faassen and de Boeij (2004a, 2004b) for a variety of molecular excitations. For instance, one finds that results for certain $\pi \to \pi^*$ transitions are somewhat improved over the ALDA, whereas $n \to \pi^*$ type excitations tend to be overestimated. We can summarize the observations as follows:

---

[8]In the SPA, the current response of an excitation dominated by the occupied and empty Kohn–Sham levels i and a is proportional to $\varphi_i^0 \nabla \varphi_a^0 - \varphi_a^0 \nabla \varphi_i^0$ (assuming real orbitals). See also eqn (10.67).
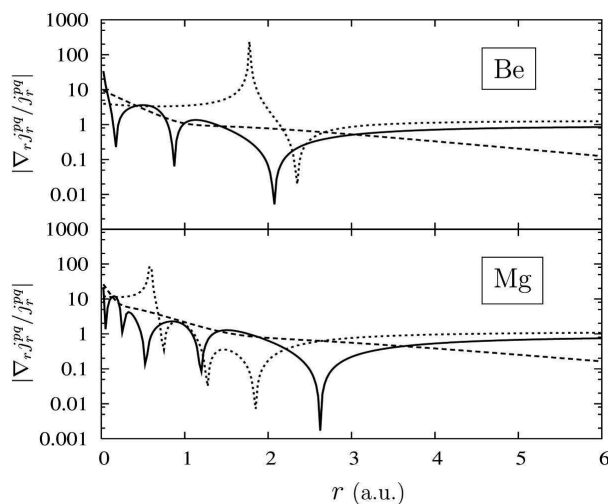
Fig. 10.9 Test of the criterion (10.59) for the Be and Mg atoms. Dashed line: local k_F. Full and dotted lines: $|\nabla j/j|$ associated with the lowest $s \to s$ and $s \to p$ excitations, respectively. [Adapted with permission from AIP from Ullrich and Burke (2004), ©2004.]

- The performance of the VK functional for atomic and molecular systems depends on the type of excitation. Those excitations which are accompanied by large current fluctuations, such that the criteria (10.59), and (10.60) are violated, are usually poorly described. For those excitations that do satisfy the criteria of validity, the VK functional improves the performance compared with ALDA only marginally.
- When atomic and molecular excitations are calculated, a large contribution comes from high-density (small r_s) regions close to the nuclei. But for $r_s < 1$, the xc kernels of the uniform electron liquid (see Section 8.3.3) are not very well known. While this is not a fault of the VK functional itself, it may be a contributing factor to the bad performance for some types of excitation.
- Since the VK xc potential is complex and frequency-dependent, excitation energies in finite systems have nonvanishing imaginary parts. This unphysical behavior[9] comes from the fact that the VK functional treats any system—finite or extended—locally as a weakly modulated uniform electron liquid.

Some improvements of the VK functional are possible, such as gradient corrections (Tao and Vignale, 2006; Tao *et al.*, 2007), and we could also try to find better approximations to the xc kernels in the high-density regions. Nevertheless, it is quite clear that the VK functional is not meant to be used for excitation energies in atomic and molecular systems; for this purpose, adiabatic GGA and hybrid xc kernels (see Chapter 9) are much better suited.

[9]An excitation energy in a finite system is the difference between two (real) energy eigenvalues of the total Hamiltonian, and therefore must be a real number. However, this is not so for extended systems; see also the discussion of the analytic structure of the response function in Section 7.1.3.

Optical absorption spectra of bulk solids.   We will discuss the performance of the VK functional for solids in Section 12.4.2. It will turn out that there are difficulties similar to those for atoms and molecules.

Linewidth of collective excitations.   Are there excitations for which the VK functional *is* well suited? The answer is yes:

> The VK functional works well for extended metallic or quasi-metallic systems such as simple bulk metals or doped semiconductor quantum wells. In these systems, excitations of a collective, plasmon-like type, which are characterized by small current and velocity gradients, are well described. In particular, the VK theory yields quantitatively accurate linewidths of these excitations.

In extended systems, unlike finite systems, dissipation is an important physical feature of collective excitations, and, if applied in the appropriate circumstances, the VK functional is ideally suited for the calculation of linewidths of such excitations. To see how this works at the most basic level, let us consider the two-level system in considered Section 7.4. The generalization of eqn (7.110) for the VK functional of TDCDFT reads (Ullrich, 2009)

$$\Omega = \omega_{21} + 2\left[K_{12,12}^{\text{ALDA}} + S_{12,12}(\Omega)\right] , \tag{10.65}$$

where $K_{12,12}^{\text{ALDA}}$ is defined in eqn (7.106) using the ALDA xc kernel $f_{\text{xc}}^{\text{ALDA}}(\mathbf{r}, \mathbf{r}')$, and

$$S_{12,12}(\omega) = \frac{i}{4\omega}\sum_{\mu\nu}\int d^3r\, u_{\mu}^{12}(\mathbf{r})\nabla_{\nu}\sigma_{\text{xc},\mu\nu}^{12}(\mathbf{r}, \omega) . \tag{10.66}$$

Notice that $S_{12,12}(\omega)$ has a real and an imaginary part, where

$$\mathbf{u}^{12}(\mathbf{r}) = \frac{1}{n_0(\mathbf{r})}\left[\varphi_1^0(\mathbf{r})\nabla\varphi_2^0(\mathbf{r}) - \varphi_2^0(\mathbf{r})\nabla\varphi_1^0(\mathbf{r})\right] \tag{10.67}$$

is the velocity field associated with the $1 \rightarrow 2$ excitation, and $\sigma_{\text{xc},\mu\nu}^{12}(\mathbf{r}, \omega)$ is the viscoelastic xc stress tensor (10.46) evaluated with $\mathbf{u}^{12}(\mathbf{r})$.

It is interesting to compare this with eqn (I.18) in Appendix I, which gives the average rate of energy dissipation (loss of kinetic energy) in classical fluid dynamics. Inspired by this, we define

$$P_{\text{visc}}^{12}(\omega) = \sum_{\mu\nu}\int d^3r\, u_{\mu}^{12}(\mathbf{r})\nabla_{\nu}\sigma_{\text{xc},\mu\nu}^{12}(\mathbf{r}, \omega) \tag{10.68}$$

as the rate of change of the energy (which has the dimensions of a power, but is a complex quantity) associated with the viscoelastic xc stress forces during the $1 \rightarrow 2$ excitation. Equation (10.65) then becomes

$$\Omega = \Omega_{\text{ALDA}} + \frac{i}{2\Omega}P_{\text{visc}}^{12}(\Omega) . \tag{10.69}$$

This is the dressed SPA for excitation energies in the VK approximation, and leads to complex values of Ω. The proper way to solve eqn (10.69) requires the frequency-dependent xc kernels $f_{\text{xc}}^{L,T}$, which enter into the definition of the xc viscosity coefficients, to be evaluated via analytic continuation, as explained in Section 8.3.4. To

Table 10.2 Lowest intersubband plasmon excitation energies and linewidths of GaAs/AlGaAs single and double quantum wells (Ullrich and Vignale, 1998*a*). Experimental data is compared with ALDA and nonadiabatic calculations, using the GK and VK xc kernels in the GK and NCT parametrizations of f_{xc}^L.

	Experiment	ALDA	GK_{GK}	GK_{NCT}	VK_{GK}	VK_{NCT}
Ω (single)	10.7	10.25	10.63	10.23	10.31	10.24
Γ (single)	0.53	—	0.683	0.655	0.128	0.104
Ω (double)	14.6	13.85	14.24	13.88	20.64	12.55
Γ (double)	1.17	—	1.00	0.403	8.55	4.15

make our lives a bit simpler, we can find an approximate solution of eqn (10.69) by replacing Ω with Ω_{ALDA} on the right-hand side. This is justified because the viscosity effects usually give only a relatively small correction to the ALDA xc energy. The result is

$$\Omega = \Omega_{ALDA} - \frac{\Im P_{visc}^{12}(\Omega_{ALDA})}{2\Omega_{ALDA}} + i\frac{\Re P_{visc}^{12}(\Omega_{ALDA})}{2\Omega_{ALDA}} . \tag{10.70}$$

The viscoelastic xc effects therefore give a correction to the real part of the ALDA excitation energy, and they introduce an imaginary part. The shift of the real part is due to the *elastic* behavior of the interacting electrons, whereas the imaginary part reflects the electronic *viscosity*. The dissipated power P_{diss} in a classical fluid is a real, negative quantity, as discussed in Appendix I; likewise, $\Re P_{visc}^{12}$ is negative, which means that the excitation energy Ω acquires a negative imaginary part. A complex excitation energy corresponds to a spectral line with a Lorentzian line shape whose half-width at half-maximum (HWHM) Γ is given by the imaginary part of the excitation energy. We therefore get the following VK result:

$$\Gamma = \left| \Re P_{visc}^{12}(\Omega)/2\Omega \right| . \tag{10.71}$$

The simple linewidth formula (10.71) was derived using the SPA in a two-level system. A somewhat more general expression for the linewidth is (Ullrich and Vignale, 1998*b*)

$$\Gamma = \frac{|\Re \sum_{\mu\nu} \int d^3r \, u_{1\mu}(\mathbf{r},\Omega)\nabla_\nu \sigma_{xc,\mu\nu}(\mathbf{r},\Omega)|}{\int d^3r \, n_0(\mathbf{r})|\mathbf{u}_1(\mathbf{r},\Omega)|^2} , \tag{10.72}$$

where $\mathbf{u}_1(\mathbf{r},\Omega)$ is the velocity profile associated with the excitation energy Ω.[10] Instead of using these approximate expressions, the linewidth can also be calculated exactly by determining the excitation energy as a pole in the complex frequency plane, or by determining the photoabsorption cross section.

Now let us see how this works in practice. We consider two kinds of GaAs/AlGaAs quantum well (see Fig. 10.10 and Appendix K): a single well of width 40 nm with $N_s =$

---

[10]It is easy to see how the two linewidth formulas are related: the excitation energy Ω in the denominator in eqn (10.71) is replaced in eqn (10.72) by the average classical kinetic energy. Equation (10.72) is thus independent of the amplitude of the eigenmode associated with the excitation Ω.
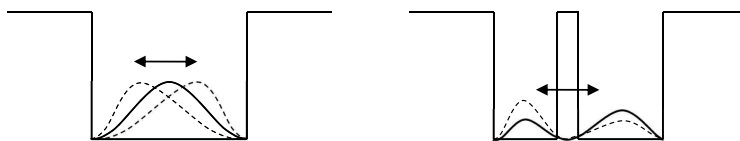
Fig. 10.10 Illustration of the electron dynamics of the intersubband transitions of Table 10.2. In the double well, the electrons tunnel back and forth through the barrier.

$1 \times 10^{11}\,\mathrm{cm}^{-2}$, and an asymmetric double well consisting of two wells of widths 8.5 nm and 7.3 nm separated by a 2.3 nm barrier, with $N_s = 2 \times 10^{11}\,\mathrm{cm}^{-2}$. The intersubband electron dynamics in the double well is such that electrons are periodically forced to tunnel through the barrier. Tunneling is an intrinsically single-electron phenomenon, which disrupts the collective flow and causes large stresses in the electron liquid. Owing to the noncollective nature of the electron dynamics in the double well, which cannot be described by a simple laminar flow pattern, we don't expect the VK functional to work there very well.

This is indeed confirmed by the numbers in Table 10.2, comparing experimental results with TD(C)DFT calculations of intersubband excitation energies and linewidths. The ALDA, as expected, gives zero linewidth and reasonable plasmon frequencies. Let us now look at the performance of the nonadiabatic xc kernels. We compare results obtained using the GK approximation, eqn (10.1), and the VK functional, using two parametrizations of f_{xc}^L (GK and NCT).[11]

For the single well, the real parts of Ω don't differ much from the ALDA results; with the VK functional, we obtain a linewidth that is much lower than experiment. This is to be expected, since the experimental data also include other dissipation mechanisms (see below). The GK functional, on the other hand, gives a linewidth that is greater than the experimental value, which is consistent with the fact that it violates the harmonic potential theorem of TDDFT and therefore tends to cause overdamping.

The situation is different for the double well. Here, the GK functional gives reasonable results, whereas the VK functional completely breaks down, giving unreasonably large damping. This can again be understood by looking at whether the criteria of validity (10.58), (10.59), and (10.60) are satisfied. Indeed, a full analysis (Ullrich and Vignale, 1998a) shows that the intersubband plasmon has a strongly peaked velocity field in the barrier region, which comes from single-electron tunneling between the wells (see Fig. 10.10). Such applications are clearly out of bounds for the VK functional.

We should also mention that the spin-dependent VK functional (10.61) has been applied to calculate linewidths of intersubband spin plasmons in quantum wells (D'Amico and Ullrich, 2006).

---

[11] These calculations were carried out using the 3D form of the VK functional. The question of dimensionality is somewhat subtle: one one hand, a quantum well of finite width is of course a 3D system; but on the other hand, owing to finite-size quantization into subbands, there is no continuous excitation spectrum. As a consequence, application of the 3D VK functional to quantum wells may be a bit problematic and can lead to an overestimation of dissipation, particularly if the wells are very narrow (D'Agosta *et al.*, 2007). The correct form of the VK functional for geometrically confined systems such as quantum wells (with dimensionality between 2D and 3D) remains an open question.

10.5.3   Intrinsic and extrinsic dissipation

The electron dynamics in all realistic extended systems is subject to *dissipation*. In the broadest sense, this means that energy is irreversibly transferred from the electronic degrees of freedom to the environment. The word "environment" can have many meanings: it could be ionic vibrations, an infinite "outside" region (such as metallic leads) connected to a finite "inside" region, or, in a more abstract sense, the total electronic Hilbert space into which a more restricted subspace is embedded.

In practice, dissipation is caused by some kind of scattering or damping forces. In the following, we shall distinguish between two kinds of scattering mechanisms:

- *extrinsic* scattering is caused by some form of disorder, such as impurities, interface roughness, or phonons (since lattice vibrations represent a deviation from the perfect crystal);
- *intrinsic* scattering is caused by electronic interactions and occurs even in an otherwise perfect (i.e., not disordered) system.

This distinction make sense from the viewpoint of TD(C)DFT: intrinsic effects are in principle treated exactly via the xc potential, whereas all extrinsic effects must come from some external scattering potential or via coupling to the lattice dynamics.

A full treatment of disordered electronic systems is far beyond the scope of this book. We will discuss some TDDFT approaches for open systems in Section 15.3.5. A linear-response TDCDFT approach for weakly disordered systems has been developed to study intrinsic and extrinsic contributions to the linewidth of intersubband plasmons in quantum wells (Ullrich and Vignale, 2001, 2002) and to study such contributions to transport and optical conductivities in dilute magnetic semiconductors (Kyrychenko and Ullrich, 2009). Schematically, one obtains an expression for the current–current response function of the disordered system in terms of TD(C)DFT response functions of the clean system:

$$\chi_{j_\alpha j_\beta}^{\text{dis}}(\mathbf{q},\omega) = \chi_{j_\alpha j_\beta}^{\text{clean}}(\mathbf{q},\omega) + \sum_{\mathbf{k}} \frac{k_\alpha k_\beta}{\omega^2} \langle \hat{U}_{\text{sc}}(\mathbf{k})\hat{U}_{\text{sc}}(-\mathbf{k})\rangle \left[\chi_{nn}^{\text{dis}}(\mathbf{q}-\mathbf{k},\omega) - \chi_{nn}^{\text{clean}}(-\mathbf{k},0)\right].$$

(10.73)

Here, $\langle \hat{U}_{\text{sc}}(\mathbf{k})\hat{U}_{\text{sc}}(-\mathbf{k})\rangle$ represents a system average over the product of disorder-scattering-potential operators (these couple to the density fluctuations, which is why the density-density response functions show up on the right-hand side).[12] Equation (10.73) needs to be solved self-consistently for the disordered response function. This is similar to other approaches in the literature, such as diagrammatic techniques for strongly disordered systems (Lee and Ramakrishnan, 1985).

In the limit of weak disorder, we can replace the disordered by the clean response function on the right-hand side, thus getting rid of the self-consistency. In this way, extrinsic scattering is treated approximately, while intrinsic dissipation through electronic many-body effects is still in principle treated exactly via TDDFT.

Figure 10.11 shows intersubband plasmon frequencies and linewidths compared with experimental data (Williams *et al.*, 2001). Under the influence of a static electric

---

[12]In practice, one needs to find a model for the disorder scattering potential. Often, one assumes a random screened Coulomb potential; other, correlated forms of disorder potentials are also possible.
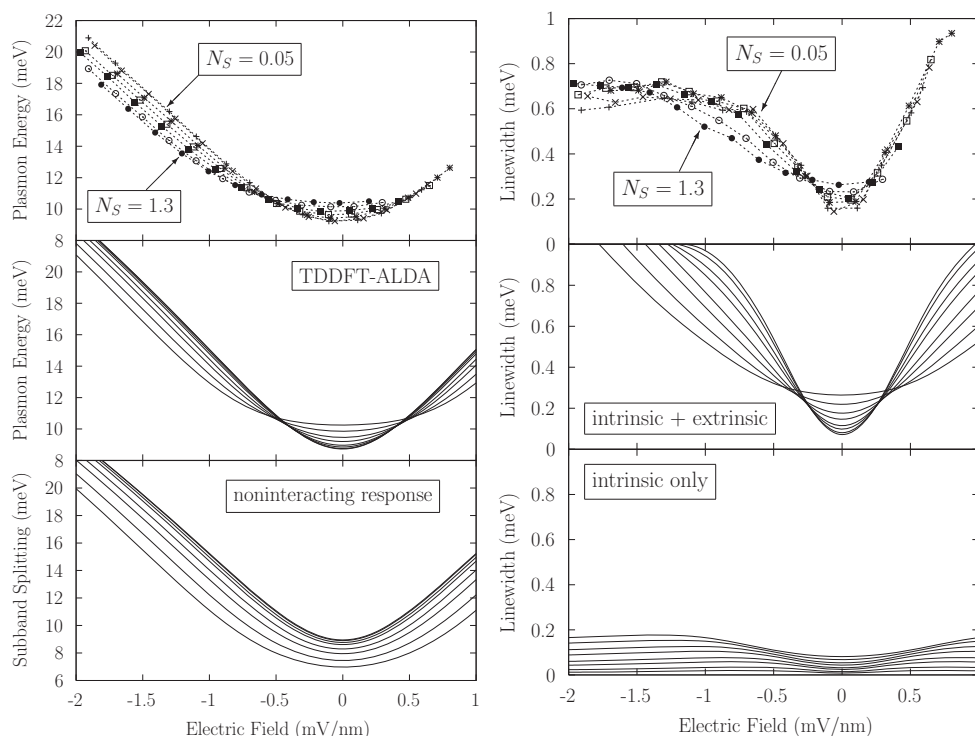
Fig. 10.11 Intersubband plasmon frequencies and linewidths for a 40 nm GaAs/AlGaAs quantum well with N_s between 0.05 and 1.3×10^{11} cm^{-2}. A static electric field "tilts" the quantum well and pushes the electrons more towards the quantum well edge. [Adapted with permission from APS from Ullrich and Vignale (2002), ©2002.]

field, the plasmon frequency Ω exhibits a quadratic Stark effect, but only TDDFT describes correctly the crossing of the Ω-curves for different values of N_s. The bottom right panel of Fig. 10.11 shows the intrinsic plasmon linewidth due to the nonadiabatic xc effects discussed above. We see that these effects make a nonnegligible contribution (up to 30% of the experimental linewidth, for large N_s and small field). Good agreement with experiment is achieved through including the dominant contribution of interface roughness scattering.

10.6   Memory effects: elasticity and dissipation

So far, we have discussed nonadiabatic xc effects in TDCDFT mainly in the frequency-dependent linear-response regime. As we have seen, these effects cause shifts of the excitation energies (which we attributed to the elasticity of the electron liquid) and damping of the excitations (due to the viscosity). We shall now move over to the real-time domain, which will clarify our understanding of several open questions:

- How do nonadiabatic xc effects manifest themselves in the time domain, in particular, what are the signatures of elasticity and viscosity in the xc potential?
- Where does the energy go that is dissipated owing to the electronic viscosity?
- How does the transition from finite to extended systems take place?

10.6.1 A simple exercise: the classical damped harmonic oscillator

Dissipation is, of course, also present in classical mechanics. As a warm-up exercise, it is very helpful to take a look at the classical damped harmonic oscillator. What interests us here in particular is when and how the various kinds of forces act during the (quasi-)periodic motion of the oscillator. The equation of motion of the damped harmonic oscillator is

$$m\frac{\partial^2 x}{\partial t^2} + \lambda\frac{\partial x}{\partial t} + kx = 0 \,, \tag{10.74}$$

with a spring constant k and a damping parameter λ. There is a nice, clean separation between elastic and dissipative effects: the former are related to the restoring force $F_E = -kx$ of the spring, described by Hooke's law, and the latter are related to a velocity-dependent damping force $F_D = -\lambda(\partial x/\partial t)$. Let us introduce $\omega_0^2 = k/m$ as the frequency of the undamped oscillator, and define $\gamma = \lambda/2m$. In the underdamped case ($\gamma < \omega_0$), the motion is periodic with an exponentially decreasing amplitude:

$$x(t) = e^{-\gamma t}A\cos(\omega t - \phi) \,, \qquad \omega = \sqrt{\omega_0^2 - \gamma^2} \,, \tag{10.75}$$

where the amplitude A and phase ϕ are defined via the initial conditions.

Figure 10.12 illustrates the free motion of a very weakly damped classical oscillator (setting $\phi = 0$), whose initial amplitude A essentially remains unchanged during the two cycles that are shown. The position of the point mass and the elastic and damping forces are given by

$$x(t) \sim \cos(\omega t) \,, \tag{10.76}$$

$$F_E(t) \sim -\cos(\omega t) = \cos(\omega t + \pi) \,, \tag{10.77}$$

$$F_D(t) \sim \sin(\omega t) = \cos(\omega t + \pi/2) \,. \tag{10.78}$$

From this example, we can draw the following conclusions, which remain valid for general elastic/dissipative systems:

The elastic and dissipative forces both lag behind the motion of system, and are distinguished by their characteristic phase shifts.
The elastic forces are in opposition to the instantaneous out-of-equilibrium displacement. They lag behind by a half-cycle, i.e., they are phase-shifted by π.
The dissipative forces are in opposition to the instantaneous velocity. They lag behind the position of the system by a quarter-cycle, or a phase shift of $\pi/2$.
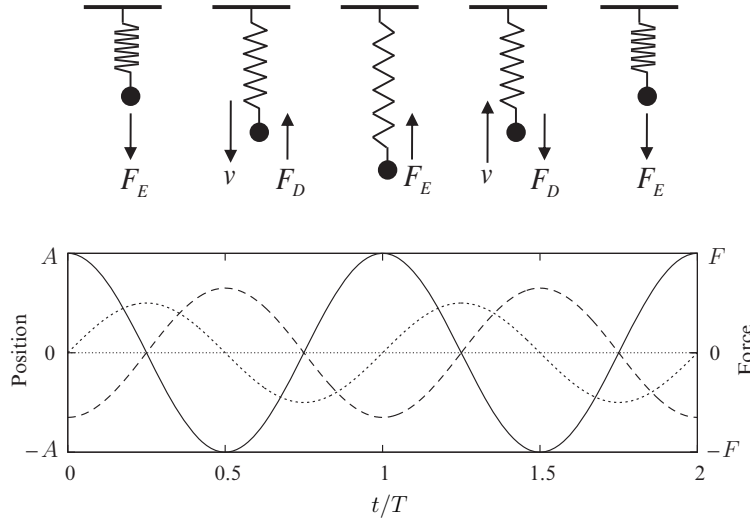
Fig. 10.12 Free motion of a classical, weakly damped harmonic oscillator with nearly constant amplitude. Top: position, velocity, and forces during one cycle. Bottom: position (full line), elastic force (dashed line), and damping force (dotted line), as a function of time. The damping force is not drawn to scale; it is assumed to be much smaller than the elastic force.

10.6.2 The VK functional in the time domain

The VK functional can be transformed into the time domain and applied beyond the linear response (Vignale *et al.*, 1997; Wijewardane and Ullrich, 2005; Ullrich and Tokatly, 2006). As we will see, this leads to an xc potential with memory effects explicitly built in. In this subsection, we will study its properties.

The linearized, frequency-dependent vector potential of eqn (10.51) can be transformed into the following time-dependent expression:

$$\frac{\partial}{\partial t} A_{\mathrm{xc},\mu}^{\mathrm{VK}}(\mathbf{r}, t) = -\nabla_\mu v_{\mathrm{xc}}^{\mathrm{ALDA}}(\mathbf{r}, t) + \frac{1}{n(\mathbf{r}, t)} \sum_\nu \nabla_\nu \sigma_{\mathrm{xc},\mu\nu}(\mathbf{r}, t) \,, \tag{10.79}$$

where the time-dependent xc stress tensor is given by

$$\sigma_{\mathrm{xc},\mu\nu}(\mathbf{r}, t) = \int_{-\infty}^t dt' \left\{ \eta_{\mathrm{xc}}(\mathbf{r}, t, t') \left[\nabla_\nu u_\mu(\mathbf{r}, t') + \nabla_\mu u_\nu(\mathbf{r}, t') - \frac{2}{3} \nabla \cdot \mathbf{u}(\mathbf{r}, t') \delta_{\mu\nu} \right] \right.$$
$$\left. + \zeta_{\mathrm{xc}}(\mathbf{r}, t, t') \nabla \cdot \mathbf{u}(\mathbf{r}, t') \delta_{\mu\nu} \right\}. \tag{10.80}$$

The viscosity coefficients in eqn (10.80) are defined as the following Fourier transforms:

$$\eta_{\mathrm{xc}}(\mathbf{r}, t, t') = \int \frac{d\omega}{2\pi} \; \eta_{\mathrm{xc}}(\bar{n}, \omega) e^{-i\omega(t-t')} \Big|_{\bar{n}=n(\mathbf{r}, t)} \tag{10.81}$$

and similarly for $\zeta_{\mathrm{xc}}(\mathbf{r}, t, t')$.

Notice that we are now no longer in the linear-response regime. In other words, the velocity $\mathbf{u}(\mathbf{r}, t)$ itself can be large, but we still assume that its spatial gradients are small. We will give a more detailed discussion of the derivation and range of validity of eqn (10.79) in Appendix L.

The form of the nonlinear xc vector potential (10.79) is dictated by a number of rather general requirements. For instance, it is still the case that the xc force density follows from a symmetric stress tensor, which ensures that Newton's third law is satisfied. Furthermore, the expression needs to reduce to the proper VK form (10.51) in the linear regime, and should be valid up to second order in the spatial derivatives. This also resolves the apparent ambiguity of whether $\eta_{\mathrm{xc}}(\mathbf{r}, t, t')$ should be evaluated at $n(\mathbf{r}, t)$ or $n(\mathbf{r}, t')$: the difference is of higher order in the gradients.

In Appendix J, we show how to construct the xc scalar potential from the vector potential for a quasi-one-dimensional system such as a quantum well (which has a spatial dependence only in one direction, say z, and is uniform along the other two directions). Let us now use the same technique to derive the time-dependent scalar xc potential that corresponds to $A_{\mathrm{xc},\mu}^{\mathrm{VK}}(z, t)$. We obtain

$$v_{\mathrm{xc}}^{\mathrm{VK}}(z, t) = v_{\mathrm{xc}}^{\mathrm{ALDA}}(z, t) + v_{\mathrm{xc}}^{\mathrm{M}}(z, t) \,, \tag{10.82}$$

where the nonadiabatic contribution (the "M" stands for memory) is given by

$$v_{\mathrm{xc}}^{\mathrm{M}}(z, t) = -\int_{-\infty}^{z} \frac{dz'}{n(z', t)} \nabla_{z'} \int_{-\infty}^{t} dt' \, Y\Big(n(z', t), t - t'\Big) \nabla_{z'} u_{z'}(z', t') \,. \tag{10.83}$$

Assuming that the system starts out from its ground state at t_0, the lower limit of the time integration in eqn (10.83) can be replaced by t_0, since the velocity is zero prior to that. The memory kernel Y is defined as

$$Y(n, t - t') = \frac{4}{3} \eta_{\mathrm{xc}}(n, t - t') + \zeta_{\mathrm{xc}}(n, t - t') \,. \tag{10.84}$$

It can be expressed in the following alternative form:

$$Y(n, t - t') = \frac{4}{3} \mu_{\mathrm{xc}} - \frac{n^2}{\pi} \int \frac{d\omega}{\omega} \Im f_{\mathrm{xc}}^{L}(n, \omega) \cos[\omega(t - t')] \,, \tag{10.85}$$

which is obtained using the Kramers–Kronig relations for the xc kernel and contour integration in the complex ω-plane. The xc shear modulus μ_{xc} is defined in eqn (8.54).

The short-time behavior $(t - t' \to 0)$ of the memory kernel is of particular interest, since it governs the high-frequency dynamics. From the Kramers–Kronig relation (8.39) we have

$$\int \frac{d\omega}{\pi} \frac{\Im f_{\mathrm{xc}}^{L}(\omega)}{\omega} = \Re f_{\mathrm{xc}}^{L}(0) - f_{\mathrm{xc}}^{L}(\infty) \,, \tag{10.86}$$

so that

$$Y(n, 0) = n^2 \left(f_{\mathrm{xc}}^{L}(\infty) - \frac{d^2 e_{\mathrm{xc}}^{h}}{dn^2} \right) . \tag{10.87}$$

The infinite-frequency limit of f_{xc}^{L} is given in eqn (8.43). We also immediately see from eqn (10.85) that
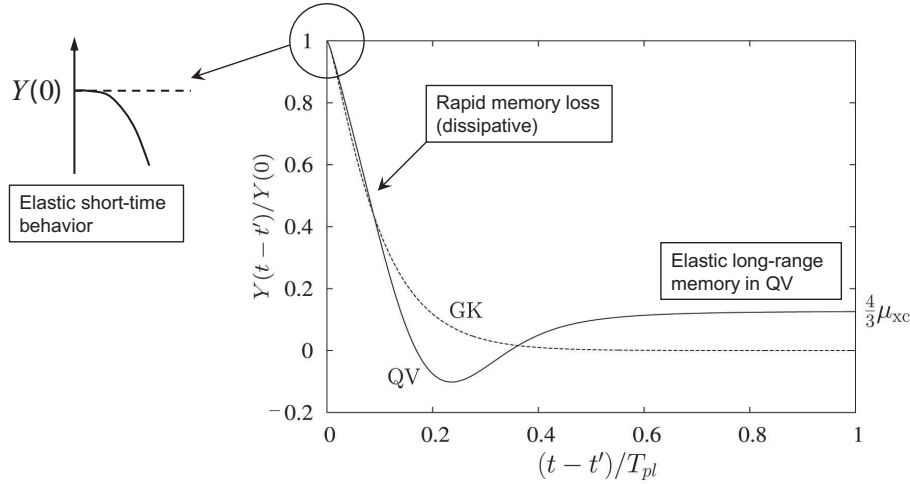
Fig. 10.13 Scaled memory kernel $Y(n, t - t')$ for $r_s = 3$ in the GK and QV parametrizations.

$$\left. \frac{d}{dt} Y(n, t - t') \right|_{t - t' \to 0} = 0 \,. \tag{10.88}$$

Figure 10.13 shows the memory kernel $Y(n, t - t')$ at $r_s = 3$, evaluated with the GK and QV parametrizations for $f_{xc}^L(\omega)$, and scaled by the short-time limit $Y(n, 0)$. Here, $T_{pl} = 2\pi/\omega_{pl}$ is the characteristic timescale associated with the plasma frequency $\omega_{pl} = \sqrt{4\pi n}$. Looking at eqn (10.83), we see that $Y(n, t - t')$ is not defined for $t - t' < 0$. The kernel at $t - t' = 0$ accounts for the dependence on the instantaneous velocity gradients, and for positive $t - t'$ it decides how the xc potential depends on prior velocity gradients. Going to the right in Fig. 10.13 thus means going more and more deeply into the past.

We can distinguish three different regimes of the memory kernel:

1. *Short times.* For $t - t' \to 0$, the memory kernel approaches its limiting value $Y(n, 0)$ with zero slope [see eqn (10.88)], which is schematically illustrated in Fig. 10.13. This indicates an elastic behavior of the short-term memory of the electron liquid, which makes sense: short times correspond to the high-frequency regime, for which the dynamics of any liquid—quantum or classical—becomes purely elastic. The two parametrizations Y^{GK} and Y^{QV} are identical at $t = t'$ and have a similar short-time behavior, since both satisfy the correct high-frequency limit (8.45) for $f_{xc}^L(\omega)$.

2. *Intermediate times.* After the very short initial phase, the memory kernel rapidly decreases, which can be interpreted as a loss of memory of the electron liquid—in other words, dissipation. This dissipative phase takes place within about half a plasma cycle for a large range of values of r_s. Since $T_{pl} \sim n^{-1/2}$, this means that a system with a higher electron density forgets more rapidly.

3. *Long times.* Y^{GK} goes exponentially to zero for large $t - t'$, and thus has no long-term memory at all. On the other hand, Y^{QV} passes through a minimum around
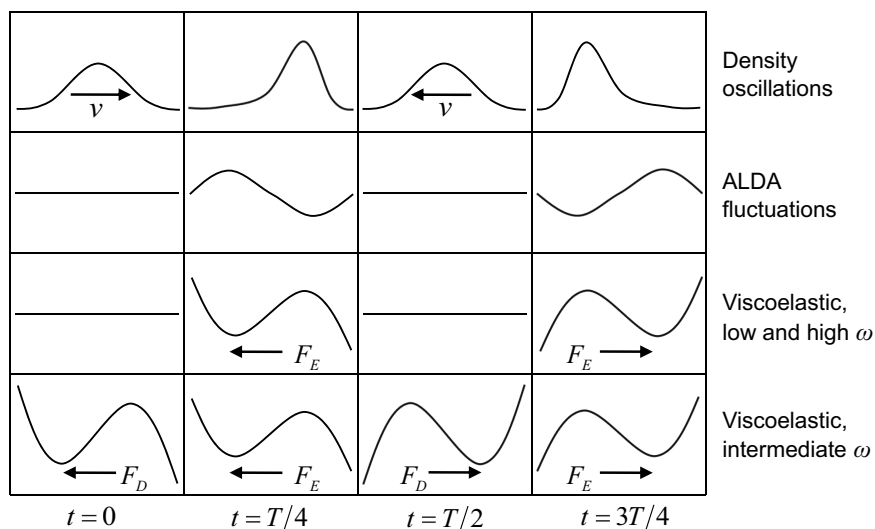
Fig. 10.14 Snapshots of the time-dependent VK potential during one cycle of a given charge-density oscillation (top row). Second row: ALDA fluctuations, $v_{\mathrm{xc}}^{\mathrm{ALDA}}(t) - v_{\mathrm{xc}}^{\mathrm{LDA}}$. Third and fourth row: the viscoelastic, memory-dependent part $v_{\mathrm{xc}}^{\mathrm{M}}(t)$ at low and high frequencies (purely elastic) and at intermediate frequencies (elastic and dissipative).

$0.22 T_{pl}$ and then approaches a finite limit $4\mu_{\mathrm{xc}}/3$, where $\mu_{\mathrm{xc}} \to 0$ for large r_s.[13] This is due to the finite xc shear modulus of the electron liquid in the static limit. At much larger times $(t - t' \gg T_{pl})$, intrinsic collision mechanisms will set in with a characteristic relaxation time τ, driving the system towards thermodynamic equilibrium (see Section 8.3.2), and the memory kernel will eventually go to zero. However, such large timescales are not relevant to the present problem.

In the general case of a time-dependent process, the electron dynamics may cover a broad range of the frequency spectrum, which means that the elastic and dissipative memory effects of all regions of the memory kernel can play a role. To test the behavior of the memory-dependent xc potential, it is therefore advantageous to consider the case where the system oscillates with a fixed frequency. In this manner, one can clearly distinguish between the different regimes.

This is schematically illustrated in Fig. 10.14, which shows snapshots of a given oscillating density during one cycle of the oscillation, and the xc potentials that are produced by it. At times $t = 0$ and $T/2$, the density passes through the equilibrium position at maximum velocity. At times $t = T/4$ and $3T/4$, the density is at the turning points and is at rest there for a split second.

---

[13]Around the minimum, Y^{QV} briefly passes through negative values, which indicates a softening of the elastic contribution caused by this part of the memory. On the other hand, the dissipative behavior is reversed when the slope of Y^{QV} is rising. This part of the memory causes a driving force (which, however, is vastly dominated by the dissipation from those parts where the slope is negative).

The other panels of Fig. 10.14 show the various components of the xc potential. In the second row, we have the ALDA fluctuations, i.e., the difference $v_{xc}^{ALDA}(t) - v_{xc}^{LDA}$. The ALDA depends on the instantaneous density only, and is thus in sync with the charge-density oscillations. There is no difference whether the oscillations are fast or slow; the ALDA always behaves in the same way.

In contrast, the viscoelastic potential $v_{xc}^{M}(t)$ depends strongly on how fast the density is oscillating. In the low- and high-frequency regimes, the electron dynamics is purely elastic, and v_{xc}^{M} exerts an elastic restoring force that is largest when the oscillation is at the turning points. There is no contribution as the density passes through the equilibrium position.

At intermediate frequencies, on the other hand, dissipative forces are present, which are largest when the density passes through the equilibrium position at maximum velocity. The signature in $v_{xc}^{M}(t)$ is that it builds up a potential barrier that opposes the instantaneous motion of the density.

The conclusion from this example is therefore that the elastic and dissipative components of the VK potential can be distinguished by their phase shifts relative to the motion of the density, just as for a classical damped harmonic oscillator: elastic contributions lag behind by π, and viscous contributions are phase-shifted by $\pi/2$. This argument works for any time dependence of the density (not just for periodic oscillations), since the dynamics can always be represented as a superposition of oscillations at different frequencies and amplitudes.

10.6.3   Dissipation, multiple excitations, and thermodynamic limit

In the preceding subsection, we took a close look at how the VK xc potential works in the time domain, and we saw that its memory dependence gives rise to viscoelastic forces on the moving electrons. To study these effects, we assumed that a time-dependent oscillating density was given, and then simply evaluated the xc potential with it. Now let us go further and see how the electron dynamics is affected when we use the VK xc potential for an actual self-consistent time propagation.

Figure 10.15 shows the dipole oscillations $d(t)$ in a quantum well that is initially in a static electric field, which is suddenly switched off at time $t = 0$. The resulting charge-density oscillations, which correspond to intersubband plasmon dynamics in the quantum well (see Appendix K, in particular Fig. K.5), were obtained from the TDKS equation using the ALDA or the VK potential (in the QV parametrization). We compare two cases: a weak initial field (0.01 mV/nm) and a stronger field (0.5 mV/nm).

In the weak-field case, the ALDA gives charge-density oscillations with a constant amplitude, $d(t) = d_0 \cos(\omega t)$, whereas the VK potential leads to an exponential decay of the amplitude, $d(t) = d_0 e^{-\Gamma t} \cos(\omega t)$. The rate of decay Γ is the linewidth of the excitation (HWHM), which we discussed in Section 10.5.2.

In the strong-field case, the dynamics is much richer: the ALDA gives an oscillation pattern that arises from a superposition of the lowest and higher intersubband plasmons. Owing to their larger velocity, the higher-frequency spectral components in $d(t)$ are more rapidly damped for the VK potential, so that the dipole oscillations soon become smooth.
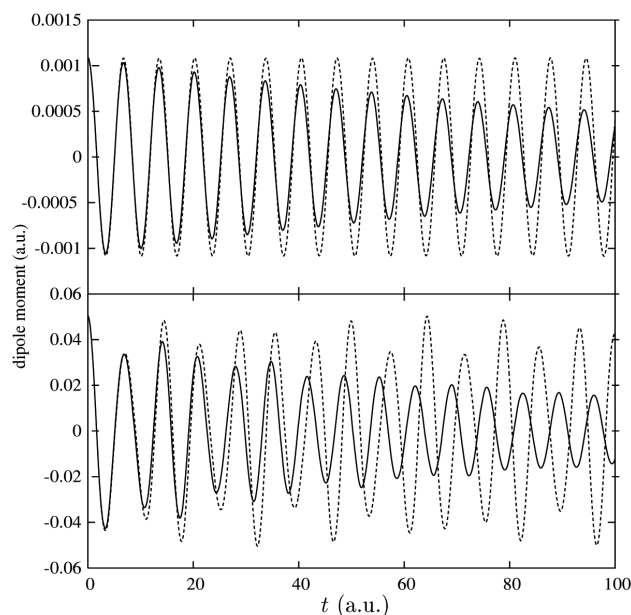
Fig. 10.15 Dipole moment $d(t)$ of a 40 nm GaAs/AlGaAs quantum well with $N_s = 10^{11}$ cm^{-2}. The well is initially in a uniform electric field of 0.01 mV/nm (top) and 0.5 mV/nm (bottom), which is abruptly switched off at $t = 0$. Dashed lines: ALDA. Solid lines: VK. [Reproduced with permission from APS from Wijewardane and Ullrich (2005), ©2005.]

Let us now come to the underlying physical mechanism which causes the damping in the VK theory. The key point is the following:

> The VK functional of TDCDFT uses viscosity coefficients η_{xc} and ζ_{xc} that are derived from a homogeneous reference system as input; in other words, any interacting inhomogeneous electronic system—finite or extended—is treated locally as if it were a weakly modulated homogeneous electron liquid. But a homogeneous, infinite reference system has a continuous spectrum of excitations, which acts as a reservoir that provides intrinsic dissipation channels into which an excitation of the inhomogeneous system can decay.

Later, in Section 12.2, we will discuss plasmon modes in bulk metals in more detail. It will turn out that there are collective plasmon modes and incoherent single particle–hole excitations. The decay of a plasmon into single-particle excitations is called Landau damping, and is already included in the ALDA and any other adiabatic approach. The damping due to the electronic viscosity is caused by decay of an excitation into multiple particle–hole excitations: these are beyond the adiabatic approximation.

We now discuss one last example to illustrate nonadiabatic effects in TD(C)DFT. The system is very simple: two interacting electrons in a two-dimensional rectangular area (a so-called quantum strip) with a given width (10 a.u.) and a variable length,
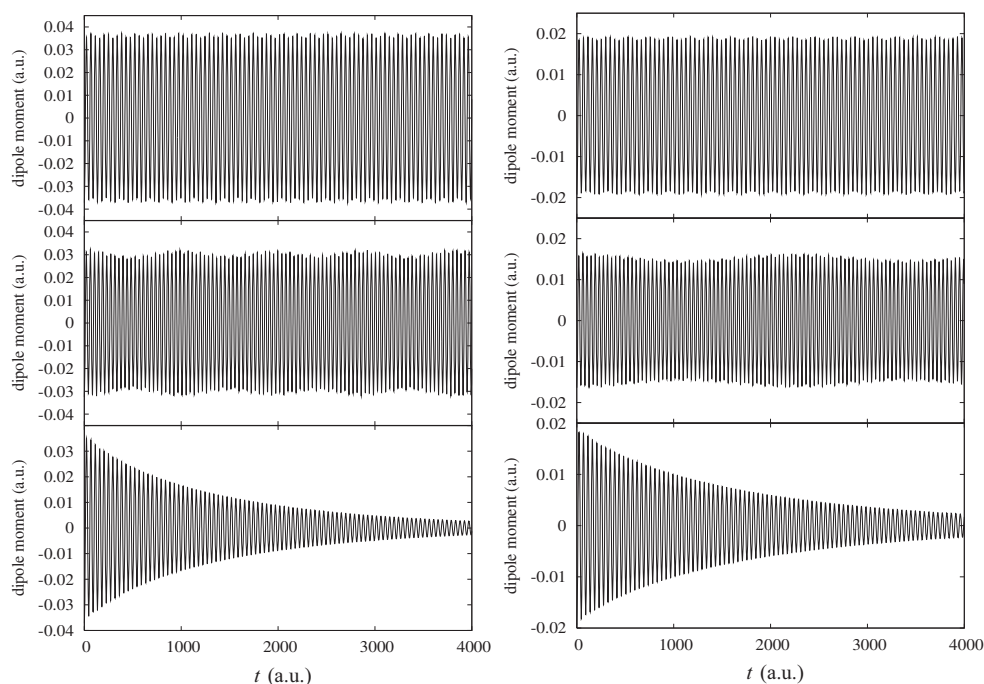
Fig. 10.16 Time-dependent dipole moment associated with charge-density oscillations of two interacting electrons in a quantum strip of width 10 a.u. and length 50 a.u. (left) and 100 a.u. (right). Top panels: ALDA. Middle panels: exact calculation. Bottom panels: VK. [Adapted with permission from AIP from Ullrich (2006), ©2006.]

$L = 50$ a.u. or 100 a.u. We use hard-wall boundary conditions across the strip (z-direction), and periodic boundary conditions along the strip (x-direction). The density is therefore uniform along x, but quantum-confined along z. We now consider free charge-density oscillations along the z-direction, triggered by a uniform electric field that is suddenly switched off at $t = 0$. The density remains uniform along the length of the strip during these oscillations.

The system is simple enough to permit a fully numerical solution of the two-electron time-dependent Schrödinger equation; the results are shown in the middle panels in Fig. 10.16. We propagate for a long time, and see many oscillations. But what is particularly interesting to see is that the amplitude of the oscillations is modulated. A detailed analysis of the spectral composition shows (Ullrich, 2006) that these modulations are due to the presence of *doubly excited states*. It is therefore not surprising that these beating patterns are absent in an ALDA calculation (top panels), since an adiabatic xc functional can only describe single excitations, as we have discussed at length in Section 9.3.

How could the exact xc potential manage to reproduce the modulated charge-density oscillations? The exact $v_{xc}(t)$ would have to act in such a way that the amplitude of the oscillations is periodically suppressed and enhanced. In other words, the

oscillations are periodically damped and then driven back to their previous condition—the exact xc potential alternates between being dissipative and elastic.

How does the VK functional perform? As expected: the charge-density oscillations in the quantum strip are exponentially damped, which is of course wrong for a finite system. The VK functional dissipates in an irreversible manner[14] and cannot drive the system back to where it was before, which would be needed to reproduce the modulations.

But we now make another interesting observation: the period of the amplitude modulations increases when the quantum strip becomes longer. It is therefore natural to think of what will happen in the thermodynamic limit, where we make the strip longer and longer, but keep adding electrons such that the charge density does not change. Under these conditions, the period of the amplitude modulations, known as the *recurrence time*, will keep growing until, at infinite length and particle number, the recurrence time will also be infinite. This means that the amplitude keeps decreasing and doesn't come back—which is precisely what the VK functional predicts. This leads us to the following conclusion:

> The VK functional becomes physically correct in the thermodynamic limit of an extended system, provided that the conditions (10.58)–(10.60) are satisfied for the ground state and the excitation under consideration. The intrinsic damping of collective excitations, which arises through interference with a continuum of (multiple) excitations, will then be quantitatively correctly described.

Exercise 10.1 Show that the torque due to the Hartree force $\mathbf{F}_H$ vanishes (see Section 10.3.3).

Exercise 10.2 Prove the relation (10.25) between the noninteracting density–density and current–current response functions.

Exercise 10.3 Verify the steps leading from eqn (10.43) to eqn (10.44), which is the fluid-dynamical form of the linearized xc vector potential for homogeneous systems.

Exercise 10.4 Show that the VK functional satisfies the harmonic potential theorem. Hint: go back to Section 6.3.2 and determine the velocity field associated with the time-dependent density $n(\mathbf{r}, t)$ of eqn (6.45).

Exercise 10.5 Consider the classical harmonic oscillator described by the equation of motion (10.75). But now, instead of the damping-force term $\lambda \, \partial x / \partial t$, which depends on the instantaneous velocity, introduce a memory-dependent term as follows:

$$m\frac{\partial^2 x}{\partial t^2} - \int_0^t dt' \, Y_{\mathrm{cl}}(t - t')\frac{\partial x}{\partial t'} + kx = 0 \,. \tag{10.89}$$

---

[14]The irreversibility of the energy dissipation of the VK functional, and the increase in entropy that goes along with it, was demonstrated by D'Agosta and Vignale (2006).

The classical memory kernel $Y_{\rm cl}(t - t')$ describes how the system depends on its previous velocities. Try out the following two cases:

(a) Infinite memory: $Y_{\rm cl}(t - t') = \beta$, where β is a constant. What difference does it make whether β is positive or negative?

(b) Exponential memory loss: $Y_{\rm cl}(t - t') = \beta e^{-\lambda(t - t')}$, where λ is a positive constant.

In each case assume β to be small, so that $x(t) = A \cos(\omega t)$ with an almost constant amplitude during several cycles. Then plug $x(t)$ into the memory term, evaluate the time integral analytically, and discuss elastic and dissipative effects.

If you wish to explore further, you can try your hand at more complicated memory kernels similar to the QV kernel shown in Fig. 10.13, which have different types of short- and long-range memory. You may have to evaluate the resulting memory integral numerically.

A full time propagation of the oscillator equation (10.89) with various forms of $Y_{\rm cl}(t - t')$ would make a nice computational project. You could also extend the model to a system of two coupled oscillators with different spring constants but similar damping terms; this would give you a simple model for the nonlinear dynamics shown in the bottom panel of Fig. 10.15.

Exercise 10.6 Convince yourself that a complex excitation energy $\Omega - i\Gamma$, where $\Gamma > 0$, corresponds to a line shape with a Lorentzian profile and HWHM Γ, i.e., a spectral signal proportional to $[(\omega - \Omega)^2 + \Gamma^2]^{-1}$. A simple way to see this is via eqns (7.47) and (7.48).

Exercise 10.7 Consider the zero-frequency limits of the real parts of the viscosity coefficients (10.47) and (10.48). Using results from Chapter 8, show that $\Re\eta_{\rm xc}(0)$ is finite, but $\Re\zeta_{\rm xc}(0)$ vanishes.

Exercise 10.8 The so-called STLS scheme (Singwi *et al.*, 1968; Giuliani and Vignale, 2005) was originally developed as a self-consistent approach to calculating correlation energies in homogeneous electronic systems. It was recently generalized to inhomogeneous systems (Dobson *et al.*, 2002). In the linear-response regime, the inhomogeneous STLS scheme leads to the following expression for the tensor xc kernel (Dobson, 2009):

$$f_{{\rm xc},\mu\nu}^{\rm STLS}(\mathbf{r}, \mathbf{r}', \omega) = -\frac{1}{\omega^2}[g_0(\mathbf{r}, \mathbf{r}') - 1]\nabla_\mu \frac{1}{|\mathbf{r} - \mathbf{r}'|}\nabla'_\nu \,, \tag{10.90}$$

where $g_0(\mathbf{r}, \mathbf{r}')$ is the ground-state pair correlation function, defined in analogy to eqn (C.13). In the full STLS scheme, g_0 is obtained self-consistently via the adiabatic-connection fluctuation–dissipation theorem (see Section 14.1). Notice that this tensor xc kernel has a long spatial range, but a trivial frequency dependence.

In the exchange-only limit, the STLS kernel takes on the following form, which strongly resembles the scalar PGG kernel, eqn (11.67):

$$f_{{\rm x},\mu\nu}^{\rm STLS}(\mathbf{r}, \mathbf{r}', \omega) = \frac{2}{\omega^2} \frac{\left|\sum_{k=1}^{\rm occ} \varphi_k^0(\mathbf{r})\varphi_k^{0*}(\mathbf{r}')\right|^2}{n_0(\mathbf{r})n_0(\mathbf{r}')} \nabla_\mu \frac{1}{|\mathbf{r} - \mathbf{r}'|}\nabla'_\nu \,. \tag{10.91}$$

Compare the x-only STLS and PGG kernels for a 1D system, using the techniques of Appendix J to transform between the scalar and tensor kernels. You will find that the correspondence is not perfect, because of the way the ∇_μ operator is positioned in eqn (10.91). What happens in the case of a two-electron spin-singlet system (e.g., the helium atom)?

The x-only limit of the STLS kernel for a two-electron spin-singlet system can also be obtained directly from eqn (10.90). For this, you need to show that the noninteracting pair correlation function (assuming a single Slater determinant) is given by $g_0(\mathbf{r}, \mathbf{r}') = 1/2$.

11

The time-dependent optimized effective potential

The most important challenge in static and time-dependent DFT is the construction of good approximations to the xc potential. We know from the basic theorems that the xc potentials are formally defined as functionals of the density, and we indicate this by writing $v_{\mathrm{xc}}^0[n_0](\mathbf{r})$ in DFT and $v_{\mathrm{xc}}[n](\mathbf{r}, t)$ in TDDFT. A large number of widely used approximations, such as the LDA and GGA, are constructed as explicit functionals of the density and its gradients, and we have considered many examples and applications.

In this chapter, we shall deal with a new class of xc potentials, which are defined as *implicit* density functionals but *explicit* orbital functionals; we will explain below what we mean by "implicit" versus "explicit." The construction of these functionals proceeds via the optimized-effective-potential (OEP) method.[1]

The static OEP method has a long history (Sharp and Horton, 1953; Talman and Shadwick, 1976; Krieger *et al.*, 1992a) and is the subject of several reviews (Grabo *et al.*, 2000; Engel, 2003; Baerends and Gritsenko, 2005; Görling, 2005; Kümmel and Kronik, 2008). The time-dependent generalization (TDOEP) is of more recent origin (Ullrich *et al.*, 1995b) and has gained considerable popularity in the linear-response regime lately.

The basics and applications of the OEP and TDOEP will be discussed in this chapter. There are many formal and practical reasons why this is worth our effort:

- Developing approximate xc energy functionals in terms of the orbitals, rather than the density, allows greater flexibility. To construct the associated Kohn–Sham potentials one can use the (TD)OEP method, thus bringing orbital functionals formally under the umbrella of (TD)DFT.
- The (TD)OEP allows us to give a precise definition of what we mean by *exact exchange* in (TD)DFT, and how this differs from (TD)HF theory. In fact, the large majority of applications of the (TD)OEP are in the exact-exchange limit.
- In practice, the (TD)OEP can be used to construct xc potentials that have many desirable properties, such as the correct asymptotic behavior or the discontinuity with respect to a change in the total particle number. A variety of applications take advantage of these properties, often with excellent results.
- We shall see later, in Chapter 13, that the (TD)OEP can be viewed in the context of many-body perturbation theory. This will give us important formal insights.

---

[1] The OEP approach has occasionally been called the optimized-potential method (or model) (OPM) in the older literature, but this abbreviation is no longer much in use.

11.1 The static OEP approach for orbital functionals

11.1.1 Explicit versus implicit density functionals

The static Kohn–Sham scheme in spin-resolved form was defined in eqns (2.41)–(2.44). For any approximate form of the xc energy $E_{\text{xc}}[n_{0\uparrow}, n_{0\downarrow}]$ that is given as an explicit functional form of the spin densities $n_{0\sigma}$, such as the LSDA (2.83), we can directly evaluate the functional derivative in eqn (2.44) and thus construct the xc potential.

Since the Kohn–Sham effective potential $v_{s\sigma}^0$ is a functional of the spin densities, the Kohn–Sham orbitals $\varphi_{j\sigma}^0(\mathbf{r})$ become a functional of the densities as well, and we can make this clear by writing them as $\varphi_{j\sigma}^0[n_{0\sigma}](\mathbf{r})$. This functional dependence is an *implicit* one: by this, we mean that one cannot write down a closed functional form of the orbitals in which the spin densities $n_{0\sigma}$ appear explicitly.[2] Instead, the functional dependence of the $\varphi_{j\sigma}^0[n_{0\sigma}](\mathbf{r})$ is defined in an operational sense, via the *procedure* of solving the Kohn–Sham equation featuring a density-dependent effective potential.

Since the orbitals are density functionals if they come from a Kohn–Sham equation, any xc functional that is built from these orbitals, or orbital densities $n_{j\sigma}^0 = |\varphi_{j\sigma}^0|^2$, automatically becomes a density functional as well, albeit an implicit one. In other words, we can write the xc energy (or any other density functional) as

$$E_{\text{xc}}[n_{0\sigma}] = E_{\text{xc}}\left[\{\varphi_{j\sigma}^0[n_{0\sigma}]\}\right] = E_{\text{xc}}\left[\{\varphi_{j\sigma}^0\}\right] , \tag{11.1}$$

where the curly brackets in $E_{\text{xc}}\left[\{\varphi_{j\sigma}^0\}\right]$ indicate dependence on a set of orbitals.

Since we have

$$n_{0\sigma}(\mathbf{r}) = \sum_{j=1}^{N_\sigma} n_{j\sigma}^0(\mathbf{r}) = \sum_{j=1}^{N_\sigma} |\varphi_{j\sigma}^0|^2 , \tag{11.2}$$

every explicit density functional can trivially be written as an explicit orbital functional. But, vice versa, an orbital functional can *not* always be written as an explicit density functional. This is most prominently the case for the exact exchange energy given in eqn (2.51), which we here repeat for convenience:

$$E_{\text{x}}^{\text{exact}}[\{\varphi_{j\sigma}^0\}] = -\frac{1}{2} \sum_\sigma \sum_{i,j=1}^{N_\sigma} \int d^3r \int d^3r' \, \frac{\varphi_{i\sigma}^{0*}(\mathbf{r}')\varphi_{j\sigma}^0(\mathbf{r}')\varphi_{i\sigma}^0(\mathbf{r})\varphi_{j\sigma}^{0*}(\mathbf{r})}{|\mathbf{r} - \mathbf{r}'|} . \tag{11.3}$$

Another example is the SIC for an approximate xc energy functional [see eqn (2.107)]:

$$\begin{aligned} E_{\text{xc}}^{\text{SIC}}[\{n_{j\sigma}^0\}] = {} & E_{\text{xc}}^{\text{app}}[n_{0\uparrow}, n_{0\downarrow}] \\ & - \sum_j \left(E_{\text{H}}[n_{j\uparrow}^0] + E_{\text{xc}}^{\text{app}}[n_{j\uparrow}^0, 0]\right) - \sum_j \left(E_{\text{H}}[n_{j\downarrow}^0] + E_{\text{xc}}^{\text{app}}[0, n_{j\downarrow}^0]\right) . \end{aligned} \tag{11.4}$$

Further examples can be found on the third and higher rungs of the ladder of approximations shown in Fig. 2.7.

There are two "traditional" ways to deal with these and other orbital-dependent xc energy functionals. The first is to use them in a non-self-consistent manner. This means

---

[2]The only exception is for systems with one or two electrons, where $\varphi_{1\sigma}^0[n_{0\sigma}](\mathbf{r}) = \sqrt{n_{0\sigma}(\mathbf{r})}$, assuming the spin orbitals to be real.

that one obtains a set of single-particle orbitals using some other method (for instance, the LDA or GGA), and then simply inserts them into the orbital-dependent xc energy functionals. This is the usual way in which meta- and hyper-GGAs are implemented.

The second option is to carry out a variation with respect to the orbitals, rather than the density, which leads to single-particle equations different from the Kohn–Sham equations: in the case of $E_{\mathrm{x}}^{\mathrm{exact}}$ one arrives at the HF scheme with a nonlocal exchange potential (see Appendix D), and in the case of $E_{\mathrm{xc}}^{\mathrm{SIC}}$ one finds a set of single-particle equations with a local but state-dependent xc potential (Perdew and Zunger, 1981).

Neither of these two methods is a DFT approach in the proper sense. As we shall now discuss, the OEP method is the formally correct way to treat orbital functionals within the realm of DFT.

11.1.2   The OEP integral equation

First derivation.   Let us assume we have an xc energy functional that is an explicit orbital functional. The associated Kohn–Sham xc potential is formally obtained from the functional derivative

$$v_{\mathrm{xc}\sigma}^0(\mathbf{r}) = \frac{\delta E_{\mathrm{xc}}[\{\varphi_{j\sigma}^0\}]}{\delta n_{0\sigma}(\mathbf{r})} \ . \tag{11.5}$$

At this point we don't know how to evaluate this functional derivative directly, but we can make use of the chain rule:

$$v_{\mathrm{xc}\sigma}^0(\mathbf{r}) = \sum_{\sigma'} \sum_{j'=1}^{N_{\sigma'}} \int d^3r' \left\{ \frac{\delta E_{\mathrm{xc}}[\{\varphi_{j\sigma}^0\}]}{\delta \varphi_{j'\sigma'}^0(\mathbf{r}')} \frac{\delta \varphi_{j'\sigma'}^0(\mathbf{r}')}{\delta n_{0\sigma}(\mathbf{r})} + \frac{\delta E_{\mathrm{xc}}[\{\varphi_{j\sigma}^0\}]}{\delta \varphi_{j'\sigma'}^{0*}(\mathbf{r}')} \frac{\delta \varphi_{j'\sigma'}^{0*}(\mathbf{r}')}{\delta n_{0\sigma}(\mathbf{r})} \right\} \ . \tag{11.6}$$

At least we now have a functional derivative of the xc energy which we *do* know how to evaluate, and we define the (generally complex) state-dependent potential $\mathcal{V}_{\mathrm{xc}j\sigma}^0(\mathbf{r})$:

$$\mathcal{V}_{\mathrm{xc}j\sigma}^0(\mathbf{r}) = \frac{1}{\varphi_{j\sigma}^{0*}(\mathbf{r})} \frac{\delta E_{\mathrm{xc}}[\{\varphi_{j\sigma}^0\}]}{\delta \varphi_{j\sigma}^0(\mathbf{r})} \ . \tag{11.7}$$

This leaves us with another functional derivative under the integral in eqn (11.6) to deal with, and we invoke the chain rule again:

$$v_{\mathrm{xc}\sigma}^0(\mathbf{r}) = \sum_{\sigma'\sigma''} \sum_{j'=1}^{N_{\sigma'}} \int d^3r' \int d^3r'' \, \varphi_{j'\sigma'}^{0*}(\mathbf{r}') \mathcal{V}_{\mathrm{xc}j'\sigma'}^0(\mathbf{r}') \frac{\delta \varphi_{j'\sigma'}^0(\mathbf{r}')}{\delta v_{s\sigma''}^0(\mathbf{r}'')} \frac{\delta v_{s\sigma''}^0(\mathbf{r}'')}{\delta n_{0\sigma}(\mathbf{r})} + \text{c.c.} \tag{11.8}$$

The last derivative on the right-hand side can be brought over to the other side:

$$\sum_{\sigma'} \int d^3r' \, v_{\mathrm{xc}\sigma'}^0(\mathbf{r}') \frac{\delta n_{0\sigma'}(\mathbf{r}')}{\delta v_{s\sigma}^0(\mathbf{r})} = \sum_{\sigma'} \sum_{j'=1}^{N_{\sigma'}} \int d^3r' \, \varphi_{j'\sigma'}^{0*}(\mathbf{r}') \mathcal{V}_{\mathrm{xc}j'\sigma'}^0(\mathbf{r}') \frac{\delta \varphi_{j'\sigma'}^0(\mathbf{r}')}{\delta v_{s\sigma}^0(\mathbf{r})} + \text{c.c.} \tag{11.9}$$

We identify the static response function of the Kohn–Sham system,

$$\chi_{s,\sigma'\sigma}(\mathbf{r}',\mathbf{r}) = \frac{\delta n_{0\sigma'}(\mathbf{r}')}{\delta v_{s\sigma}^0(\mathbf{r})} = \delta_{\sigma\sigma'} \sum_{j'=1}^{N_{\sigma'}} \sum_{\substack{j=1 \\ j\neq j'}}^{\infty} \frac{\varphi_{j\sigma}^0(\mathbf{r}')\varphi_{j'\sigma}^{0*}(\mathbf{r}')\varphi_{j\sigma}^{0*}(\mathbf{r})\varphi_{j'\sigma}^0(\mathbf{r})}{\varepsilon_{j'\sigma} - \varepsilon_{j\sigma}} + \text{c.c.} \tag{11.10}$$

[this expression follows directly from eqn (7.86)], and from nondegenerate first-order perturbation theory we have

$$\frac{\delta\varphi^0_{j'\sigma'}(\mathbf{r}')}{\delta v^0_{s\sigma}(\mathbf{r})} = \delta_{\sigma\sigma'}\sum_{\substack{j=1\\j\neq j'}}^{\infty}\frac{\varphi^0_{j\sigma}(\mathbf{r}')\varphi^{0*}_{j\sigma}(\mathbf{r})\varphi^0_{j'\sigma}(\mathbf{r})}{\varepsilon_{j'\sigma} - \varepsilon_{j\sigma}}\,. \tag{11.11}$$

Inserting eqns (11.10) and (11.11) into eqn (11.9) gives

$$\sum_{j=1}^{N_\sigma}\int d^3r'\left[v^0_{\text{xc}\sigma}(\mathbf{r}') - \mathcal{V}^0_{\text{xc}j\sigma}(\mathbf{r}')\right]\varphi^0_{j\sigma}(\mathbf{r})\varphi^{0*}_{j\sigma}(\mathbf{r}')\sum_{\substack{k=1\\k\neq j}}^{\infty}\frac{\varphi^0_{k\sigma}(\mathbf{r}')\varphi^{0*}_{k\sigma}(\mathbf{r})}{\varepsilon_{j\sigma}-\varepsilon_{k\sigma}} + \text{c.c.} = 0\,. \tag{11.12}$$

This is the OEP equation. Equation (11.12) determines the xc potential $v^0_{\text{xc}\sigma}(\mathbf{r})$ as a functional of the Kohn–Sham orbitals (and, thus, as an implicit density functional) via solution of an integral equation. We shall discuss its properties below.

Second derivation. Before we go into the properties of the OEP integral equation, it is instructive to show an alternative way of deriving it. The idea is to minimize the total energy of the system with respect to variations in the effective potential:

$$\frac{\delta E[\{\varphi^0_{j\sigma}\}]}{\delta v^0_{s\sigma}(\mathbf{r})} = 0\,. \tag{11.13}$$

Here, $E[\{\varphi^0_{j\sigma}\}]$ is the total energy [see eqn (2.30)], written as an orbital functional. We again employ the chain rule,

$$\sum_{\sigma'}\sum_{j'=1}^{N_{\sigma'}}\int d^3r'\frac{\delta E[\{\varphi^0_{j\sigma}\}]}{\delta\varphi^0_{j'\sigma'}(\mathbf{r}')}\frac{\delta\varphi^0_{j'\sigma'}(\mathbf{r}')}{\delta v^0_{s\sigma}(\mathbf{r})} + \text{c.c.} = 0\,, \tag{11.14}$$

plus the fact that the orbitals satisfy the static Kohn–Sham equation

$$\left[-\frac{\nabla^2}{2} + v^0_{s\sigma}(\mathbf{r})\right]\varphi^0_{j\sigma}(\mathbf{r}) = \varepsilon_{j\sigma}\varphi^0_{j\sigma}(\mathbf{r})\,. \tag{11.15}$$

After a few straightforward steps, which will be left as an exercise, the OEP integral equation (11.12) emerges.

Historically, this was the way in which the OEP equation was first derived (Talman and Shadwick, 1976; Krieger *et al.*, 1992*a*). It also explains the name: the total energy is minimized by a set of orbitals $\{\varphi^0_{j\sigma}(\mathbf{r})\}$ under the additional constraint that the orbitals come from a single-particle equation featuring a common *local* optimized effective potential $v^0_{s\sigma}(\mathbf{r})$.[3]

The derivations of the OEP equation which we have discussed here assume that the ground state is nondegenerate. Generalizing the OEP to degenerate ground states is quite straightforward (Krieger *et al.*, 1992*a*).

---

[3]An *unconstrained* minimization of the energy with respect to the orbitals leads, in general, to a nonlocal and/or state-dependent effective potential, such as in HF theory.

11.1.3 Properties of the OEP

The OEP integral equation (11.12) for $v_{\text{xc}\sigma}^0(\mathbf{r})$ cannot be solved analytically, except for the trivial case of one- or two-electron systems, where only a single orbital is occupied for each spin. We will later consider some approximate solutions, but for now let us consider some of the exact properties of the OEP equation.

First of all, there are two rather obvious properties, which are both very easy to verify. The first is that eqn (11.12) determines the xc potential only to within an overall additive constant. In other words, if $v_{\text{xc}\sigma}^0(\mathbf{r})$ is a solution, then so is $v_{\text{xc}\sigma}^0(\mathbf{r}) + C_\sigma$. How should we choose C_σ? We'll come to it in a minute when we discuss asymptotics.

The other "easy" property is that if E_{xc} is an explicit density functional, rather than an orbital functional, we immediately obtain $v_{\text{xc}\sigma}^0(\mathbf{r}) = \delta E_{\text{xc}}[n_0]/\delta n_0(\mathbf{r})$, as expected. This follows trivially, since in this case $\mathcal{V}_{\text{xc}j\sigma}^0(\mathbf{r}) = \delta E_{\text{xc}}[n_0]/\delta n_0(\mathbf{r})$, independent of j.

Now we come to the more interesting properties of the OEP. We will skip the detailed proofs here (Krieger *et al.*, 1992*a*; Grabo *et al.*, 2000) and just list the results.

Asymptotic behavior. For finite systems, the orbitals decay exponentially for $r \to \infty$, where the exponent depends on the orbital eigenvalue. The highest occupied orbital, $\varphi_{N_\sigma\sigma}^0$, is therefore the one that decays most slowly,[4] which means that there is an "outer region" in space where it dominates over all other orbitals $\varphi_{j\sigma}^0$ with $j < N_\sigma$. We can then dramatically simplify the OEP equation (11.12) and obtain

$$v_{\text{xc}\sigma}^0(\mathbf{r}) = \mathcal{V}_{\text{xc}N_\sigma\sigma}^0(\mathbf{r}) + \left(\bar{v}_{\text{xc}N_\sigma\sigma}^0 - \bar{\mathcal{V}}_{\text{xc}N_\sigma\sigma}^0\right), \qquad r \to \infty. \tag{11.16}$$

Here, we introduce the notation

$$\bar{v}_{\text{xc}p\sigma}^0 = \int d^3r \, \varphi_{p\sigma}^*(\mathbf{r}) v_{\text{xc}\sigma}^0(\mathbf{r}) \varphi_{p\sigma}^0(\mathbf{r}) \tag{11.17}$$

for the average of the xc potential over the $(p\sigma)$ orbital, and similarly for $\bar{\mathcal{V}}_{\text{xc}p\sigma}^0$ [in eqn (11.16), we have $p = N_\sigma$].

The xc potential should vanish asymptotically as $-1/r$, as we discussed in Section 2.2.1. It turns out that all $\mathcal{V}_{\text{xc}N_\sigma\sigma}^0(\mathbf{r})$ of practical interest share this property. Thus, we choose the constant C_σ such that $v_{\text{xc}\sigma}^0(\mathbf{r}) = 0$ for $r \to \infty$, which implies

$$\bar{v}_{\text{xc}N_\sigma\sigma}^0 = \bar{\mathcal{V}}_{\text{xc}N_\sigma\sigma}^0. \tag{11.18}$$

We therefore have $v_{\text{xc}\sigma}^0(\mathbf{r}) = \mathcal{V}_{\text{xc}N_\sigma\sigma}^0(\mathbf{r})$ for $r \to \infty$, which in particular means

$$v_{\text{x}\sigma}^0(\mathbf{r}) \longrightarrow -\frac{1}{r}, \qquad r \to \infty, \tag{11.19}$$

for the exact-exchange case.

---

[4]There is a subtle issue for open-shell systems where the highest occupied orbital has a nodal surface. It turns out that along the nodal surface, the xc potential can approach a different asymptotic value, which is determined by the second-highest occupied orbital (Della Sala and Görling, 2002; Kümmel and Kronik, 2008).
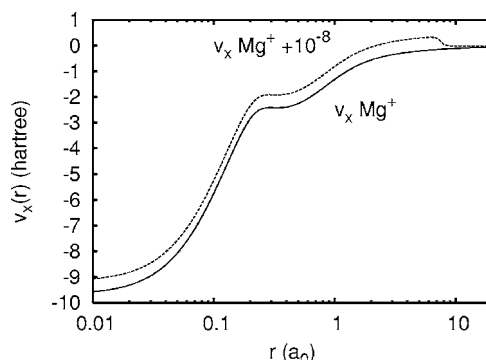
Fig. 11.1 Discontinuity in the OEP exact exchange potential for the Mg^+ ion. A discontinuity in the potential develops if a very small fractional charge is added. [Adapted with permission from APS from Kümmel and Kronik (2008), ©2008.]

Koopmans theorem.   The solutions of the OEP scheme satisfy the Koopmans theorem:

$$\varepsilon_{N_\sigma\sigma} = E^0(N) - E_u^0(N-1) \,, \tag{11.20}$$

where $\varepsilon_{N_\sigma\sigma}$ is the highest occupied orbital eigenvalue of spin σ, $E^0(N)$ is the OEP ground-state energy of the N-electron system, and $E_u^0(N-1)$ is the unrelaxed ground-state energy of the $(N-1)$-electron system (which means that it is obtained by evaluating it with the OEP eigenfunctions of the N-electron system). This property follows from eqn (11.18) (Krieger *et al.*, 1992*a*).

Discontinuity.   In Section 2.2.3, we discussed the fact that the exact xc potential has a very interesting property: if the particle number N of a finite system is allowed to be a continuous variable, then the xc potential jumps by a constant whenever N passes through an integer. Another way of putting this is to say that the xc energy has a derivative discontinuity Δ_{xc} [see eqn (2.65)]. This plays an important role in the DFT definition of the band gap in a solid.

The OEP is an ideal method to construct xc potentials that have a discontinuity upon change of particle number (Krieger *et al.*, 1992*a*), and it is easy to see why. Again, the key is eqn (11.18). Let us consider the x-only case for a total particle number $N+f$, where $f \ll 1$, which means that we assume that the orbital with $j = N_\sigma + 1$ is now occupied by a very small fraction f of an electron. No matter how small f is, there exists an "outer" region with $r > R$ where the newly occupied orbital dominates over all other orbitals, and the asymptotic behavior changes from the $-1/r$ form of eqn (11.19) to

$$v_{\mathrm{x}\sigma}^0(\mathbf{r}; N_\sigma + f) \longrightarrow -\frac{f}{r} \,, \qquad r \to \infty \,. \tag{11.21}$$

As long as $f \ll 1$, the inner orbitals (up to $j = N_\sigma$) don't care that the $(N_\sigma + 1)$ orbital is occupied by a tiny bit of charge, and the OEP equation (11.12) gives the same result for the xc potential for $r < R$, up to a constant. But the way we determine this adjustable constant has now changed!

This is nicely illustrated in Fig. 11.1, which shows the OEP exact exchange potential for the magnesium cation (Kümmel and Kronik, 2008). If a fractional charge with $f = 10^{-8}$ is added, the newly occupied orbital starts to dominate the asymptotics around $R = 7$ a.u. For $r < R$, the exchange potential jumps by a constant, and at $r = 7$ a.u. a step develops. As $f \to 0$, this step moves further and further out to infinity, which indicates the true discontinuity limit.

11.1.4   The KLI approximation and related schemes

There exist several schemes for obtaining an approximate solution of eqn (11.12), which have contributed much to the popularity of the OEP. Let us begin with the approximation of Krieger, Li, and Iafrate (KLI) (Krieger *et al.*, 1992*a*). The key idea is quite simple, namely, to replace the energy differences $\varepsilon_{j\sigma} - \varepsilon_{k\sigma}$ in eqn (11.12) by some average value $\Delta\varepsilon$:

$$\sum_{j=1}^{N_\sigma} \int d^3r' \left[v_{\mathrm{xc}\sigma}^{\mathrm{KLI}}(\mathbf{r}') - \mathcal{V}_{\mathrm{xc}j\sigma}^0(\mathbf{r}') \right] \varphi_{j\sigma}^0(\mathbf{r}) \varphi_{j\sigma}^{0*}(\mathbf{r}') \sum_{\substack{k=1 \\ k \neq j}}^{\infty} \frac{\varphi_{k\sigma}^0(\mathbf{r}') \varphi_{k\sigma}^{0*}(\mathbf{r})}{\Delta\varepsilon} + \mathrm{c.c.} = 0 \,. \quad (11.22)$$

The $\Delta\varepsilon$ can be pulled in front of all the summations and simply cancels out. We can now make use of the closure relation for the single-particle orbitals, which leads to

$$\sum_{\substack{k=1 \\ k \neq j}}^{\infty} \varphi_{k\sigma}^0(\mathbf{r}') \varphi_{k\sigma}^{0*}(\mathbf{r}) = \delta(\mathbf{r} - \mathbf{r}') - \varphi_{j\sigma}^0(\mathbf{r}') \varphi_{j\sigma}^{0*}(\mathbf{r}) \,. \quad (11.23)$$

Substituting this into eqn (11.22) gives the following formula after a few simple steps:

$$v_{\mathrm{xc}\sigma}^{\mathrm{KLI}}(\mathbf{r}) = \frac{1}{2n_\sigma(\mathbf{r})} \sum_{j=1}^{N_\sigma} n_{j\sigma}(\mathbf{r}) \left[\mathcal{V}_{\mathrm{xc}j\sigma}^0(\mathbf{r}) + (\bar{v}_{\mathrm{xc}j\sigma}^{\mathrm{KLI}} - \bar{\mathcal{V}}_{\mathrm{xc}j\sigma}^0) \right] + \mathrm{c.c.} \quad (11.24)$$

This certainly looks much simpler than the original OEP equation (11.12)! A particularly nice feature is that we have managed to get rid of the summation over unoccupied orbitals, and that we now have an expression where the xc potential shows up explicitly on the left-hand side.

As it stands, eqn (11.24) still contains the orbital averages $\bar{v}_{\mathrm{xc}j\sigma}^{\mathrm{KLI}}$ [see eqn (11.17)] on the right-hand side, so we are still formally dealing with an integral equation. But, fortunately, this integral equation can be solved relatively easily (Krieger *et al.*, 1992*a*); working out the details will be the subject of Exercise 11.4. As a result, we obtain an explicit xc functional of the orbitals which can be implemented in a straightforward manner.

A further simplification can be achieved if the orbital-dependent constants in eqn (11.24) are dropped. We then obtain

$$v_{\mathrm{xc}\sigma}^{\mathrm{Slater}}(\mathbf{r}) = \frac{1}{2n_\sigma(\mathbf{r})} \sum_{j=1}^{N_\sigma} n_{j\sigma}(\mathbf{r}) \left[\mathcal{V}_{\mathrm{xc}j\sigma}^0(\mathbf{r}) + \mathcal{V}_{\mathrm{xc}j\sigma}^{0*}(\mathbf{r}) \right] \,. \quad (11.25)$$

For historical reasons, we call the expression (11.25) the Slater approximation, since it was first proposed by Slater (1951) as a local approximation to the HF exchange potential.

The KLI and Slater potentials are the most widely used approximations to the OEP. They share several important exact properties with the exact OEP: for instance, both $v_{\mathrm{xc}\sigma}^{\mathrm{KLI}}$ and $v_{\mathrm{xc}\sigma}^{\mathrm{Slater}}$ are determined to within an arbitrary constant C_σ, and they have the same asymptotic behavior as the OEP potential, namely, they approach $\mathcal{V}_{\mathrm{xc}N_\sigma\sigma}^0(\mathbf{r})$ as $r \to \infty$. For the exact-exchange case, this means that the KLI and Slater potentials approach $-1/r$ asymptotically. Furthermore, the KLI potential (but not the Slater potential) satisfies the Koopmans theorem and has a discontinuity as the total number of particles passes through an integer.

The KLI and Slater potentials are by no means the only approximations available in the literature, but they are certainly the most widely used ones. We should mention here the common-energy-denominator approximation (Gritsenko and Baerends, 2001), which is equivalent to the so-called localized HF approximation (Della Sala and Görling, 2001); both are slightly more accurate than the KLI potential. On the other hand, $v_{\mathrm{xc}\sigma}^{\mathrm{Slater}}$ can be simplified even further by a "global" averaging method (GAM),

$$v_{\mathrm{xc}\sigma}^{\mathrm{GAM}}(\mathbf{r}) = \frac{1}{2N_\sigma} \sum_{j=1}^{N_\sigma} \left[\mathcal{V}_{\mathrm{xc}j\sigma}^0(\mathbf{r}) + \mathcal{V}_{\mathrm{xc}j\sigma}^{0*}(\mathbf{r}) \right]. \tag{11.26}$$

The GAM, in spite of being a very crude approximation to the OEP,[5] has the correct asymptotic behavior, and can be useful for the description of highly excited states and ionization processes (Ullrich *et al.*, 2000).

11.1.5 Exact-exchange DFT versus HF theory

Let us pause for a moment and consider the meaning of exchange and correlation in DFT. Recall that in Chapter 2 we defined the xc energy in eqn (2.32) as that part of the total energy of an interacting many-body system which is not contained in the sum of the noninteracting kinetic energy, the interaction energy with the external potential, and the classical Coulomb energy. Hence, on a fundamental level there is no logical necessity to consider exchange and correlation as two separate, additive contributions to $E_{\mathrm{xc}}[n]$ or $v_{\mathrm{xc}}^0[n]$. What we call "exchange" and what we mean by "correlation" is a matter of convention, at least to a certain extent.[6]

When we speak of "exact-exchange DFT", we generally mean the x-only OEP. However, the *exact* DFT exchange energy is defined as $E_{\mathrm{x}}^{\mathrm{exact}}[\{\varphi_{j\sigma}^{0,\mathrm{exact}}\}]$, evaluated with the self-consistent orbitals coming from the *exact* local Kohn-Sham potential. Notice that this is not quite the same as the x-only OEP exchange energy, which is evaluated with the x-only OEP orbitals; the difference, however, is usually extremely small. The exact DFT exchange energy is different from the HF exchange energy, $E_{\mathrm{x}}^{\mathrm{exact}}[\{\varphi_{j\sigma}^{\mathrm{HF}}\}]$. HF and x-only DFT have the same orbital functional for the total energy, but the HF ground-state energy is lower:

$$E_{v_0}^{\mathrm{HF}}[\{\varphi_{j\sigma}^{\mathrm{HF}}\}] \le E_{v_0}^{\mathrm{HF}}[\{\varphi_{j\sigma}^0\}]. \tag{11.27}$$

---

[5]For instance, the GAM is not size-consistent, owing to its explicit dependence on N_σ. Size-consistency here means that if a system has the form of two well-separated subsystems, then the energy of the total system should be the sum of the energies of the individual subsystems.

[6]There is no ambiguity about exchange and correlation in the definition of the LDA, since the exchange energy of a homogeneous electron liquid of constant density n is defined via the HF theory.

Table 11.1 Atomic total energies (in a.u.) in various x-only schemes (Krieger *et al.*, 1992*a*). The HF energy is always lower than the energy obtained from the OEP; the KLI potential is an excellent approximation to the OEP.

	$-E_{\mathrm{HF}}$	$E_{\mathrm{OEP}} - E_{\mathrm{HF}}$	$E_{\mathrm{KLI}} - E_{\mathrm{OEP}}$	$E_{\mathrm{Slater}} - E_{\mathrm{EOP}}$	$E_{\mathrm{LSDA}} - E_{\mathrm{OEP}}$
Be	14.5730	0.0006	0.0002	0.0111	0.0044
Ne	128.5471	0.0017	0.0006	0.0447	0.0179
Mg	199.6146	0.0030	0.0009	0.0786	0.0143
Ar	526.8175	0.0053	0.0017	0.1092	0.0172
Ca	676.7582	0.0063	0.0022	0.1458	0.0161
Kr	2752.0550	0.0121	0.0032	0.2870	0.0322

Table 11.2 Absolute values in eV of the highest-occupied-orbital energies ε_{N_σ} for some closed-shell atoms, calculated in various x-only schemes (Krieger *et al.*, 1992*a*).

	HF	OEP	KLI	Slater	LSDA
Be	8.415	8.414	8.404	8.883	4.627
Ne	23.141	23.149	23.114	24.817	12.056
Mg	6.886	6.885	6.868	7.729	3.868
Ar	16.082	16.075	16.036	17.365	9.083
Ca	5.321	5.322	5.308	6.110	3.030
Kr	14.264	14.256	14.204	15.439	8.159

This is because the HF orbitals minimize the energy in an unconstrained variation, leading to a nonlocal potential. In the OEP, by contrast, the minimization takes place under the constraint that the effective potential is *local*. This also defines the exact correlation energy in DFT: $E_{\mathrm{c}}^{\mathrm{exact}}$ is the exact total energy minus $E_{\mathrm{x}}^{\mathrm{exact}}[\{\varphi_{j\sigma}^{0,\mathrm{exact}}\}]$. This definition differs from the traditional definition in quantum chemistry, where the correlation energy denotes all contributions to the total energy beyond the HF theory.

The results obtained with exact-exchange DFT and HF theory are often numerically very close. This is illustrated in Tables 11.1 and 11.2 for several closed-shell atoms. The OEP total ground-state energy is always greater than the HF energy, but the difference is of the order of parts per million. We also see that the KLI potential is an excellent approximation to the full OEP. The Slater potential (11.25), on the other hand, is much less accurate than the LSDA when it comes to total energies, but it delivers much better orbital eigenvalues.

Figure 11.2 shows the exchange potential for the Ne atom, and indeed the KLI potential and the OEP are hardly distinguishable. Both show a characteristic bump between the atomic shells (which is missing in the LSDA), and have the correct asymptotic behavior. The Slater potential turns out to be too deep, which is another typical
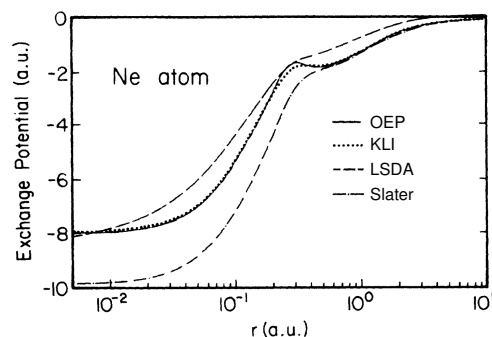
Fig. 11.2 Exact OEP exchange potential and various approximations for the Neon atom. [Adapted with permission from APS from Krieger *et al.* (1992*a*), ©1992.]

observation and consistent with the orbital eigenvalues shown in Table 11.2.

The HF theory and the x-only OEP share an important property, namely, they are self-interaction-free, at least as far as all the occupied levels are concerned. To see this, consider the OEP exact-exchange potential for the case where there is only a single occupied orbital. We have

$$
\mathcal{V}_{\mathrm{x}j\sigma}^0(\mathbf{r}) = -\frac{1}{\varphi_{j\sigma}^{0*}(\mathbf{r})} \sum_{k=1}^{N_\sigma} \int d^3r' \, \frac{\varphi_{j\sigma}^{0*}(\mathbf{r}')\varphi_{k\sigma}^0(\mathbf{r}')\varphi_{k\sigma}^{0*}(\mathbf{r})}{|\mathbf{r} - \mathbf{r}'|} \; . \tag{11.28}
$$

For $N_\sigma = 1$, is easy to see that

$$
v_{\mathrm{x}\sigma}^0(\mathbf{r}) = -\int d^3r' \, \frac{n_\sigma(\mathbf{r}')}{|\mathbf{r} - \mathbf{r}'|} \; , \tag{11.29}
$$

which cancels out the self-interaction part of the Hartree potential. In this particular case, the KLI, Slater, and GAM potential give identical results.

There is an important difference between the HF theory and the OEP when it comes to the description of unoccupied single-particle states. In Kohn–Sham theory, all orbitals—no matter whether they are occupied or unoccupied—feel the *same* effective potential. In the exact-exchange OEP, this means that *all* orbitals are subject to an exchange potential that goes as $-1/r$ for large r. This suggests the interpretation that the OEP virtual orbitals can be viewed as excited electrons interacting with $(N-1)$ remaining electrons. The OEP is thus an excellent starting point for calculating excitation energies (see Chapter 9) and, in particular, highly excited Rydberg states will be bound. Furthermore, the OEP yields good band-gap energies in solids (Städele *et al.*, 1997, 1998).

By contrast, the HF exchange potential only has the correct long-range asymptotic behavior for the *occupied* states, and drops off exponentially for virtual orbitals. As a consequence, the HF potential supports only a few bound unoccupied states, and is therefore a much poorer starting point for calculating excitation energies. A physical interpretation is that the HF LUMO orbital energy corresponds approximately to the addition energy of an extra electron in the field of the other N electrons, and is thus

Table 11.3 Static axial polarizabilities (in a.u.) for hydrogen chains of various lengths (Kümmel *et al.*, 2004; Körzdörfer *et al.*, 2008).

	H_4	H_6	H_8	H_{12}
LDA	37.6	72.7	114.6	210.5
HF	32.0	56.4	82.3	137.6
OEP x-only	32.2	56.6	84.2	138.1
KLI x-only	33.1	60.2	90.6	156.3
OEP–SIC	30.6	48.7	80.1	129.8
KLI–SIC	19.4	60.3	98.2	193.6
MP4	29.5	51.6	75.9	126.9

more like an electron affinity than an energy of an excited electron. This explains why Kohn–Sham orbital energy differences are usually much better approximations to excitation energies than HF energy eigenvalue differences, as we have seen in Chapter 9.

11.1.6 Applications

The ground-state OEP and its various approximations have been extensively tested for atomic and (mostly small) molecular systems. Most of the applications have been carried out in the x-only limit (Talman and Shadwick, 1976; Krieger *et al.*, 1992*a*), but there are also OEP studies with LSDA–SIC functionals (Norman and Koelling, 1984) and with x-only plus orbital-dependent correlation functionals (Engel, 2003). We will just go over a few highlights here; a more detailed overview of the applications of the OEP was given by Kümmel and Kronik (2008).

A common observation in all applications to small atomic and molecular systems is that the KLI approximation is very close to the full OEP. We have noticed this already in Table 11.1 for total atomic energies and in Table 11.2 for the highest-occupied-orbital eigenvalues. However, as one goes over to more extended systems, this may no longer necessarily be true. Take, for example, the static polarizabilities of chain-like molecules (Kümmel *et al.*, 2004; Körzdörfer *et al.*, 2008). As shown in Table 11.3, the LDA tends to overestimate the polarizability of extended molecules; we have already noticed this fact in Section 10.5, and found there that TDCDFT in the static limit can give excellent results for π-conjugated polymers, but performs less well for H chains.

We now find that we can get excellent polarizabilities for H chains using the OEP. In the x-only case, the OEP and HF results essentially agree, and come within less than 10% of the MP4 results. A further improvement is achieved using the OEP–SIC functional. However, in both cases the corresponding KLI results deviate significantly from those obtained with the OEP, which typically tends to overestimate the polarizabilities (albeit not as much as the LDA does).

Figure 11.3 shows (using the example of an H_8 chain) that both the OEP and the KLI exchange potential oppose an externally applied electric field along the molecular axis; this is not the case with the LDA.
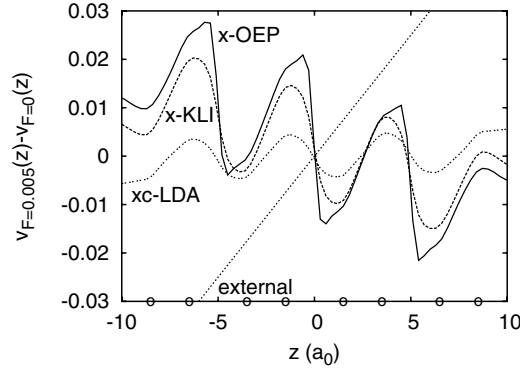
Fig. 11.3 Differences in $v_{\mathrm{x}}^{\mathrm{OEP}}$, $v_{\mathrm{x}}^{\mathrm{KLI}}$, and $v_{\mathrm{xc}}^{\mathrm{LDA}}$ with and without an external electric field applied along the axial direction of an H_8 chain. The OEP and the KLI potential produce a field-counteracting effect, which is absent in the case of the LDA. [Adapted with permission from APS from Kümmel *et al.* (2004), ©2004.]

11.2   The TDOEP scheme

11.2.1   Variational principle

In Section 6.6, we discussed the role of the action principle in TDDFT. There, we defined the action functional of the interacting system as

$$
\mathcal{A}[n] = \mathcal{A}_0[n] - \int_{t_0}^{t_1} dt \int d^3r\, n(\mathbf{r},t)v(\mathbf{r},t)
$$

$$
= \mathcal{A}_{0s}[n] - \int_{t_0}^{t_1} dt \int d^3r\, n(\mathbf{r},t)v(\mathbf{r},t) - \mathcal{A}_{\mathrm{H}}[n] - \mathcal{A}_{\mathrm{xc}}[n]\,, \qquad (11.30)
$$

where $\mathcal{A}_{0s}[n]$ and $\mathcal{A}_{\mathrm{H}}[n]$ are defined in eqns (6.73) and (6.76).

Let us now consider a more general, spin-dependent formalism, and assume that the total action is given as a functional of a set of time-dependent Kohn–Sham orbitals:

$$
\mathcal{A}[\{\varphi_{j\sigma}\}] = \sum_{\sigma}\sum_{j=1}^{N_\sigma} \int_{-\infty}^{t_1} dt \int d^3r\, \varphi_{j\sigma}^*(\mathbf{r},t)\left(i\frac{\partial}{\partial t} + \frac{\nabla^2}{2}\right)\varphi_{j\sigma}(\mathbf{r},t)
$$

$$
- \sum_{\sigma} \int_{-\infty}^{t_1} dt \int d^3r\, n_\sigma(\mathbf{r},t)v_\sigma(\mathbf{r},t)
$$

$$
- \frac{1}{2}\int_{-\infty}^{t_1} dt \int d^3r \int d^3r'\, \frac{n(\mathbf{r},t)n(\mathbf{r}',t)}{|\mathbf{r}-\mathbf{r}'|} - \mathcal{A}_{\mathrm{xc}}[\{\varphi_{j\sigma}\}]\,. \qquad (11.31)
$$

Notice that we now take the initial time to be $t_0 = -\infty$, without loss of generality; later we shall consider the specific case where the system is in its ground state until t_0, and from then on evolves under the influence of a time-dependent external potential.[7]

---

[7]A minor technical point: to make the time integration in the action functional (11.31) well defined, one has to introduce a convergence factor $\exp(\eta t)$ into the integrand, and take the limit $\eta \to 0^+$ after the time integration.

We assume that the xc action functional $\mathcal{A}_{\mathrm{xc}}[\{\varphi_{j\sigma}\}]$ is given as an explicit functional of the orbitals. Needless to say, approximations will be required, just as with the xc energy of static DFT. A straightforward procedure is the adiabatic approximation (6.79), which we adapt here for orbital functionals:

$$\mathcal{A}_{\mathrm{xc}}^{\mathrm{A}}[\{\varphi_{j\sigma}\}] = \int_{-\infty}^{t_1} dt\, E_{\mathrm{xc}}[\{\varphi_{j\sigma}^0\}]\Big|_{\{\varphi_{j\sigma}^0(\mathbf{r})\}\to\{\varphi_{j\sigma}(\mathbf{r},t)\}} . \tag{11.32}$$

This automatically generates an xc action functional from any given xc energy functional. An example is the exact-exchange action

$$A_{\mathrm{x}}^{\mathrm{exact}}[\{\varphi_{j\sigma}\}] = -\frac{1}{2}\sum_{\sigma}\sum_{i,j=1}^{N_\sigma}\int_{-\infty}^{t_1} dt \int d^3r \int d^3r'\, \frac{\varphi_{i\sigma}^*(\mathbf{r}',t)\varphi_{j\sigma}(\mathbf{r}',t)\varphi_{i\sigma}(\mathbf{r},t)\varphi_{j\sigma}^*(\mathbf{r},t)}{|\mathbf{r}-\mathbf{r}'|} . \tag{11.33}$$

This exchange action functional leads to the TDHF scheme if the traditional Dirac–Frenkel principle is used, in which the total action is made stationary with respect to variations of the time-dependent orbitals. But here we want to pursue a different avenue, namely, we are looking for a *local* time-dependent xc potential that is associated with an orbital-dependent xc action. This will lead us to the TDOEP scheme.

The very first and most important question is: given the orbital-dependent action, what is the appropriate variational principle? Following reasoning similar to that which led us to eqn (6.67), we obtain

$$\delta\mathcal{A}[\{\varphi_{j\sigma}\}] = i\sum_{j=1}^{N_\sigma}\int d^3r\, \varphi_{j\sigma}^*(\mathbf{r},t_1)\delta\varphi_{j\sigma}(\mathbf{r},t_1) , \tag{11.34}$$

which takes into account the fact that unconstrained density variations at time $t < t_1$ will in general cause a variation of the orbitals at the upper limit t_1. In other words, the action is not stationary. But, as we shall see shortly, the resulting TDOEP formalism will turn out to be perfectly causal.

11.2.2 The TDOEP equation: derivation and properties

In the following, we shall work with the time-dependent version of the static OEP variational principle (11.13). In other words, we wish to determine the local effective potential $v_{s\sigma}(\mathbf{r},t)$ from the following condition:

$$\frac{\delta\mathcal{A}[\{\varphi_{j\sigma}\}]}{\delta v_{s\sigma}(\mathbf{r},t)} = i\sum_{j=1}^{N_\sigma}\int d^3r\, \varphi_{j\sigma}^*(\mathbf{r},t_1)\frac{\delta\varphi_{j\sigma}(\mathbf{r},t_1)}{\delta v_{s\sigma}(\mathbf{r},t)} , \tag{11.35}$$

where the orbitals $\{\varphi_{j\sigma}\}$ are constrained to obey the TDKS equation

$$\left[-\frac{\nabla^2}{2} + v_{s\sigma}(\mathbf{r},t)\right]\varphi_{j\sigma}(\mathbf{r},t) = i\frac{\partial}{\partial t}\,\varphi_{j\sigma}(\mathbf{r},t) . \tag{11.36}$$

Using the chain rule, we obtain from eqn (11.35)

$$\sum_{\sigma'} \sum_{j'=1}^{N_{\sigma'}} \int_{-\infty}^{\infty} dt' \int d^3 r' \left\{ \frac{\delta \mathcal{A}[\{\varphi_{j\sigma}\}]}{\delta \varphi_{j'\sigma'}(\mathbf{r}',t')} \frac{\delta \varphi_{j'\sigma'}(\mathbf{r}',t')}{\delta v_{s\sigma}(\mathbf{r},t)} + \frac{\delta \mathcal{A}[\{\varphi_{j\sigma}\}]}{\delta \varphi_{j'\sigma'}^*(\mathbf{r}',t')} \frac{\delta \varphi_{j'\sigma'}^*(\mathbf{r}',t')}{\delta v_{s\sigma}(\mathbf{r},t)} \right\}$$

$$= i \sum_{j=1}^{N_\sigma} \int d^3 r \, \varphi_{j\sigma}^*(\mathbf{r},t_1) \frac{\delta \varphi_{j\sigma}(\mathbf{r},t_1)}{\delta v_{s\sigma}(\mathbf{r},t)} \,. \tag{11.37}$$

The first thing to do is to calculate the functional derivatives $\delta \mathcal{A}/\delta \varphi_{j\sigma}$ and $\delta \mathcal{A}/\delta \varphi_{j\sigma}^*$, keeping in mind that there is no fixed boundary condition at t_1, i.e., $\delta \varphi_{j\sigma}(t_1) \neq 0$ in general. This plays an important role when integrating by parts.

Defining

$$\mathcal{V}_{\text{xc}j\sigma}(\mathbf{r},t) = \frac{1}{\varphi_{j\sigma}^{0*}(\mathbf{r},t)} \frac{\delta \mathcal{A}_{\text{xc}}[\{\varphi_{j\sigma}\}]}{\delta \varphi_{j\sigma}(\mathbf{r},t)} \,, \tag{11.38}$$

we obtain

$$\frac{\delta \mathcal{A}[\{\varphi_{j\sigma}\}]}{\delta \varphi_{j'\sigma'}^*(\mathbf{r}',t')} = \left[i\frac{\partial}{\partial t'} + \frac{\nabla'^2}{2} - v_{\sigma'}(\mathbf{r}',t') - v_{\text{H}}(\mathbf{r}',t') - \mathcal{V}_{\text{xc}j'\sigma'}^*(\mathbf{r}',t') \right]$$

$$\times \varphi_{j'\sigma'}(\mathbf{r}',t') \, \theta(t_1 - t')$$

$$= \left[v_{\text{xc}\sigma'}(\mathbf{r}',t') - \mathcal{V}_{\text{xc}j'\sigma'}^*(\mathbf{r}',t') \right] \varphi_{j'\sigma'}(\mathbf{r}',t') \, \theta(t_1 - t') \,, \tag{11.39}$$

where we have used the TDKS equation (11.36) in the last step. Similarly, we find

$$\frac{\delta \mathcal{A}[\{\varphi_{j\sigma}\}]}{\delta \varphi_{j'\sigma'}(\mathbf{r}',t')} = \left[v_{\text{xc}\sigma'}(\mathbf{r}',t') - \mathcal{V}_{\text{xc}j'\sigma'}(\mathbf{r}',t') \right] \varphi_{j'\sigma'}^*(\mathbf{r}',t') \, \theta(t_1 - t')$$

$$+ i\varphi_{j'\sigma'}^*(\mathbf{r}',t_1)\delta(t_1 - t') \,, \tag{11.40}$$

where the last term on the right-hand side comes from a partial integration.

Inserting eqns (11.39) and (11.40) into eqn (11.37), we find that the boundary terms cancel out, and we obtain

$$\sum_{\sigma'} \sum_{j'=1}^{N_{\sigma'}} \int_{-\infty}^{t_1} dt' \int d^3 r' \left[v_{\text{xc}\sigma'}(\mathbf{r}',t') - \mathcal{V}_{\text{xc}j'\sigma'}(\mathbf{r}',t') \right] \varphi_{j'\sigma'}^*(\mathbf{r}',t') \frac{\delta \varphi_{j'\sigma'}(\mathbf{r}',t')}{\delta v_{s\sigma}(\mathbf{r},t)} + \text{c.c.} = 0 \,.$$

$$\tag{11.41}$$

The next step is to evaluate the functional derivatives $\delta \varphi_{j'\sigma'}/\delta v_{s\sigma}$ and $\delta \varphi_{j'\sigma'}^*/\delta v_{s\sigma}$. To do this, we consider the $\{\varphi_{j\sigma}\}$ as unperturbed states in the time interval $[-\infty, t_1]$, and consider the TDKS equation (11.36) subject to an additional small time-dependent perturbing potential $\delta v_{s\sigma}(\mathbf{r},t)$:

$$\left[-\frac{\nabla^2}{2} + v_{s\sigma}(\mathbf{r},t) + \delta v_{s\sigma}(\mathbf{r},t) \right] \varphi_{j\sigma}'(\mathbf{r},t) = i\frac{\partial}{\partial t} \, \varphi_{j\sigma}'(\mathbf{r},t) \,. \tag{11.42}$$

This situation is a bit different from the usual time-dependent perturbation theory as it is presented in quantum mechanics textbooks, where one considers stationary systems that are subject to some time-dependent perturbation. Instead, we have here a system that is already explicitly time-dependent, and now feels an *additional* small time-dependent potential.

We expand the perturbed orbitals $\varphi'_{j\sigma}(\mathbf{r}, t)$ in terms of the unperturbed time-dependent Kohn–Sham orbitals, which form a complete set at each given time t:

$$\varphi'_{j\sigma}(\mathbf{r}, t) = \sum_{k=1}^{\infty} c_{jk\sigma}(t)\varphi_{k\sigma}(\mathbf{r}, t) . \tag{11.43}$$

Making the usual ansatz of a perturbation expansion,

$$c_{jk\sigma}(t) = c_{jk\sigma}^{(0)}(t) + c_{jk\sigma}^{(1)}(t) + \dots , \tag{11.44}$$

where the superscripts indicate orders of the perturbation $\delta v_{s\sigma}$, we obtain[8]

$$\frac{\partial}{\partial t} c_{jk\sigma}^{(0)}(t) = 0 , \tag{11.45}$$

$$\frac{\partial}{\partial t} c_{jk\sigma}^{(1)}(t) = \frac{1}{i} \sum_{l=1}^{\infty} c_{jl\sigma}^{(0)}(t) \int d^3r \; \varphi_{k\sigma}^*(\mathbf{r}, t)\delta v_{s\sigma}(\mathbf{r}, t)\varphi_{l\sigma}(\mathbf{r}, t) . \tag{11.46}$$

Now all we need to do is integrate eqn (11.46), and we will have what we need. But there is a very important point to keep in mind, namely, we need to ensure that causality is respected. And to do this, we use the following trick: we start at the *upper* time limit $t = t_1$, where we impose the initial condition $\varphi'_{j\sigma}(\mathbf{r}, t_1) = \varphi_{j\sigma}(\mathbf{r}, t_1)$, and then propagate eqn (11.42) *backwards* in time. In this way, it is ensured that the resulting functional derivatives $\delta\varphi_{j'\sigma'}/\delta v_{s\sigma}$ and $\delta\varphi_{j'\sigma'}^*/\delta v_{s\sigma}$ are causal.

Thus, we have $c_{jl\sigma}^{(0)}(t) = \delta_{jl}$ and $c_{jk\sigma}^{(1)}(t_1) = 0$, and we obtain

$$c_{jk\sigma}^{(1)}(t) = \frac{1}{i} \int_{t_1}^{t} dt' \int d^3r \; \varphi_{k\sigma}^*(\mathbf{r}, t')\delta v_{s\sigma}(\mathbf{r}, t')\varphi_{j\sigma}(\mathbf{r}, t') . \tag{11.47}$$

From this, we obtain the desired functional derivative as

$$\frac{\delta\varphi_{j'\sigma'}(\mathbf{r}', t')}{\delta v_{s\sigma}(\mathbf{r}, t)} = i\delta_{\sigma\sigma'} \sum_{j=1}^{\infty} \varphi_{j\sigma}^*(\mathbf{r}, t)\varphi_{j'\sigma}(\mathbf{r}, t)\varphi_{j\sigma}(\mathbf{r}', t')\theta(t_1 - t)\theta(t - t') , \tag{11.48}$$

and the complex conjugate of this expression for $\delta\varphi_{j'\sigma'}^*/\delta v_{s\sigma}$.

Inserting this into eqn (11.41) gives the final result:

$$i \sum_{j=1}^{N_\sigma} \int_{-\infty}^{t_1} dt' \int d^3r' \left[v_{\mathrm{xc}\sigma}(\mathbf{r}', t') - \mathcal{V}_{\mathrm{xc}j\sigma}(\mathbf{r}', t') \right] \varphi_{j\sigma}(\mathbf{r}, t)\varphi_{j\sigma}^*(\mathbf{r}', t')K_\sigma(\mathbf{r}, t, \mathbf{r}', t')$$
$$+ \text{c.c.} = 0 , \tag{11.49}$$

where the integral kernel K_σ is given by

$$K_\sigma(\mathbf{r}, t, \mathbf{r}', t') = \sum_{k=1}^{\infty} \varphi_{k\sigma}^*(\mathbf{r}, t)\varphi_{k\sigma}(\mathbf{r}', t')\theta(t - t') . \tag{11.50}$$

Equation (11.49) is the TDOEP integral equation, which determines the local time-dependent xc potential associated with an orbital-dependent xc action functional. Let us now discuss some of its properties:

---

[8]Filling in the steps in between will be the subject of Exercise 11.7.

- *Causality.* Compared with the static OEP equation (11.12), we see that the TDOEP involves an additional time integration. Owing to the step function $\theta(t - t')$ that is contained in the kernel $K_\sigma(\mathbf{r}, t, \mathbf{r}', t')$, it is immediately clear that causality is guaranteed, i.e., the xc potential $v_{\mathrm{xc}\sigma}(\mathbf{r}, t)$ depends only on the orbitals at times $t' \le t$; the dependence on the upper time limit t_1 drops out.

- *Memory.* The TDOEP xc potential $v_{\mathrm{xc}\sigma}(\mathbf{r}, t)$ depends on the *entire history* of the system, all the way back to $t = -\infty$. Even if we wish to determine the xc potential over only a finite time interval, the entire previous history must be taken into account. Notice in particular that the orbital-dependent xc potential has a memory even if we use the xc action in the adiabatic approximation.

- *Additive function.* Another property of eqn (11.49) is the fact that it determines $v_{\mathrm{xc}\sigma}(\mathbf{r}, t)$ only to within an additive, purely time-dependent function $c_\sigma(t)$, as expected in view of the Runge–Gross theorem. The proof is left as Exercise 11.9.

- *Density functionals.* It is easy to see that we simply retrieve the ordinary time-dependent xc potential in the adiabatic approximation if the action is an explicit density functional.

- *First alternative form.* The TDOEP scheme (11.49) can be rewritten in the following, slightly modified form:

$$
i \sum_{j=1}^{N_\sigma} \int_{-\infty}^{t} dt' \int d^3r' \left[v_{\mathrm{xc}\sigma}(\mathbf{r}', t') - \mathcal{V}_{\mathrm{xc}j\sigma}(\mathbf{r}', t') \right] \varphi_{j\sigma}(\mathbf{r}, t) \varphi_{j\sigma}^*(\mathbf{r}', t')
$$
$$
\times \sum_{\substack{k=1 \\ k \ne j}}^{\infty} \varphi_{k\sigma}^*(\mathbf{r}, t) \varphi_{k\sigma}(\mathbf{r}', t') + \mathrm{c.c.} = 0 , \quad (11.51)
$$

which is obtained by removing the $j = k$ term from the integral kernel (11.50). For this to be true, the following condition must be satisfied:

$$
i \sum_{j=1}^{N_\sigma} n_{j\sigma}(\mathbf{r}, t) \int_{-\infty}^{t} dt' \int d^3r' \left[\mathcal{V}_{\mathrm{xc}j\sigma}(\mathbf{r}', t') - \mathcal{V}_{\mathrm{xc}j\sigma}^*(\mathbf{r}', t') \right] n_{j\sigma}(\mathbf{r}', t') = 0 . \quad (11.52)
$$

There is a good reason why we prefer eqn (11.51), as we shall soon see when we consider the static limit. But is the condition (11.52) always fulfilled? This obviously depends on the explicit functional form of the xc action functional, and in the following we shall admit only those functionals $\mathcal{A}[\{\varphi_{j\sigma}\}]$ that do satisfy eqn (11.52). An important, broad class of xc action functionals is made up of those that depend on the orbitals through the combinations $\varphi_{j\sigma}(\mathbf{r}, t)\varphi_{j\sigma}^*(\mathbf{r}', t)$ for all $(j\sigma)$. This includes as a special case the exact-exchange action functional (11.33), which depends on the time-dependent spin-density matrix $\sum_{j}^{N_\sigma} \varphi_{j\sigma}(\mathbf{r}, t)\varphi_{j\sigma}^*(\mathbf{r}', t)$.

- *Static limit.* An important consistency requirement for every time-dependent theory is that it must reduce to the proper static limit; in the case of the TDOEP, this should be the static OEP. Let us now see how this works. In a static situation, we can write the time-dependent orbitals as follows:

$$
\varphi_{j\sigma}(\mathbf{r}, t) = \varphi_{j\sigma}^0(\mathbf{r}) e^{-i\varepsilon_{j\sigma}(t-t_0)} . \quad (11.53)
$$

In this case the adiabatic approximation (11.32) becomes exact, and we have

$$
\mathcal{V}_{\mathrm{xc}j\sigma}^{\mathrm{static}}(\mathbf{r},t) = \frac{1}{\widetilde{\varphi}_{j\sigma}^*(\mathbf{r})} \frac{\delta E_{\mathrm{xc}}[\{\widetilde{\varphi}_{j\sigma}\}]}{\delta \widetilde{\varphi}_{j\sigma}(\mathbf{r})}\Bigg|_{\widetilde{\varphi}_{j\sigma}(\mathbf{r})=\varphi_{j\sigma}^0(\mathbf{r})e^{-i\varepsilon_{j\sigma}(t-t_0)}} . \tag{11.54}
$$

It turns out that this expression is independent of time [all time-dependent phase factors compensate each other, since we assume the condition (11.52) to hold in the static limit as well], and we have $\mathcal{V}_{\mathrm{xc}j\sigma}^{\mathrm{static}}(\mathbf{r},t) = \mathcal{V}_{\mathrm{xc}j\sigma}^0(\mathbf{r})$. We therefore obtain

$$
i\sum_{j=1}^{N_\sigma} \int_{-\infty}^{t} dt' \int d^3r' \left[v_{\mathrm{xc}\sigma}^0(\mathbf{r}') - \mathcal{V}_{\mathrm{xc}j\sigma}^0(\mathbf{r}') \right] \varphi_{j\sigma}^0(\mathbf{r})\varphi_{j\sigma}^{0*}(\mathbf{r}')
$$

$$
\times \sum_{\substack{k=1 \\ k\neq j}}^{\infty} \varphi_{k\sigma}^{0*}(\mathbf{r})\varphi_{k\sigma}^0(\mathbf{r}')\, e^{-i(\varepsilon_{j\sigma}-\varepsilon_{k\sigma})(t-t')} + \mathrm{c.c.} = 0 . \tag{11.55}
$$

If we carry out the time integration over t' (including the usual convergence factor $\lim_{\eta\to 0^+} e^{i\eta t}$ to take care of the lower time limit $-\infty$), it is straightforward to see that this reduces to the static OEP integral equation (11.12).

- *Second alternative form.* In practice, we usually deal with situations where the system is in its ground state for all times up until t_0. At $t = t_0$, an explicitly time-dependent external potential is switched on, and we wish to calculate the time-dependent xc potential for the subsequent time evolution. In this scenario, the TDOEP scheme (11.51) becomes

$$
\sum_{j=1}^{N_\sigma} \sum_{\substack{k=1 \\ k\neq j}}^{\infty} \left\{ i \int_{t_0}^{t} dt' \int d^3r' \left[v_{\mathrm{xc}\sigma}(\mathbf{r}',t') - \mathcal{V}_{\mathrm{xc}j\sigma}(\mathbf{r}',t') \right] \varphi_{j\sigma}(\mathbf{r},t)\varphi_{j\sigma}^*(\mathbf{r}',t')\varphi_{k\sigma}^*(\mathbf{r},t)\varphi_{k\sigma}(\mathbf{r}',t') \right.
$$

$$
\left. + \int d^3r' \left[v_{\mathrm{xc}\sigma}^0(\mathbf{r}') - \mathcal{V}_{\mathrm{xc}j\sigma}^0(\mathbf{r}') \right] \varphi_{j\sigma}(\mathbf{r},t)\varphi_{k\sigma}^*(\mathbf{r},t)\frac{\varphi_{j\sigma}^{0*}(\mathbf{r}')\varphi_{k\sigma}^0(\mathbf{r}')}{\varepsilon_{j\sigma}-\varepsilon_{k\sigma}} \right\} + \mathrm{c.c.} = 0 . \tag{11.56}
$$

To conclude this subsection, we should mention that the derivation of the TDOEP scheme which we have discussed here is not the only one. The TDOEP scheme can also be shown to emerge from an action principle based on Keldysh Green's functions (van Leeuwen, 1996, 1998), and from a special form of time-dependent perturbation theory (Görling, 1997). We will say more about these approaches in Chapter 13.

11.2.3   Approximations

Adiabatic TDOEP.   The adiabatic approximation was first introduced in Section 4.3, and appears in many applications throughout this book. Let us now address the question of how the adiabatic approximation to the TDOEP (the AOEP) should be defined.

For pure density functionals such as the LDA, defining the adiabatic approximation is straightforward: all we need to do is replace the static density by the time-dependent density. The simplest example of this procedure is the ALDA. But for the case of the OEP [see eqn (11.12)], it is not so obvious how to define the adiabatic approximation.

If it depended only on the orbitals, then it would be easy—we would simply replace the static orbitals by time-dependent ones. But the static OEP also depends on the energy eigenvalues, whose meaning in the dynamical regime is not obvious.

We define the AOEP as the static OEP whose associated ground-state density equals the instantaneous $n(t)$. This requires two steps at each t:

1. First, find the static Kohn–Sham potential v_s^t which produces $n(t)$ as its self-consistent ground-state density and whose xc part is the static OEP. Since the external part of v_s^t is in general different from the actual time-dependent external potential, and a priori unknown, v_s^t must be found by numerical inversion of the static Kohn–Sham equation (see Appendix E).

2. Next, plug the resulting complete set of orbitals $\varphi_{j\sigma}^t(\mathbf{r})$ and eigenvalues $\varepsilon_{j\sigma}^t$ into the static OEP integral equation (11.12). Solution of this equation gives the AOEP xc potential at time t.

The AOEP so defined becomes identical to the TDOEP in the static limit where the system remains in its ground state, and both reduce to the static OEP in this case.

Time-dependent KLI and Slater potentials.   In Section 11.1.4, we discussed several approximations to the static OEP; the most important ones are the KLI and Slater potentials, defined in eqns (11.24) and (11.25). We saw that the KLI potential is, for most purposes, an excellent approximation to the full OEP, giving total ground-state energies and orbital eigenvalues in close agreement.

In the time-dependent case, the KLI and Slater approximations to the TDOEP equation (11.51) are defined as follows:

$$v_{\mathrm{xc}\sigma}^{\mathrm{Slater}}(\mathbf{r},t) = \frac{1}{2n_\sigma(\mathbf{r},t)} \sum_{j=1}^{N_\sigma} n_{j\sigma}(\mathbf{r},t) \left[\mathcal{V}_{\mathrm{xc}j\sigma}(\mathbf{r},t) + \mathcal{V}_{\mathrm{xc}j\sigma}^*(\mathbf{r},t) \right], \qquad (11.57)$$

$$v_{\mathrm{xc}\sigma}^{\mathrm{KLI}}(\mathbf{r},t) = v_{\mathrm{xc}\sigma}^{\mathrm{Slater}}(\mathbf{r},t) + \frac{1}{n_\sigma(\mathbf{r},t)} \sum_{j=1}^{N_\sigma} n_{j\sigma}(\mathbf{r},t) \left[\bar{v}_{\mathrm{xc}j\sigma}^{\mathrm{KLI}}(t) - \frac{1}{2} \left(\bar{\mathcal{V}}_{\mathrm{xc}j\sigma}(t) + \bar{\mathcal{V}}_{\mathrm{xc}j\sigma}^*(t) \right) \right].$$
$$(11.58)$$

These are simply the static expressions (11.24) and (11.25) evaluated with time-dependent orbitals; the memory of the full TDOEP is lost. The time-dependent KLI and Slater potentials thus appear to be merely adiabatic approximations based on their static counterparts, but they actually are more than just that: there is also another way of arriving at eqn (11.58), rather than by simply making an adiabatic approximation based on the static KLI expression. It turns out that the TDOEP equation (11.51) can be rewritten as a partial differential equation, which has the same form as eqn (11.58) except for some additional orbital-dependent terms that vanish when averaged over the respective orbital densities. The time-dependent KLI (TDKLI) potential emerges if these terms are neglected. A similar derivation was given earlier for the static case by Krieger *et al.* (1992*b*), and later generalized to the time-dependent case (Ullrich *et al.*, 1995*b*).

In practice, the TDKLI potential is implemented in the same way as the static KLI potential: at each time t, inversion of a small matrix of dimension N_σ is required (see Exercise 11.4).

Most applications of time-dependent, orbital-dependent potentials have been carried out using the TDKLI approximation; we will discuss a few of them in the following. But before we come to these examples, an important point needs to be mentioned, namely, that the TDKLI potential does not satisfy the zero-force theorem of TDDFT (see Section 6.2.2) (Mundt *et al.*, 2007). As a consequence, the total force caused by $v_{\mathrm{xc}\sigma}^{\mathrm{KLI}}$ on a given system may be nonvanishing; incidentally, this also affects the static KLI potential. The root of the problem lies in the ad hoc way in which the KLI and TDKLI potentials are derived, namely, by neglecting certain terms in the full (TD)OEP equation. In other words, the KLI and TDKLI potentials are not derived from a variational principle.

How serious is this violation of the zero-force theorem in a time-dependent situation? Mundt *et al.* (2007) studied small neutral sodium clusters in which the electron cloud is subject to a weak initial momentum boost that triggers small plasmon-like oscillations. After a while, these oscillations spontaneously tend to self-amplify and eventually develop into catastrophic numerical instabilities; no such behavior was observed with the ALDA. On the other hand, many applications of the TDKLI potential to systems that are more strongly confined and less polarizable than neutral sodium clusters (such as positively charged clusters, atoms, and quantum wells) or systems driven by strong external fields do not show any unusual behavior. This indicates that zero-force theorem violations do not play a role in many situations of practical interest, but this should be checked on a case-by-case basis.

11.2.4   First case study: full versus approximate TDOEP

The full TDOEP integral equation (11.56) poses formidable practical challenges and has so far only been implemented in exact exchange for a quasi-one-dimensional quantum well (Wijewardane and Ullrich, 2008). We will study this example in the following because it illustrates a number of general features.

The system is a doped GaAs/AlGaAs square quantum well of width 40 nm which contains a number of electrons per unit area (2.2×10^{11} cm^{-2}) such that the two lowest subbands are initially occupied.[9] The system either is driven by an external dipole potential at a given frequency or carries out free charge-density oscillations after an initial sudden excitation.

Equation (11.56) is an integral equation for $v_{\mathrm{xc}\sigma}(\mathbf{r}, t)$ in space and time; the xc potential at time t depends on the orbitals at times $t' < t$, which means that in practice these earlier orbitals must be stored in memory. Depending on the desired length of the time interval $[t_0, t_1]$ for which the system is to be propagated, this can place a heavy demand on computational resources. In this sense, the TDOEP is similar to other TDKS time propagation schemes with memory, such as the memory-dependent xc potential of the nonlinear VK theory (see Section 10.6).

But there is more. In Sections 4.4 and 4.5, we discussed the meaning of self-consistency in TDDFT and showed how to achieve it in practice using step-by-step time propagation (for instance with the Crank–Nicolson algorithm) combined with a

---

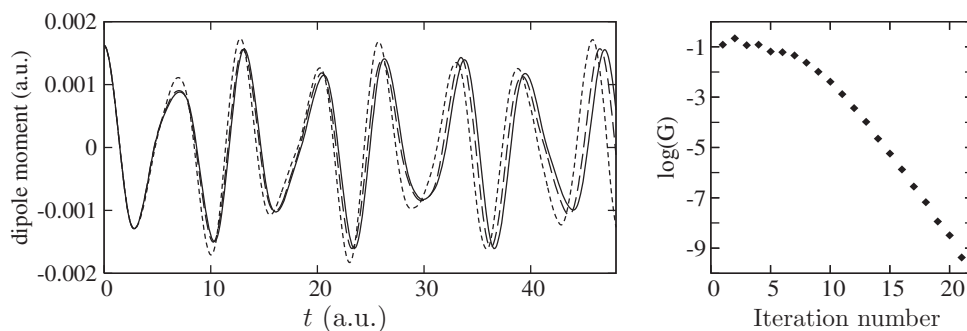[9]See Appendix K for a discussion of the basics of quantum wells.

Fig. 11.4 Left: time-dependent dipole moment of free charge-density oscillations in a quantum well with two occupied subbands. Full line, TDKLI; long-dashed line, AOEP; dotted line, TDOEP. Right: convergence index G [see eqn (11.59)]. [Adapted with permission from APS from Wijewardane and Ullrich (2008), ©2008.]

predictor–corrector scheme. This is how essentially all TDKS calculations are implemented. But, in the case of the TDOEP, we encounter a difficulty which prevents us from using this standard propagation approach.

Let us discretize the time integral in eqn (11.56) using the trapezoidal rule; the integral then becomes a finite sum, where the number of terms depends on how small the time step $\Delta\tau$ is taken to be. The term in this sum that arises from the upper limit t of the time integral is of particular significance, because it contains the xc potential at time $\tau_j = t$ which we wish to calculate (assuming that the potential at all earlier times $\tau_j < t$ has already been determined). But it is easy to see in eqn (11.56) that the integrand vanishes at the upper limit $t' = t$ of the time integral! In other words, eqn (11.56) only determines $v_{\mathrm{xc}\sigma}(\mathbf{r}, t')$ for $t' < t$, and not at the time t itself. Hence, the step-by-step propagation algorithm of Section 4.5 cannot be used for the TDOEP.[10]

We are therefore forced to resort to an alternative propagation method: the global self-consistency scheme of TDDFT (see Section 4.4 and, in particular, Fig. 4.3). But does this scheme actually converge? To monitor the convergence, we define the index

$$G_l = \frac{\int_{t_0}^{t_1} dt\, |d_l(t) - d_{l-1}(t)|}{\int_{t_0}^{t_1} dt\, |d_l(t)|}\,, \tag{11.59}$$

where $d_l(t)$ is the time-dependent dipole moment as obtained in the lth iteration step. Our test case is a situation where the quantum well is initially in an electric field which is suddenly switched off at $t = t_0$, and this in turn causes the density to freely oscillate back and forth. As seen in Fig. 4.3, G_l decreases rapidly, which indicates stable and robust convergence towards a self-consistent solution of the TDKS equation with the TDOEP exchange potential. All in all, about 20 global iteration cycles are needed.

Let us now see how the different methods compare when it comes to calculating the time-dependent dipole moment of the charge-density oscillations in the quantum

[10]This is consistent with the observation that alternative step-by-step time propagation schemes for the TDOEP were plagued by numerical instabilities (Mundt and Kümmel, 2006).
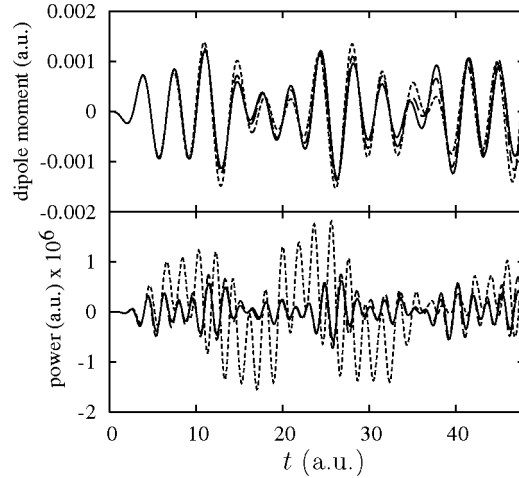
Fig. 11.5 Top: dipole oscillations in a quantum well driven by an external field of frequency 20 meV and intensity 20 W/cm^2. Full line, TDKLI; long-dashed line, AOEP; dotted line, TDOEP. Bottom: xc power [see eqn (11.60)]. [Adapted with permission from APS from Wijewardane and Ullrich (2008), ©2008.]

well. We observe in Fig. 11.4 that the TDKLI and AOEP results are extremely close to each other, which does not come as a surprise considering the fact that the static KLI potential is an excellent approximation to the OEP. The full TDOEP, on the other hand, differs a bit more, and leads to charge-density oscillations that are slightly faster. Somehow, this must be related to the memory inherent in the TDOEP, which the AOEP ignores.

For further insight, let us define the xc power

$$P(t) = \int dz \, j(z,t) \nabla_z \left[v_{\mathrm{xc}\sigma}(z,t) - v_{\mathrm{xc}\sigma}^0(z,t) \right] \; , \tag{11.60}$$

where it is assumed that the quantum well confinement direction is along the z-axis. We consider the same quantum well as above, now subject to an external field (in the dipole approximation) of frequency 20 meV, which corresponds roughly to twice the lowest intersubband plasmon frequency. The top part of Fig. 11.5 again confirms that the AOEP and TDKLI results are generally in very close agreement, and not too different compared with the full TDOEP. We can see from the bottom panel of Fig. 11.5 that $P(t)$ oscillates twice as fast as $d(t)$, since it is defined as the product of two oscillating quantities, the current $j(z,t)$ and the dynamical xc force $\nabla_z \left[v_{\mathrm{xc}\sigma}(z,t) - v_{\mathrm{xc}\sigma}^0(z,t) \right]$.

But now we learn two interesting things from the xc power $P(t)$:

1. On average, $P(t)$ is zero, which means that there is no dissipation.
2. For the TDOEP, $P(t)$ (and therefore the time-dependent exchange potential) picks up a phase shift compared with the AOEP and TDKLI results, which themselves are completely in sync. This is a clear indication of memory-induced elasticity.
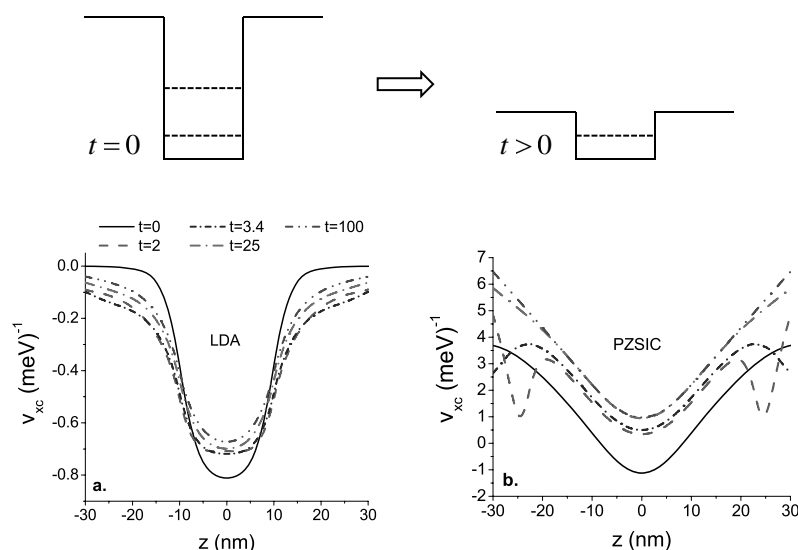
Fig. 11.6 Snapshots of the time-dependent xc potential in the LDA and TDKLI–SIC approaches for an electron escape process triggered by sudden barrier suppression in a quantum well. In the SIC case, the ionization of the second subband produces a jump in the xc potential. [Adapted with permission from the PCCP Owner Societies from Vieira *et al.* (2009), ©2009.]

11.2.5 Second case study: discontinuity in the xc potential

The second example which we shall discuss in detail also involves electron dynamics in quantum wells. Now the goal is to find out how the discontinuity in the xc potential with changes in the particle number—a prominent feature of the static OEP—carries over into the time domain (Vieira *et al.*, 2009). In this study, the calculations were done with the TDKLI approach, using the ALDA–SIC functional as input [see eqn (11.4)].

In Section 6.7, we saw that $v_{xc}(\mathbf{r}, t)$ jumps by a constant during an ionization process as the number of electrons passes through an integer or, equivalently, as a single-particle level is completely depleted. To see how this constant shift develops in the TDKLI potential, we consider a scenario in which the depth of a quantum well with two initially occupied subbands is suddenly decreased to one-third of its initial value (see Fig. 11.6).[11] The shallow quantum well now has only one bound level, and density rapidly spills out. Figure 11.6 shows how the xc potential changes with time. In the case of the ALDA, the xc potential gradually changes and becomes a bit more shallow overall. In the case of the TDKLI–SIC approach, on the other hand, one can see very nicely that a step structure forms as ionization sets in. These steps quickly migrate away from the quantum well, along with the escaping electrons, and in the end one is left with an xc potential that looks almost identical to the original one, just

[11]Such a scenario is, of course, not very realistic. In practice, one could suddenly switch on a static electric field which suppressed the barrier on one side.
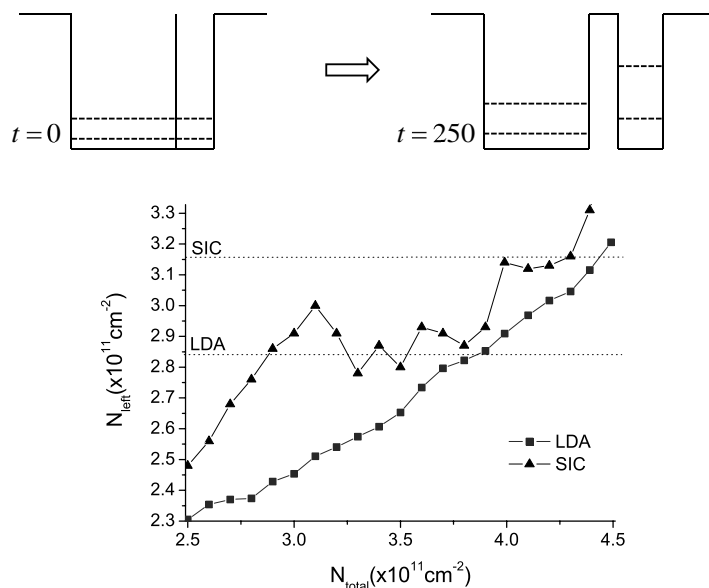
Fig. 11.7 Number of electrons in the left well, N_{left}, as a function of the total electron number of a dissociating double quantum well after $t = 250$ a.u. The SIC potential predicts an abrupt decrease in N_{left} approaching the region where the second subband would be filled in the isolated well. [Adapted with permission from the PCCP Owner Societies from Vieira *et al.* (2009), ©2009.]

shifted by a constant. Similar effects were also observed in simulations of a 1D lithium atom (Mundt and Kümmel, 2005).

Now that we have confirmed that the TDKLI–SIC approach does indeed produce steps and jumps in the time-dependent xc potential, the question is whether and how any physical observables are affected by this. We focus on a dissociating asymmetric double quantum well (see Fig. 11.7), where the left well has a width of 32 nm and the right one has a width of 8 nm, and both have the same depth. At $t = 0$, the system starts out with a very thin barrier so that the electrons share the two wells; this is analogous to a molecular orbital in a diatomic molecule. The two wells are then slowly pulled apart, until, at $t = 250$ a.u., they can be considered separate.[12]

The double-well system is populated with a total number of electrons $N_{\text{total}} = N_{\text{left}} + N_{\text{right}}$, and we are interested in the final distribution of electrons in the left and right wells. In a diatomic molecule, we know that the separated atomic systems should have integer charge; since the quantum wells here are extended systems, charge cannot be counted directly, but we expect nevertheless to see some signature of the discontinuity in the xc potential in the final electron distributions. This is confirmed in Fig. 11.7, which shows the final value of N_{left} at $t = 250$ a.u. versus N_{total}.

[12]Again, not a very realistic example, since quantum wells cannot simply "dissociate."
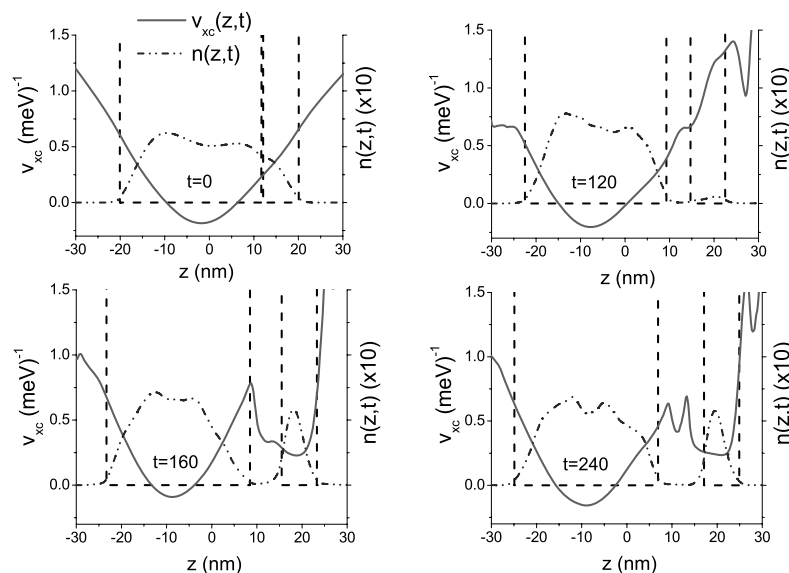
Fig. 11.8 Snapshots of the time-dependent density and xc potential in the TDKLI–SIC approach for the dissociating double well shown in Fig. 11.7. [Reproduced with permission from the PCCP Owner Societies from Vieira *et al.* (2009), ©2009.]

The horizontal dotted lines in the lower part of Fig. 11.7 indicate the value of N_{left} at which, in a ground-state calculation of the left well only, the second subband would become occupied (the LDA value is smaller than the SIC one). The ALDA predicts a smooth increase in N_{left}, but the TDKLI–SIC result behaves dramatically differently: the electrons seem to resist filling the left well if it means that the second subband would be populated. N_{left} forms a sort of plateau, and crosses the threshold to the second subband only much later. Since the process is dynamical, the plateau has some structure.

Figure 11.8 shows snapshots of the TDKLI–SIC xc potential at different times during the dissociation process of a quantum well with $N_{\text{total}} = 3.3 \times 10^{11} \text{ cm}^{-2}$. These snapshots clearly illustrate the mechanism preventing the left quantum well from being filled: once the double well starts dissociating, the xc potential builds up step structures with a pronounced peak in the barrier region. The system resists filling the second subband: at the moment at which this happens, the potential on the left side jumps up relative to the minimum that develops simultaneously on the right side. As a result, electrons flow back to the right, as seen from the density plots.

This example demonstrates that the TDKLI–SIC method captures the effects of the discontinuity in the xc potential, which are crucial for generic dissociation or fragmentation processes. However, the step structures and jumps in the xc potential become more and more washed out the more abrupt the dynamics becomes, owing to increasingly strong density and current fluctuations.

11.3   TDOEP in the linear regime

We will now consider the TDOEP in the linear-response regime, where the goal is to derive an expression for the xc kernel $f_{\mathrm{xc},\sigma\sigma'}(\mathbf{r},\mathbf{r}',\omega)$ as a functional of the orbitals. In doing so, we are motivated by the expectation that this xc kernel will produce good excitation energies, because of all the nice properties of the OEP (mainly the freedom from self-interaction and the resulting correct asymptotics).

Let us begin with the definition of the xc kernel [see eqn (7.89)]:

$$f_{\mathrm{xc},\sigma\sigma'}(\mathbf{r},t,\mathbf{r}',t') = \left.\frac{\delta v_{\mathrm{xc}\sigma}(\mathbf{r},t)}{\delta n_{\sigma'}(\mathbf{r}',t')}\right|_{n_{0\uparrow}(\mathbf{r}),n_{0\downarrow}(\mathbf{r})}. \tag{11.61}$$

Here, the xc potential is given through the TDOEP as an orbital functional, so we need to use the chain rule for functional derivatives, as we have already done on several occasions:

$$f_{\mathrm{xc},\sigma\sigma'}(\mathbf{r},t,\mathbf{r}',t') = \sum_{\sigma_1\sigma_2}\sum_{j=1}^{\infty}\int d^3r_1\int dt_1\int d^3r_2\int dt_2$$
$$\times \left.\frac{\delta v_{\mathrm{xc}\sigma}(\mathbf{r},t)}{\delta\varphi_{j\sigma_1}(\mathbf{r}_1,t_1)}\frac{\delta\varphi_{j\sigma_1}(\mathbf{r}_1,t_1)}{\delta v_{s\sigma_2}(\mathbf{r}_2,t_2)}\frac{\delta v_{s\sigma_2}(\mathbf{r}_2,t_2)}{\delta n_{\sigma'}(\mathbf{r}',t')}\right|_{\varphi_{j\sigma}^0(\mathbf{r})} + \mathrm{c.c.}\,, \tag{11.62}$$

where we have used the abbreviation $\varphi_{j\sigma}^0(t) \equiv \varphi_{j\sigma}^0(\mathbf{r})e^{-i\varepsilon_{j\sigma}t}$. The last functional derivative on the right-hand side of eqn (11.62) can be identified as the inverse Kohn–Sham response function, and we can bring it over to the left:

$$\sum_{\sigma''}\int d^3r''\int dt'' f_{\mathrm{xc},\sigma\sigma'}(\mathbf{r},t,\mathbf{r}'',t'')\chi_{s,\sigma''\sigma'}(\mathbf{r}'',t'',\mathbf{r}',t') \tag{11.63}$$
$$= \sum_{\sigma''}\sum_{j=1}^{\infty}\int d^3r''\int dt''\,\mathcal{F}_{\mathrm{xc}j,\sigma\sigma''}(\mathbf{r},t,\mathbf{r}'',t'')\varphi_{j\sigma''}^*(\mathbf{r}'',t'')\left.\frac{\delta\varphi_{j\sigma''}(\mathbf{r}'',t'')}{\delta v_{s\sigma'}(\mathbf{r}',t')}\right|_{\varphi_{j\sigma}^0(\mathbf{r})} + \mathrm{c.c.}\,,$$

where

$$\mathcal{F}_{\mathrm{xc}j,\sigma\sigma'}(\mathbf{r},t,\mathbf{r}',t') = \left.\frac{1}{\varphi_{j\sigma'}^*(\mathbf{r}',t')}\frac{\delta v_{\mathrm{xc}\sigma}(\mathbf{r},t)}{\delta\varphi_{j\sigma'}(\mathbf{r}',t')}\right|_{\varphi_{j\sigma}^0(\mathbf{r})}. \tag{11.64}$$

To evaluate the functional derivative $\delta\varphi_{j\sigma}/\delta v_{s\sigma'}$, we use time-dependent perturbation theory, similarly to what we did in Section 11.2.2 when we derived eqn (11.48). However, things are now different in the sense that causality arises here via the usual forward time propagation, and we obtain

$$\frac{\delta\varphi_{j\sigma''}(\mathbf{r}'',t'')}{\delta v_{s\sigma'}(\mathbf{r}',t')} = -i\delta_{\sigma''\sigma'}\theta(t''-t')\sum_{k=1}^{\infty}\varphi_{k\sigma'}^*(\mathbf{r}',t')\varphi_{k\sigma'}(\mathbf{r}'',t'')\varphi_{j\sigma'}(\mathbf{r}',t')\,. \tag{11.65}$$

Equation (11.63) gives, in principle, the exact TDOEP xc kernel. Just like the xc potential, it is defined via an integral equation; the additional difficulty compared with the TDOEP equation (11.49) is that $\mathcal{F}_{\mathrm{xc}j,\sigma\sigma'}(\mathbf{r},t,\mathbf{r}',t')$ cannot be easily obtained,

since $v_{\text{xc}\sigma}(\mathbf{r}, t)$ is only given as an implicit orbital functional. It is possible to transform eqn (11.63) into an integral equation which directly involves functional derivatives of the xc action, $\delta \mathcal{A}_{\text{xc}}/\delta \varphi_{j\sigma}$ and $\delta^2 \mathcal{A}_{\text{xc}}/\delta \varphi_{j\sigma} \delta \varphi_{j'\sigma'}$ (Petersilka *et al.*, 1998). However, the resulting expression is quite complicated, and we shall not pursue it here any further.

Does that mean that we have to abandon our hope of arriving at a practically useful expression for the TDOEP xc kernel? Fortunately not: there are two elegant alternative approaches to constructing $f_{\text{xc},\sigma\sigma'}$, which have been particularly useful in the exact-exchange limit. The first approach uses perturbation theory along the adiabatic connection (Görling, 1998*a*, 1998*b*), and the second uses many-body perturbation theory (Hellgren and von Barth, 2008). We shall discuss details of the latter in Chapter 13, and will also give an explicit expression for the exact frequency-dependent exchange kernel $f_{\text{x}}(\mathbf{r}, \mathbf{r}', \omega)$ there.

On the other hand, it is possible to arrive at approximate solutions for the xc kernel in a relatively simple manner. If we compare eqn (11.63) with the TDOEP equation, eqn (11.49), we notice that there exists some formal similarity between the two. In that case, why not try using similar approximation methods? The most straightforward thing is to try a form similar to the Slater approximation (11.57); this leads us to propose the following approximate expression, known as the PGG xc kernel (Petersilka *et al.*, 1996, 1998):

$$f_{\text{xc},\sigma\sigma'}^{\text{PGG}}(\mathbf{r}, t, \mathbf{r}', t') = \frac{1}{2 n_{0\sigma'}(\mathbf{r}')} \sum_{j=1}^{N_\sigma} |\varphi_{j\sigma'}^0(\mathbf{r}')|^2 \left[\mathcal{F}_{\text{xc}j,\sigma\sigma'}(\mathbf{r}, t, \mathbf{r}', t') + \text{c.c.} \right]. \tag{11.66}$$

We evaluate eqn (11.64) with the explicit analytical form $v_{\text{xc}\sigma}^{\text{Slater}}(\mathbf{r}, t)$. This gives

$$f_{\text{x},\sigma\sigma'}^{\text{PGG}}(\mathbf{r}, t, \mathbf{r}', t') = -\delta(t - t')\delta_{\sigma\sigma'} \frac{\left| \sum_{k=1}^{N_\sigma} \varphi_{k\sigma}^0(\mathbf{r})\varphi_{k\sigma}^{0*}(\mathbf{r}') \right|^2}{|\mathbf{r} - \mathbf{r}'| n_{0\sigma}(\mathbf{r}) n_{0\sigma}(\mathbf{r}')}. \tag{11.67}$$

For a homogeneous system, the PGG kernel becomes (Lein *et al.*, 2000)

$$f_{\text{x}}^{\text{PGG}}(q, \omega) = -\frac{3\pi}{10 k_F^2} \left\{ 11 + 2Q^2 + \left(\frac{2}{Q} - 10Q \right) \ln \frac{1+Q}{|1-Q|} \right.$$
$$\left. + (2Q^4 - 10Q^2) \ln \left| 1 - \frac{1}{Q^2} \right| \right\}, \tag{11.68}$$

where $Q = q/2k_F$ and we take the spin-unpolarized form for simplicity.

The PGG xc kernel has been successfully applied to the excitation energies and optical spectra of atoms (Petersilka *et al.*, 2000; Burke *et al.*, 2002) and small clusters (Marques *et al.*, 2001). In Section 12.3, we will show that it also gives good result for exciton binding energies in semiconductors.

Exercise 11.1 Show that the OEP integral equation (11.12) follows from eqns (11.14) and (11.15).

Exercise 11.2 Show that eqn (11.16) follows from the OEP integral equation (11.12) in the asymptotic region where all contributions to the sum over j can be neglected except $j = N_\sigma$.

Exercise 11.3 Prove that the second derivation of the OEP integral equation, starting from eqn (11.13), is consistent with the Hohenberg–Kohn variational principle and eqn (11.5).

Exercise 11.4 The KLI approximation is defined in eqn (11.24). This is formally an integral equation for $v_{\text{xc}\sigma}^{\text{KLI}}(\mathbf{r})$, but it can be solved relatively easily. To do this, you need to find the orbital-dependent constants $\bar{v}_{\text{xc}j\sigma}^{\text{KLI}}$. Show that one ends up with a final expression of the form

$$v_{\text{xc}\sigma}^{\text{KLI}}(\mathbf{r}) = w_{\text{xc}\sigma}(\mathbf{r}) + \frac{1}{n_\sigma(\mathbf{r})} \sum_{j,k}^{N_\sigma} n_{j\sigma}(\mathbf{r}) \left(\Pi_\sigma^{-1}\right)_{jk} \bar{w}_{\text{xc}k\sigma} , \qquad (11.69)$$

with the $N_\sigma \times N_\sigma$ matrix

$$\Pi_{kj\sigma} = \delta_{kj} - \int d^3r \, \frac{n_{k\sigma}(\mathbf{r})n_{j\sigma}(\mathbf{r})}{n_\sigma(\mathbf{r})} , \qquad (11.70)$$

and

$$w_{\text{xc}\sigma}(\mathbf{r}) = \frac{1}{2n_\sigma(\mathbf{r})} \sum_{j=1}^{N_\sigma} n_{j\sigma}(\mathbf{r}) \left[\mathcal{V}_{\text{xc}j\sigma}^0(\mathbf{r}) - \bar{\mathcal{V}}_{\text{xc}j\sigma}^0\right] + \text{c.c.} \qquad (11.71)$$

Exercise 11.5 Explain why the correlation energy of a system in its ground state is always a negative quantity.

Exercise 11.6 Go over the derivation of the TDOEP equation again (see Sections 11.2.1 and 11.2.2). Show that in the x-only case one arrives at the TDHF equations by an unconstrained variation with respect to the orbitals.

Exercise 11.7 Derive eqn (11.46) for $c_{jk\sigma}^{(1)}(t)$. The idea is to insert eqn (11.43) into the perturbed TDKS equation (11.42), then make the ansatz (11.44) and collect terms of the same order in the perturbation.

Exercise 11.8 Show that the kernel $K_\sigma(\mathbf{r}, t, \mathbf{r}', t')$ plays the role of the Green's function in the following differential equation:

$$\left[i\frac{\partial}{\partial t'} + \frac{\nabla'^2}{2} - v_{s\sigma}(\mathbf{r}', t')\right] K_\sigma(\mathbf{r}, t, \mathbf{r}', t') = -i\delta(\mathbf{r} - \mathbf{r}')\delta(t - t') \qquad (11.72)$$

with the initial condition $K_\sigma(\mathbf{r}, t, \mathbf{r}', t') = 0$ for $t' > t$.

Exercise 11.9 Show that the TDOEP integral equation (11.49) determines the xc potential only to within a purely time-dependent constant $c_\sigma(t)$.

Exercise 11.10 Show that the integrand of the TDOEP integral equation vanishes at the upper time limit t.

Exercise 11.11 Carry out the steps leading to the PGG kernel (11.67) via eqn (11.66).

Exercise 11.12 Prove that xc action functionals that depend on the orbitals through the combinations $\varphi_{j\sigma}(\mathbf{r}, t)\varphi_{j\sigma}^*(\mathbf{r}', t)$ satisfy condition (11.52).

Exercise 11.13 Show that the PGG kernel (11.68) for a homogeneous system approaches a constant as $Q \to 0$.

12
Extended systems

This chapter deals with electron dynamics in extended systems—more specifically, we shall be concerned with 3D periodic solids only, and stay mostly within the linear-response regime. Periodic solids can be metallic, insulating, or semiconducting and, accordingly, their response properties will be very different. We will therefore begin with a general overview of the electronic structure and excitations in these different types of solids. In the following, it is assumed that the reader has some basic knowledge of the essential concepts of solid-state physics.

The spectroscopy of materials is an important subject with a vast range of techniques and applications (Kuzmany, 2009; Yu and Cardona, 2010). A comprehensive treatment of the theoretical and experimental aspects of solid-state spectroscopy is, of course, far beyond the scope of this book; many important topics such as lattice dynamics and electron–phonon interactions will be omitted.[1] Instead, this chapter takes a much more selective view and focuses on those aspects of spectroscopy where the TDDFT approach to periodic solids can be particularly clearly illustrated.

A central goal of this chapter will be to explain the fundamental differences in the excitation spectra of metals and semiconductors/insulators, in particular with regard to the dominant collective electronic excitations: in metals these are the *plasmons*, and in semiconductors and insulators these are the *excitons*. TDDFT can in principle describe all types of electronic excitations in solids exactly, including plasmons and excitons. However, it will come as no surprise that the common approximations, while computationally efficient, are not always successful in practice. We will explain what the main challenges are and how they can be overcome. Much of the recent progress in the application of TDDFT to optical excitations in solids is based on the many-body techniques which we will introduce in Chapter 13.

12.1 Electronic structure and excitations of periodic solids

12.1.1 Band structure: metals versus insulators

The fundamental way to characterize a solid is via its electronic band structure. We consider the nuclei to be fixed and infinitely heavy (i.e., we make the Born–Oppenheimer approximation; see Chapter 17), and arranged in a periodic lattice. The nuclei cause a Coulomb potential with the same lattice periodicity; in other words, $v_0(\mathbf{r} + \mathbf{R}) = v_0(\mathbf{r})$, where $\mathbf{R}$ is an arbitrary lattice vector. Under these circumstances the static Kohn–Sham equation becomes

---

[1]Chapter 17 describes the coupling of electronic and nuclear dynamics, but mainly for molecules.
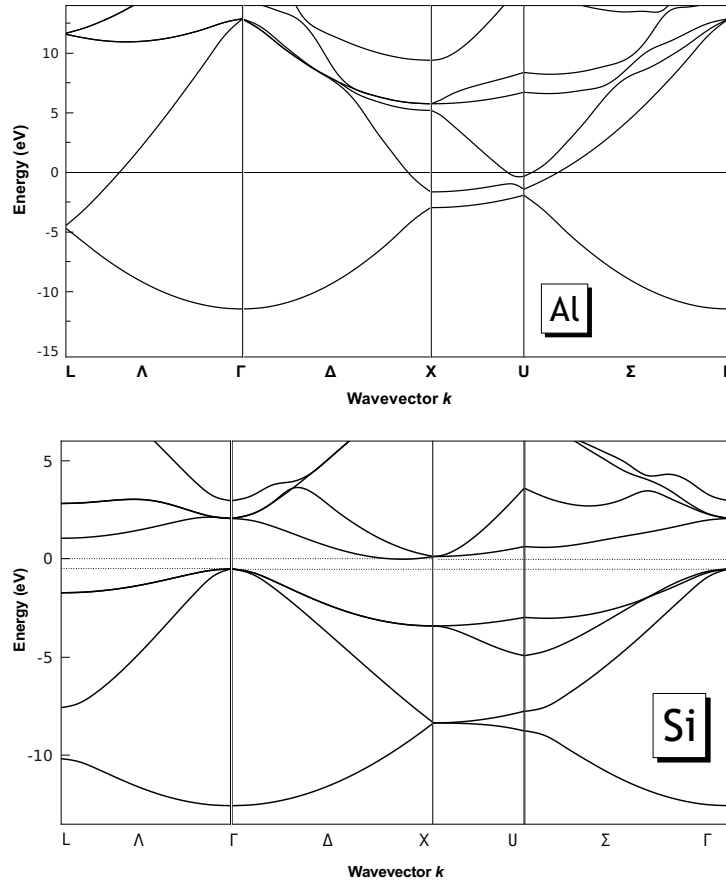
Fig. 12.1 Electronic band structures of bulk aluminum and silicon, calculated in the LDA. [Figure courtesy of A. Leonardo.]

$$\left[-\frac{\nabla^2}{2} + v_s^0[n_0](\mathbf{r}) \right] \varphi_{j\mathbf{k}}^0(\mathbf{r}) = \varepsilon_{j\mathbf{k}} \varphi_{j\mathbf{k}}^0(\mathbf{r}) \,, \tag{12.1}$$

where the Kohn–Sham effective potential has the same periodicity as the nuclear potential, i.e., $v_s^0(\mathbf{r} + \mathbf{R}) = v_s^0(\mathbf{r})$. The Kohn–Sham orbitals of the ground state of the solid satisfy Bloch's theorem and can be written in the form of modulated plane waves:

$$\varphi_{j\mathbf{k}}^0(\mathbf{r}) = e^{i\mathbf{k}\cdot\mathbf{r}} u_{j\mathbf{k}}^0(\mathbf{r}) \,. \tag{12.2}$$

Here, j is the band index, $\mathbf{k}$ is the wave vector or crystal momentum, and $u_{j\mathbf{k}}^0(\mathbf{r})$ is a lattice-periodic function, also known as a Bloch function.

The Kohn–Sham energy eigenvalues $\varepsilon_{j\mathbf{k}}$ define the band structure of the system. Let us consider two examples. Figure 12.1 shows the band structures of aluminum, a simple metal, and of silicon, a semiconductor (the calculations were done in the LDA using the ABINIT code; see Appendix O).

From the band structure, one can immediately distinguish metals and insulators: in an insulator, all bands are either completely filled or completely empty, and the highest occupied and the lowest unoccupied state are separated by a gap. By contrast, metals have one or more unfilled band, where the highest occupied states define the Fermi surface. The band gap and Fermi energy are marked by horizontal lines in Fig. 12.1.

To clarify the physical meaning of the Kohn–Sham band structure, let us keep in mind that the basic theorems of DFT guarantee that eqn (12.1) produces the exact ground-state density and with it all observables that are expressible as functionals of n_0 (provided, of course, the exact xc functional is used). In the case of solids, the ground-state observables of interest are, for instance, cohesive energies, lattice constants, and lattice vibrational frequencies. But the band structure itself has no rigorous meaning in DFT, not even with the exact v_{xc}^0, just as in the case of the Kohn–Sham energies of atoms and molecules. This has several important implications:

- The Kohn–Sham Fermi surface in a metal is, in general, not the same as the exact Fermi surface (Mearns, 1988).
- The Kohn–Sham band gap $E_{g,s}$ in an insulator is not the same as the fundamental band gap E_g (see the definitions and discussion in Section 2.2.3).
- The differences $\varepsilon_{j\mathbf{k}} - \varepsilon_{j'\mathbf{k}'}$ between the Kohn–Sham single-particle energies do not in general correspond to actual intraband or interband transitions of the many-body system, although they are often interpreted as such.

In spite of all this, the Kohn–Sham band structure is the essential first step in calculating the excitation properties of solids, and just as for atoms and molecules, the choice of approximation for the xc potential can make an important difference.

In practice, calculating the DFT band structure of a solid means that one has to choose from among a large number of computational approaches which differ in their use of basis sets and pseudopotentials (Appendix O gives a list of some popular computer codes). For an introduction to the various practical methods of electronic-structure calculations for solids see, for example, Martin (2004).

12.1.2   Linear response in periodic systems

We begin by considering eqn (7.75), transformed into the frequency domain, which expresses the density–density response function of an interacting system, χ, in terms of the response function of the Kohn–Sham system χ_s and the Hartree and xc kernels:

$$
\chi(\mathbf{r},\mathbf{r}',\omega) = \chi_s(\mathbf{r},\mathbf{r}',\omega)
$$
$$
+ \int d^3x \int d^3x'\, \chi_s(\mathbf{r},\mathbf{x},\omega) \left\{ \frac{1}{|\mathbf{x}-\mathbf{x}'|} + f_{xc}(\mathbf{x},\mathbf{x}',\omega) \right\} \chi(\mathbf{x}',\mathbf{r}',\omega). \quad (12.3)
$$

In lattice-periodic systems the translational symmetry requires that

$$
\chi(\mathbf{r},\mathbf{r}',\omega) = \chi(\mathbf{r}+\mathbf{R},\mathbf{r}'+\mathbf{R},\omega), \quad (12.4)
$$

where $\mathbf{R}$ is a lattice vector (similar relations are valid for χ_s and f_{xc}). We can Fourier analyze $\chi(\mathbf{r},\mathbf{r}',\omega)$ and obtain (Hanke, 1978; Gurtubay *et al.*, 2005)

$$
\chi(\mathbf{r},\mathbf{r}',\omega) = \frac{1}{\mathcal{V}} \sum_{\mathbf{k}\in\text{BZ}} \sum_{\mathbf{G},\mathbf{G}'} e^{-i(\mathbf{k}+\mathbf{G})\cdot\mathbf{r}} e^{i(\mathbf{k}+\mathbf{G}')\cdot\mathbf{r}'} \chi(\mathbf{k}+\mathbf{G},\mathbf{k}+\mathbf{G}',\omega), \quad (12.5)
$$

where $\mathcal{V}$ is the crystal volume, $\mathbf{k}$ is a wave vector in the first Brillouin zone (BZ), and $\mathbf{G}$ and $\mathbf{G}'$ are reciprocal-lattice vectors. In the following we shall use the notation

$$\chi_{\mathbf{G}\mathbf{G}'}(\mathbf{k},\omega) = \chi(\mathbf{k}+\mathbf{G}, \mathbf{k}+\mathbf{G}',\omega) . \tag{12.6}$$

With this, eqn (12.3) can be transformed in the following way:

$$\chi_{\mathbf{G}\mathbf{G}'}(\mathbf{k},\omega) = \chi_{s\mathbf{G}\mathbf{G}'}(\mathbf{k},\omega)$$
$$+ \sum_{\mathbf{G}_1,\mathbf{G}_2} \chi_{s\mathbf{G}\mathbf{G}_1}(\mathbf{k},\omega) \left\{ v_{\mathbf{G}_1}(\mathbf{k})\delta_{\mathbf{G}_1\mathbf{G}_2} + f_{\mathrm{xc}\mathbf{G}_1\mathbf{G}_2}(\mathbf{k},\omega) \right\} \chi_{\mathbf{G}_2\mathbf{G}'}(\mathbf{k},\omega) , \tag{12.7}$$

where the Fourier transform of the 3D Coulomb potential is given by

$$v_{\mathbf{G}}(\mathbf{k}) = \frac{4\pi}{|\mathbf{k}+\mathbf{G}|^2} . \tag{12.8}$$

The Kohn–Sham response function (7.80) becomes

$$\chi_{s\mathbf{G}\mathbf{G}'}(\mathbf{k}) = \frac{1}{\mathcal{V}} \sum_{\mathbf{k}'\in\mathrm{BZ}} \sum_{j,l=1}^{\infty} \frac{f_{l\mathbf{k}+\mathbf{k}'} - f_{j\mathbf{k}'}}{\omega + \varepsilon_{j\mathbf{k}'} - \varepsilon_{l\mathbf{k}+\mathbf{k}'} + i\eta}$$
$$\times \int d^3r \, \varphi_{j\mathbf{k}'}^{0*}(\mathbf{r}) e^{-i(\mathbf{k}+\mathbf{G})\cdot\mathbf{r}} \varphi_{l\mathbf{k}+\mathbf{k}'}^0(\mathbf{r}) \int d^3r' \, \varphi_{l\mathbf{k}+\mathbf{k}'}^{0*}(\mathbf{r}') e^{i(\mathbf{k}+\mathbf{G}')\cdot\mathbf{r}'} \varphi_{j\mathbf{k}'}^0(\mathbf{r}'), \tag{12.9}$$

featuring the Kohn–Sham band structure and wave functions from eqn (12.1).

From the response function $\chi_{\mathbf{G}\mathbf{G}'}(\mathbf{k},\omega)$, one can calculate the microscopic charge-density fluctuations in a solid induced by a scalar perturbing potential:

$$n_{1\mathbf{G}}(\mathbf{k},\omega) = \sum_{\mathbf{G}'} \chi_{\mathbf{G}\mathbf{G}'}(\mathbf{k},\omega) v_{1\mathbf{G}'}(\mathbf{k},\omega) . \tag{12.10}$$

So far, so good—but how does this relate to any spectroscopic observables of a solid? To clarify this, we will have to take a step back and look at the dielectric properties.

12.1.3   The dielectric tensor

In optical spectroscopic experiments, solids are probed by light. The appropriate framework for discussing light–matter interactions is given by Maxwell's equations,

$$\nabla \cdot \mathbf{D} = n_f , \tag{12.11}$$

$$\nabla \times \mathbf{E} = -\frac{\partial \mathbf{B}}{\partial t} , \tag{12.12}$$

$$\nabla \cdot \mathbf{B} = 0 , \tag{12.13}$$

$$\nabla \times \mathbf{H} = \mathbf{j}_f + \frac{\partial \mathbf{D}}{\partial t} . \tag{12.14}$$

All fields ($\mathbf{D}$, $\mathbf{E}$, $\mathbf{B}$, and $\mathbf{H}$) and all source terms (the density of free charges n_f and the free current density $\mathbf{j}_f$) are functions of $(\mathbf{r},t)$. The magnetic fields $\mathbf{B}$ and $\mathbf{H}$ are related via the magnetic permeability tensor $\underline{\mu}$. We restrict ourselves here to

nonmagnetic materials, for which μ is very close to the unit tensor, and in the following we will simply replace **H** with **B** everywhere.

The situation is a bit more interesting when we look at the relationship between the electric displacement **D** and the total electric field **E**:

$$\mathbf{D}(\mathbf{r}, \omega) = \int d^3 r' \, \mathfrak{e}(\mathbf{r}, \mathbf{r}', \omega) \mathbf{E}(\mathbf{r}', \omega) , \tag{12.15}$$

where $\mathfrak{e}(\mathbf{r}, \mathbf{r}', \omega)$ is the nonlocal, frequency-dependent dielectric tensor. For a periodic solid we have, in analogy with eqn (12.10),

$$\mathbf{D}_{\mathbf{G}}(\mathbf{k}, \omega) = \sum_{\mathbf{G}'} \mathfrak{e}_{\mathbf{G}\mathbf{G}'}(\mathbf{k}, \omega) \mathbf{E}_{\mathbf{G}'}(\mathbf{k}, \omega) . \tag{12.16}$$

The physical meaning of the electric displacement **D** may not be immediately obvious, so let us try to get a better feeling for the dielectric response of a solid. A weak time-varying electric field induces a current response,

$$\mathbf{j}_1 = \mathfrak{g}\mathbf{E} , \tag{12.17}$$

where $\mathfrak{g}$ is the conductivity tensor, and we drop arguments for notational simplicity.[2] In first-order linear response, $\mathbf{j}_1$ is nothing but the rate of change with time of the induced dielectric polarization, $\mathbf{j}_1 = \partial \mathbf{P}/\partial t$, where

$$\mathbf{D} = \epsilon_0 \mathbf{E} + \mathbf{P} , \tag{12.18}$$

and ϵ_0 is the vacuum permittivity (see Appendix A). Thus, we find that the dielectric and conductivity tensors are related as follows:

$$\mathfrak{e} = \epsilon_0 \mathbb{1} + \frac{i}{\omega} \, \mathfrak{g} . \tag{12.19}$$

$\mathfrak{e}$ and $\mathfrak{g}$ therefore contain similar physical information but, as we shall see shortly, for the present purposes it is more convenient to work with the dielectric tensor.

12.1.4   The macroscopic dielectric function

For comparison with experiment, one is usually interested in macroscopic quantities, i.e., quantities which are defined as averages over the unit cell. For instance, the macroscopic limit of eqn (12.16) is defined as

$$\mathbf{D}_{\mathrm{mac}}(\omega) = \mathfrak{e}_{\mathrm{mac}}(\omega)\mathbf{E}_{\mathrm{mac}}(\omega) . \tag{12.20}$$

An important observation from eqn (12.16) is that the microscopic $\mathfrak{e}_{\mathbf{G}\mathbf{G}'}(\mathbf{k}, \omega)$ is in general nondiagonal in **G** and **G**′, for inhomogeneous systems. Therefore, even a uniform external field will induce nonuniform microscopic fluctuations in the solid; these are called *local-field effects*. As a consequence, the macroscopic $\mathfrak{e}_{\mathrm{mac}}(\omega)$ cannot be

---

[2]With all arguments explicitly written, eqn (12.17) looks similar to eqn (12.16).

calculated directly; instead, one must take a detour via microscopic linear-response theory. Otherwise, local-field effects would not be properly included.

If the system were homogeneous in real space, i.e., a function of $\mathbf{r} - \mathbf{r}'$ rather than $\mathbf{r}$ and $\mathbf{r}'$ individually, taking the macroscopic limit would be easy:

$$\mathfrak{e}^{\text{hom}}_{\text{mac}}(\omega) = \lim_{q \to 0} \mathfrak{e}^{\text{hom}}(\mathbf{q}, \omega) \tag{12.21}$$

(for a homogeneous system, we can of course replace $\mathbf{k} + \mathbf{G}$ by $\mathbf{q}$). The dielectric tensor of a homogeneous system can be separated into a longitudinal and a transverse part (Pines and Nozières, 1966):

$$\mathfrak{e}^{\text{hom}}(\mathbf{q}, \omega) = \epsilon_L^{\text{hom}}(\mathbf{q}, \omega) \hat{q} \hat{q}^{\text{T}} + \epsilon_T^{\text{hom}}(\mathbf{q}, \omega) \left(\mathbb{1} - \hat{q} \hat{q}^{\text{T}} \right) , \tag{12.22}$$

where $\hat{q}$ is a unit vector along $\mathbf{q}$ and $\hat{q}^{\text{T}}$ is its transpose. In the macroscopic limit, we have $\epsilon_L^{\text{hom}}(0, \omega) = \epsilon_T^{\text{hom}}(0, \omega)$.

Things are not so simple in the inhomogeneous case. The reason is that the local-field effects continue to make their presence felt in the macroscopic dielectric constant. In the following, we shall restrict the discussion to crystals with *cubic symmetry*,[3] since this leads to the considerable simplification that the dielectric tensor becomes isotropic in the long-wavelength limit and one can carry out a decomposition into longitudinal and transverse components similar to that for the homogeneous case. It can then be shown that the macroscopic dielectric constant[4] is given by

$$\epsilon_{\text{mac}}(\omega) = \lim_{k \to 0} \left[\epsilon_{\mathbf{G}\mathbf{G}'}^{-1}(\mathbf{k}, \omega) \Big|_{\substack{\mathbf{G}=0 \\ \mathbf{G}'=0}} \right]^{-1} , \tag{12.23}$$

where $\epsilon_{\mathbf{G}\mathbf{G}'}(\mathbf{k}, \omega)$, the longitudinal component of the dielectric tensor for the cubic system, is often called the dielectric matrix.

We can now make a connection to the TDDFT response formalism of Section 12.1.2. In analogy with eqn (12.15), the scalar dielectric function is defined as

$$v_1(\mathbf{r}, \omega) = \int d^3r' \, \epsilon(\mathbf{r}, \mathbf{r}', \omega) \left[v_1(\mathbf{r}', \omega) + \int d^3r'' \frac{n_1(\mathbf{r}'', \omega)}{|\mathbf{r}' - \mathbf{r}''|} \right] . \tag{12.24}$$

From this, we obtain

$$\epsilon^{-1}(\mathbf{r}, \mathbf{r}', \omega) = \delta(\mathbf{r} - \mathbf{r}') + \int d^3r'' \frac{\chi(\mathbf{r}'', \mathbf{r}', \omega)}{|\mathbf{r} - \mathbf{r}''|} , \tag{12.25}$$

and for a periodic system we have

$$\epsilon_{\mathbf{G}\mathbf{G}'}^{-1}(\mathbf{k}, \omega) = \delta_{\mathbf{G}\mathbf{G}'} + v_{\mathbf{G}}(\mathbf{k}) \chi_{\mathbf{G}\mathbf{G}'}(\mathbf{k}, \omega) . \tag{12.26}$$

Let us now come back to the macroscopic dielectric constant. In Appendix M it is shown that $\epsilon_{\text{mac}}(\omega)$ takes on the following form (Onida *et al.*, 2002; Botti *et al.*, 2007):

---

[3]For a calculation of the macroscopic dielectric tensor without imposing cubic symmetry, see Del Sole and Fiorino (1984).

[4]Needless to say, the so-called dielectric "constant" is really a function of frequency.

$$\epsilon_{\mathrm{mac}}(\omega) = 1 - \lim_{k \to 0} v_0(\mathbf{k}) \bar{\chi}_{00}(\mathbf{k}, \omega) \,. \tag{12.27}$$

Here, $\bar{\chi}_{\mathbf{GG}'}(\mathbf{k}, \omega)$ differs from the full response function $\chi_{\mathbf{GG}'}(\mathbf{k}, \omega)$, as defined in eqn (12.7), in the following way: instead of using the full Coulomb interaction $v_{\mathbf{G}}(\mathbf{k})$ [see eqn (12.8)], it uses the modified Coulomb interaction

$$\bar{v}_{\mathbf{G}}(\mathbf{k}) = \begin{cases} 0 & \text{for } \mathbf{G} = 0 \,, \\ \dfrac{4\pi}{|\mathbf{k} + \mathbf{G}|^2} & \text{for } \mathbf{G} \neq 0 \,, \end{cases} \tag{12.28}$$

in which the long-range part $v_0(\mathbf{k}) = 4\pi/k^2$ has been left out. This seemingly small modification will later turn out to be quite important.

In the optical spectroscopy of materials, a central quantity is the complex refractive index $\widetilde{n}$, defined as (Yu and Cardona, 2010)

$$\epsilon_{\mathrm{mac}}(\omega) = \widetilde{n}^2 \,. \tag{12.29}$$

The real and imaginary parts of $\widetilde{n}$ give the usual refractive index n and the extinction coefficient κ, so that

$$\Re \epsilon_{\mathrm{mac}} = n^2 + \kappa^2 \,, \tag{12.30}$$

$$\Im \epsilon_{\mathrm{mac}} = 2n\kappa \,. \tag{12.31}$$

The extinction coefficient κ is proportional to the optical absorption coefficient; therefore, optical absorption spectra are essentially determined by $\Im \epsilon_{\mathrm{mac}}(\omega)$.

12.2 Spectroscopy of density fluctuations: plasmons

In this section, we shall consider excitations in periodic solids caused by longitudinal electric fields related to scalar perturbing potentials. These excitations are associated with fluctuations of the induced charge density, hence the name density-fluctuation excitations (Pines and Nozières, 1966).

According to the fluctuation–dissipation theorem (see Section 7.1.4), the dissipated energy follows from the imaginary part of the density–density response function. Calculating $\chi(\mathbf{r}, \mathbf{r}', \omega)$ for the material under consideration will therefore give access to its excitation spectrum, and will allow us to describe experimental results from techniques such as electron energy loss spectroscopy (EELS) and inelastic X-ray scattering spectroscopy (IXSS).

12.2.1 The excitation spectrum of a homogeneous system

Let us begin by discussing the density excitation spectrum of a homogeneous electron liquid, which will also be a good model for nearly-free-electron systems such as alkali metals. The response function of the electron liquid is given by [see eqn (8.34)]

$$\chi(q, \omega) = \frac{\chi_0(q, \omega)}{1 - [v(q) + f_{\mathrm{xc}}(q, \omega)]\chi_0(q, \omega)} \,. \tag{12.32}$$

We must find those frequencies where $\chi(q, \omega)$ has poles. Two types of poles can be distinguished (see Fig. 7.2):

- A continuous distribution of poles, which coincides with that of the noninteracting response function $\chi_0(q, \omega)$. From the analytical structure of the Lindhard function[5]

$$\chi_0(q, \omega) = 2 \int \frac{d^3k}{(2\pi)^3} \frac{\theta(k_F - k) - \theta(k_F - |\mathbf{k} + \mathbf{q}|)}{\omega + k^2/2 - |\mathbf{k} + \mathbf{q}|^2/2 + i\eta} \, , \tag{12.33}$$

one finds that the continuum of single particle–hole excitations is defined by the condition

$$\frac{q^2}{2} - qk_F \leq \omega \leq \frac{q^2}{2} + qk_F \, . \tag{12.34}$$

- Collective plasmon excitations, determined by the condition

$$1 - [v(q) + f_{\mathrm{xc}}(q, \Omega)]\chi_0(q, \Omega) = 0 \, . \tag{12.35}$$

Solution of eqn (12.35) gives the plasmon dispersion relation $\Omega(q)$. In practice this must be done numerically, but we can get an approximate analytic solution which holds for small values of q. Using the small-q expansion of the real part of the Lindhard function (Fetter and Walecka, 2003)

$$\Re\chi_0(q, \omega) = \frac{k_F^3}{3\pi^2} \frac{q^2}{\omega^2} \left[1 + \frac{3k_F^2 q^2}{5\omega^2} + \ldots \right], \tag{12.36}$$

we obtain the plasmon dispersion up to order q^2 in a straightforward manner:

$$\Omega(q) = \omega_{pl} \left[1 + \left(\frac{3k_F^2}{10\omega_{pl}^2} + \frac{1}{8\pi} f_{\mathrm{xc}}(0, \omega_{pl})\right) q^2\right], \tag{12.37}$$

where ω_{pl} is the classical plasma frequency (see Exercise 12.2). For small q, we see by comparison with the condition (12.34) that the plasmon lies outside the single-particle–hole continuum. The only source of plasmon damping is therefore the imaginary part of the xc kernel. As we discussed in Chapter 10, the physical origin of the low-q plasmon damping is decay into multiple particle–hole excitations. A frequency-independent f_{xc} leaves the plasmon undamped.

Figure 12.2 shows the plasmon dispersion of a homogeneous electron liquid with Wigner–Seitz radius $r_s = 4$, obtained from eqn (12.35) using various xc kernels (Tatarczyk *et al.*, 2001). The resulting plasmon frequencies have both real and imaginary parts. For xc kernels that are purely real (such as the ones used in Fig. 12.2), $\Im\Omega$ vanishes as long as $\Re\Omega$ is outside the single-particle–hole continuum: this means that the plasmon is undamped. As soon as the plasmon mode enters the particle–hole continuum, $\Im\Omega$ becomes finite, which indicates damping. The plasmon rapidly decays into incoherent particle–hole excitations—this is known as *Landau damping*.

There is an important technical point that must be observed when calculating damped plasmon modes. Namely, both f_{xc} (if frequency-dependent) and $\chi_0(q, \omega)$ must be evaluated for frequencies with a negative imaginary part, which requires analytic

---

[5]We restrict the discussion here to 3D systems. For lower-dimensional systems, see Giuliani and Vignale (2005).
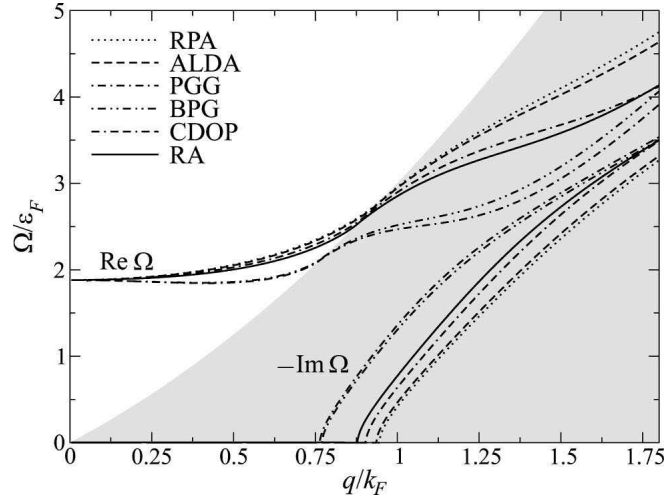
Fig. 12.2 Plasmon dispersion of a homogeneous electron liquid with $r_s = 4$, calculated from eqn (12.35) using various approximate xc kernels. The shaded region indicates the single-particle–hole continuum. [Reproduced with permission from APS from Tatarczyk *et al.* (2001), ©2001.]

continuation into the lower complex plane. In Section 8.3.4, we explained how to do this for $f_{\rm xc}(\omega)$. For the response function, one uses a similar approach and finds, for $\gamma < 0$,

$$\chi_0^{\rm lo}(q, \omega - i\gamma) = -\chi_0^{\rm up}(q, \omega + i\gamma) + 2i\Im\chi_0^{\rm up}(q, \omega - i\gamma).\qquad(12.38)$$

Here, $\chi_0^{\rm up}(q, z)$ is the usual Lindhard function, which is analytic in the upper complex plane, evaluated at the complex frequency z (Giuliani and Vignale, 2005). $\chi_0^{\rm lo}$ is the analytic continuation of $\chi_0^{\rm up}$ into the lower complex frequency plane.[6]

Coming back to Fig. 12.2, we find that all of the xc kernels under consideration give qualitatively similar results. In addition to the ALDA, these are the PGG kernel (11.68), the hybrid kernel given by Burke *et al.* (2002) (BPG), the kernel given by Corradini *et al.* (1998) (CDOP), and the kernel of Richardson and Ashcroft (1994) (RA).

12.2.2 Plasmon excitations in real metals

For simple metals whose valence electrons are delocalized and essentially free, the plasmon dispersion of the homogeneous electron liquid is a good approximation. However, for quantitative agreement with experimental data, it is necessary to include the electronic band structure and use the linear-response formalism for periodic systems that was presented in Section 12.1.2. Figure 12.3 shows results from such a calculation for the plasmon dispersions in bulk Al and Na (Quong and Eguiluz, 1993). We find that

---

[6]Notice that the first term on the right-hand side of eqn (12.38), $-\chi_0^{\rm up}(q, \omega + i\gamma)$, is the advanced response function, which is obtained similarly to the retarded response function, by replacing $\theta(\tau)$ by $\theta(-\tau)$ in eqn (7.14) and using the representation $\theta(-\tau) = -\lim_{\eta \to 0^+} (i/2\pi) \int d\omega' e^{-i\omega'\tau}/(\omega' - i\eta)$.
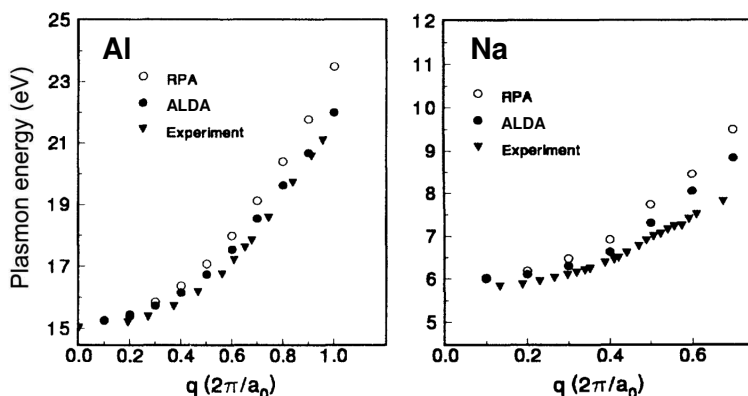
Fig. 12.3 Experimental and theoretical plasmon dispersions of bulk Al and Na. [Adapted with permission from APS from Quong and Eguiluz (1993), ©1993.]

the ALDA reproduces the experimental data very well, although the agreement for Na is perhaps not quite as good as for Al, particularly for larger wave vectors. Most of the remaining mismatch, however, can be assigned to band-structure effects known as core polarization, particularly for heavier alkali metals; xc effects beyond the ALDA play only a minor role (Ariasetiawan and Karlsson, 1994; Ku and Eguiluz, 1999).

These conclusions also hold for other metallic systems, such as the plasmon modes for the 3*d* transition metal scandium (Gurtubay *et al.*, 2005). Figure 12.4 shows a comparison of experimental data for and calculations of the dynamical structure factor for Sc in the frequency region where the valence electrons exhibit a large plasmon peak. The agreement of the calculations with experiment is excellent, reproducing details of the peak shape (which is quite different from the plasmon peaks of a homogenous electron liquid). The difference between the RPA and ALDA results is very minor. However, at higher energies, where IXSS probes the core excitations, the performance of the ALDA typically becomes less satisfactory: this is not surprising, since the underlying core states tend to be not very accurately described with the LDA.

These selected results are characteristic of the performance of TDDFT for plasmons in metals. The fact that the ALDA works well for collective excitations in gapless systems is not surprising at all, since it is based on the (gapless) homogeneous electron liquid as a reference system. We will see below that the ALDA encounters some fundamental problems in extended systems with a gap. To summarize:

> Plasmons in metallic systems are very well described by TDDFT even at the level of the ALDA. Plasmons can essentially be viewed as a classical phenomenon, in which a delocalized, nearly uniform electron distribution moves collectively with respect to a positive background. Therefore, the qualitative behavior of plasmons is already captured by the RPA, and adiabatic xc effects give only relatively minor corrections.
>
> To capture intrinsic plasmon damping caused by multiple particle–hole excitations, dynamical xc effects beyond the adiabatic approximation are essential.
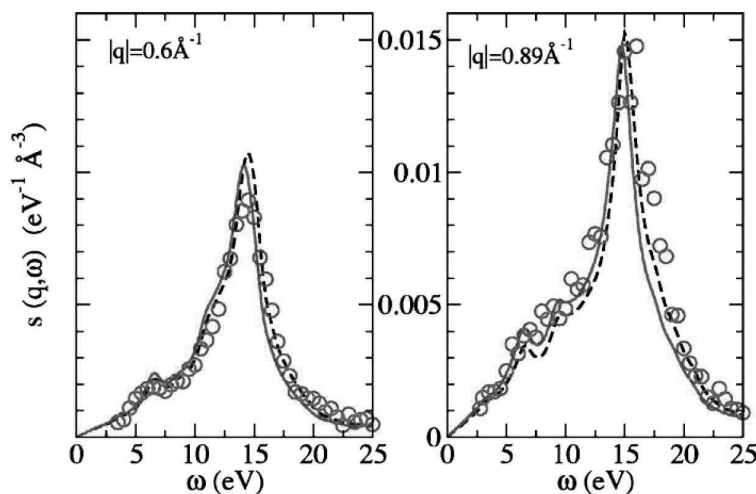
Fig. 12.4 Dynamical structure factor $S(\mathbf{q},\omega)$ of bulk scandium, calculated with the RPA (dashed line) and the ALDA (solid line), and compared with experimental IXSS data. [Reproduced with permission from APS from Gurtubay *et al.* (2005), ©2005.]

12.3   Optical absorption and excitons

In the previous section, we saw that TDDFT at its most basic level works very well for collective plasmon excitations in metallic systems. Now we will take a look at insulators and semiconductors, where things will turn out to be quite different. Insulators and semiconductors are characterized by the presence of a band gap, and interband optical excitations and their spectral features are strongly influenced by the presence of *excitons*. As we will see, excitons can also be interpreted as collective excitations, but their description with TDDFT places much higher demands on the xc functional than does the description of plasmons in metals. This will be explained in the following, and we will present successful TDDFT strategies for excitonic effects.

12.3.1   Excitons: basic models

An exciton may be defined as a bound electron–hole pair, created by some excitation process, such as absorption of a photon. The most basic model is illustrated in Fig. 12.5. An electron is promoted from the valence into the conduction band, leaving behind a hole. But the electron and the hole are not independent of each other: they feel their mutual Coulomb attraction and thus form an electron–hole pair. Owing to the reduced effective mass and the screening by the crystal background, the pair is only loosely bound and can extend over many lattice constants. This scenario is known as a *Mott–Wannier exciton*, and typically occurs in systems with relatively low band gaps.[7]

---

[7]The other extreme, in which excitons are strongly bound and the electron–hole pair essentially resides at the same atomic site, is known as a *Frenkel exciton*. This type of exciton is very important in ionic crystals and organic materials, but here we will focus more on the Mott–Wannier case.
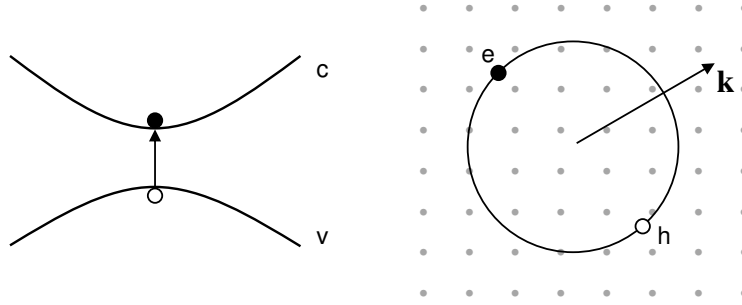
Fig. 12.5 Left: in a single-particle picture, an interband excitation in an insulator promotes an electron from the valence into the conduction band, leaving behind a hole. Right: in the Mott–Wannier model, an exciton is a bound electron–hole pair moving through the crystal.
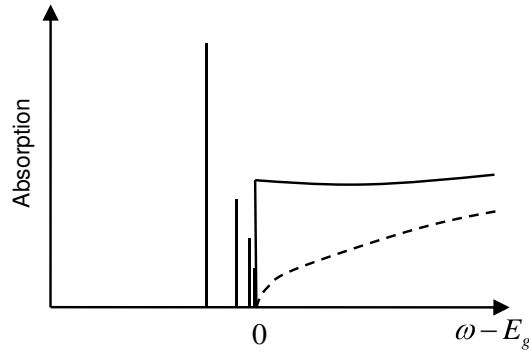

Fig. 12.6 Schematic optical absorption spectrum of a direct-band-gap insulator in the region of the band edge. Dashed line: independent-particle picture. Full lines: modified spectrum due to excitonic interactions.

The binding energy of a Mott–Wannier exciton can be estimated in a straightforward manner. Within a two-band model and using the effective-mass approximation (see Appendix K), the electron–hole pair represents a two-body system, and the center-of-mass and relative motion can be treated separately. The relative motion is described by the following one-body Schrödinger equation, known as the Wannier equation:

$$\left(-\frac{\hbar^2 \nabla^2}{2m_{eh}} - \frac{e^2}{\epsilon_r r}\right) \phi_n(\mathbf{r}) = E_n \phi_n(\mathbf{r}) .\tag{12.39}$$

Here, we depart from our usual convention of employing atomic units and explicitly indicate the fundamental constants (see also Appendix A.2). Equation (12.39) looks just like the Schrödinger equation for a hydrogen atom, except that the free-electron charge is reduced by the dielectric constant ϵ_r of the background crystal, and the free-electron mass is replaced by the reduced effective electron–hole mass, $m_{eh}^{-1} = m_e^{-1} + m_h^{-1}$.
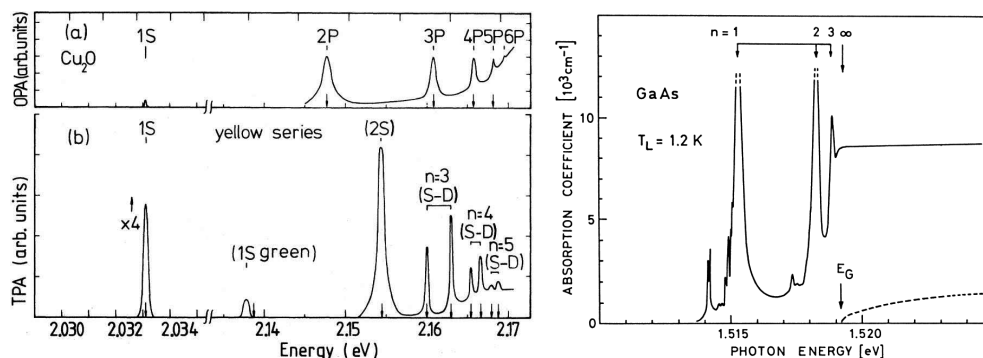
Fig. 12.7 Left: one-photon (top) and two-photon (bottom) absorption spectra of Cu_2O. [Reproduced with permission from APS from Uihlein *et al.* (1981), ©1981.] Right: high--resolution absorption spectrum of GaAs. [Reproduced with permission from Springer from Ulbrich (1985), ©1985.]

The Wannier equation can also be derived starting from a many-body Hamiltonian for interacting electrons within the TDHF approximation (Schäfer and Wegener, 2002; Haug and Koch, 2004). In addition to the effective-mass approximation and considering only two bands, one makes the assumption that the Coulomb potential varies only by a small amount over one unit cell. Whether this assumption is justified depends on the system under consideration.[8]

Solving the Wannier equation (12.39) gives a Rydberg series of excitonic bound-state solutions and a continuum. The optical absorption spectrum of an insulator is strongly modified by the presence of the excitonic interactions, as illustrated schematically in Fig. 12.6. In a single-particle picture, absorption sets in for photon energies above the band gap E_g, and the shape of the absorption spectrum is given by the joint density of states of the valence and conduction bands: close to the band edge, the absorption increases as the square root of the photon energy.

The optical spectrum in the presence of excitons shows two types of modifications:

- Bound excitons appear as discrete lines *below* the band edge E_g and form a Rydberg series with energies

$$E_n = -E_0^{\text{exc}}/n^2 , \tag{12.40}$$

  measured relative to E_g (see Fig. 12.6). Here, E_0^{exc} is the lowest exciton binding energy, given by $E_0^{\text{exc}} = \hbar^2/2m_{eh}(a_0^{\text{exc}})^2$, and the exciton Bohr radius is given by $a_0^{\text{exc}} = \hbar^2\epsilon_r/e^2 m_{eh}$.

- Above the band edge, the absorption is strongly enhanced owing to the excitonic continuum states. This effect can be quantified by the so-called Sommerfeld enhancement factor (Davies, 1998).

Figure 12.7 shows experimental data for the excitonic Rydberg series in Cu_2O and GaAs, confirming the general features of excitonic spectra discussed above.

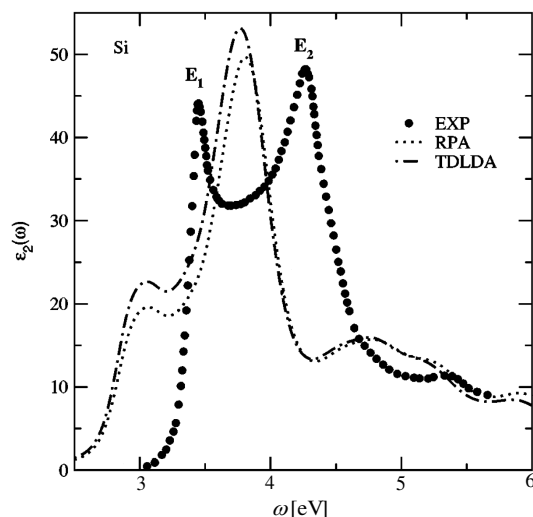[8]It is certainly not true for Frenkel excitons.

Fig. 12.8 Imaginary part of the dielectric constant of Si. The RPA and ALDA give a red-shifted spectrum and fail to reproduce the excitonic peak at the absorption edge. [Adapted with permission from APS from Botti *et al.* (2004), ©2004.]

12.3.2   TDDFT and the optical absorption of insulators

Failure of local approximations.   Figure 12.8 shows the imaginary part of the dielectric constant of Si in the region where direct interband transitions set in.[9] The experimental data (Lautenschlager *et al.*, 1987) exhibit a characteristic double-peak structure above 3 eV. The peak labeled E_1 located right above at the band edge has excitonic character.

When the experimental data are compared with theoretical results obtained using the RPA and ALDA, two main problems are observed, namely, that the onset of absorption is redshifted by about half an eV, and the first excitonic peak is almost completely absent except for a weak shoulder (Onida *et al.*, 2002; Botti *et al.*, 2004). This observation is by no means an isolated case, but rather is very characteristic of the performance of TDDFT for optical absorption spectra of insulators: standard local and semilocal xc functionals universally fail to describe excitons, and underestimate the optical gap.

On the other hand, the spectral features (apart from the missing excitons) of many semiconductors and insulators can in fact be quite well reproduced if the wrong optical gap is corrected by hand and a rigid shift of the dielectric function is made (Kootstra *et al.*, 2000a, 2000b). As an example, the dielectric constant of ZnSe is shown in Fig. 12.9. After a rigid shift of the spectra of about 1 eV is made, the ALDA results agree nicely with experiment.

---

[9]Si is an indirect-band-gap semiconductor, which means that the conduction band minimum does not coincide with the valence band maximum in the BZ. Electronic transitions at the minimum energy would, however, require the assistance of phonons. A thorough discussion of the interband transitions in Si can be found in Lautenschlager *et al.* (1987).
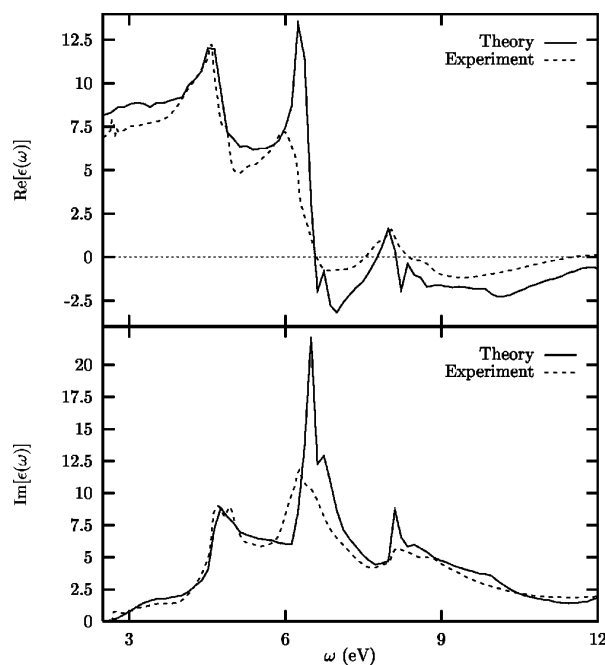
Fig. 12.9 Real and imaginary parts of the dielectric constant of ZnSe, calculated with the ALDA, and compared with the experimental data of Freeouf (1973). The calculated spectra were shifted by about 1 eV to correct for the underestimation of the optical gap. [Adapted with permission from APS from Kootstra *et al.* (2000*a*), ©2000.]

Since TDDFT is formally rigorous, it should in principle yield exact optical absorption spectra for insulators. Let us see what is required. Assume that we start from an exact ground-state calculation, which would therefore give the exact independent-particle spectrum. But now, the xc kernel $f_{\mathrm{xc}\mathbf{G}_1\mathbf{G}_2}(\mathbf{k},\omega)$ has to carry a heavy burden:

- it has to open the gap and shift the Kohn–Sham band edge to the true band edge;
- it has to cause an effective electron–hole attraction, leading to excitonic features in the spectrum.

It turns out that the xc kernel can be separated into a *quasiparticle* and an *excitonic* part,

$$f_{\mathrm{xc}} = f_{\mathrm{xc}}^{\mathrm{qp}} + f_{\mathrm{xc}}^{\mathrm{ex}}\,, \tag{12.41}$$

which are responsible for the opening of the gap and the excitonic effects. A formal justification of eqn (12.41) will be given in Section 13.3.2. For now, let us focus on the excitonic part.

Recall that the macroscopic dielectric constant $\epsilon_{\mathrm{mac}}(\omega)$ [see eqn (12.27)], requires the response function $\bar{\chi}_{00}(\mathbf{k},\omega)$ as input, which is obtained by replacing the full Coulomb interaction by the modified Coulomb interaction (12.28) in which the long-range ($\sim 1/k^2$) part has been taken out. In detail, we have

$$\bar{\chi}_{\mathbf{G}\mathbf{G}'}(\mathbf{k},\omega) = \chi_{s\mathbf{G}\mathbf{G}'}(\mathbf{k},\omega)$$
$$+ \sum_{\mathbf{G}_1,\mathbf{G}_2} \chi_{s\mathbf{G}\mathbf{G}_1}(\mathbf{k},\omega) \left\{ \bar{v}_{\mathbf{G}_1}(\mathbf{k})\delta_{\mathbf{G}_1\mathbf{G}_2} + f_{\text{xc}\mathbf{G}_1\mathbf{G}_2}(\mathbf{k},\omega) \right\} \bar{\chi}_{\mathbf{G}_2\mathbf{G}'}(\mathbf{k},\omega) . \quad (12.42)$$

Neglecting local-field effects, we therefore obtain

$$\bar{\chi}_{00}(\mathbf{k},\omega) \approx \frac{\chi_{s00}(\mathbf{k},\omega)}{1 - \chi_{s00}(\mathbf{k},\omega)f_{\text{xc}00}(\mathbf{k},\omega)} . \quad (12.43)$$

Now, notice that the Kohn–Sham noninteracting response function goes to zero as k^2 for small wave vectors:

$$\lim_{k\to 0} \chi_{s00}(\mathbf{k},\omega) \sim k^2 . \quad (12.44)$$

Therefore, the long-wavelength behavior of the modified response function $\bar{\chi}_{00}(\mathbf{k},\omega)$ will be the same as that of the Kohn–Sham response function, unless one uses an xc kernel that diverges as $1/k^2$. This explains the failure of the ALDA and other semilocal approximations:

> In local and semilocal approximations such as the ALDA, f_{xc} does not diverge but approaches a constant as $k \to 0$. Therefore, in these approximations, the only corrections to the Kohn–Sham single-particle absorption spectrum are via local-field effects, which are generally insufficient to cause excitonic interactions.

Simple approximate xc kernels for excitonic interactions. In Section 13.3, we shall discuss xc kernels derived from many-body theory which give an excellent description of the optical absorption spectra of insulators, including bound excitons. These kernels, however, are somewhat complicated. On the other hand, if one is content with the more modest goal of reproducing only certain features of the optical spectra, one can get away with much simpler approximations.

The simplest way to construct an xc kernel with the required long-range behavior is to put it in by hand:

$$f_{\text{xc}}^{\text{LR}}(\mathbf{r},\mathbf{r}') = -\frac{\alpha}{4\pi|\mathbf{r}-\mathbf{r}'|} , \quad (12.45)$$

the Fourier transform of which is $f_{\text{xc},\mathbf{G}\mathbf{G}'}^{\text{LR}}(q) = -\delta_{\mathbf{G}\mathbf{G}'}\alpha/|\mathbf{q}+\mathbf{G}|^2$ (Reining *et al.*, 2002; Botti *et al.*, 2004). The parameter α is material-dependent and related to the static dielectric constant. There also exists a frequency-dependent version (Botti *et al.*, 2005):

$$f_{\text{xc}}^{\text{LR}}(q,\omega) = -\frac{\alpha + \beta\omega^2}{q^2} . \quad (12.46)$$

As shown in Fig. 12.10, this xc kernel reproduces the main features of the double-peak structure in the optical spectrum of CdSe. The static xc kernel (12.45) does not work as well, but still performs much better than the ALDA.

12.3.3   Excitonic effects with TDDFT: a two-band model

To understand how excitonic effects are treated with TDDFT, it is helpful to consider a model which is kept as simple as possible. We will now develop such a model in analogy with the two-level system of Section 7.4.
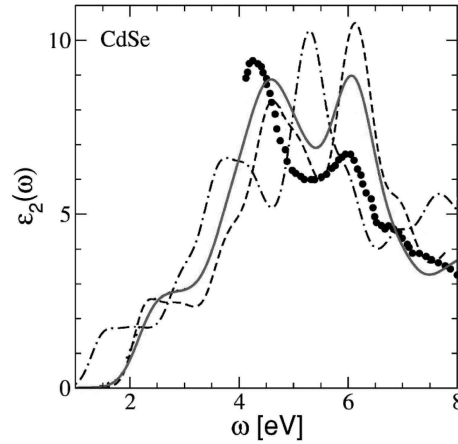
Fig. 12.10 Imaginary part of the macroscopic dielectric function for CdSe. Dots: experiment. Dotted–dashed line: ALDA. Dashed and full lines: f_{xc}^{LR} and $f_{xc}^{LR}(\omega)$, respectively [eqns (12.45) and (12.46)]. [Adapted with permission from APS from Botti *et al.* (2005), ©2005.]

Just as in atoms or molecules, the electron dynamics in a solid can be described in a TDKS scheme, with time-dependent single-particle orbitals $\varphi_{j\mathbf{k}}(\mathbf{r}, t)$, where j runs over the indices of the initially occupied bands. The system is assumed to start from the ground state, $\varphi_{j\mathbf{k}}(\mathbf{r}, t_0) = \varphi_{j\mathbf{k}}^0(\mathbf{r})$, where the Kohn–Sham Bloch functions follow from eqn (12.1). Since the $\varphi_{j\mathbf{k}}^0(\mathbf{r})$ form a complete set for each $\mathbf{k}$, we can expand the TDKS orbitals as follows:

$$\varphi_{j\mathbf{k}}(\mathbf{r}, t) = \sum_l c_{\mathbf{k}}^{jl}(t)\varphi_{l\mathbf{k}}^0(\mathbf{r}) \,. \tag{12.47}$$

The sum runs over all valence and conduction bands, including continuum states. In the following, the system interacts with an electromagnetic field in the dipole approximation. We define the density matrix $\rho_{j\mathbf{k}}^{lm}(t) = c_{\mathbf{k}}^{jl}(t)[c_{\mathbf{k}}^{jm}(t)]^*$, whose equation of motion is

$$i\frac{\partial}{\partial t}\rho_{j\mathbf{k}}(t) = [\mathbb{H}_{\mathbf{k}}(t), \rho_{j\mathbf{k}}(t)], \tag{12.48}$$

with the initial condition $\rho_{j\mathbf{k}}^{lm}(t_0) = \delta_{jl}\delta_{ml}$. The matrix elements of the Hamiltonian are

$$\begin{aligned} H_{\mathbf{k}}^{lm}(t) &= \frac{1}{\Omega} \int_\Omega d^3r \, \varphi_{l\mathbf{k}}^{0*}(\mathbf{r})H(t)\varphi_{m\mathbf{k}}^0(\mathbf{r}) \\ &= \varepsilon_{l\mathbf{k}}\delta_{lm} + \mathbf{E}(t) \cdot \mathbf{d}_{\mathbf{k}}^{lm} + \widetilde{v}_{H\mathbf{k}}^{lm}(t) + \widetilde{v}_{xc\mathbf{k}}^{lm}(t) \,, \end{aligned} \tag{12.49}$$

where Ω is the volume of the lattice unit cell, $\mathbf{E}(t)$ is the electric field amplitude, and the $\mathbf{d}_{\mathbf{k}}^{lm}$ are the dipole matrix elements. $\widetilde{v}_H(t) = v_H(t) - v_H^0$ denotes the dynamic part of the Hartree potential, and similarly for the xc part. The self-consistent solution of eqn (12.48), with the time-dependent density

$$n(\mathbf{r}, t) = 2 \sum_{j\mathbf{k}} \theta(E_F - \varepsilon_{j\mathbf{k}}) \sum_{lm} \rho_{j\mathbf{k}}^{lm}(t) \varphi_{l\mathbf{k}}^0(\mathbf{r}) \varphi_{m\mathbf{k}}^{0*}(\mathbf{r}) , \quad (12.50)$$

is equivalent to solving the TDKS equation for the solid, and is thus in principle exact.

To study optical excitation processes near the band gap, a two-band model is a reasonable and widely used approximation. We consider one valence and one conduction band, v and c, assumed to be nondegenerate. The index j of the density matrix $\rho_{j\mathbf{k}}^{lm}(t)$ refers to v and will be dropped in the following. Equation (12.48) then yields two equations for the two independent components $\rho_{\mathbf{k}}^{vv}$ and $\rho_{\mathbf{k}}^{vc}$:

$$\frac{\partial}{\partial t} \rho_{\mathbf{k}}^{vv}(t) = -2\Im \left\{ \left[\mathbf{E}(t) \cdot \mathbf{d}_{\mathbf{k}}^{cv} + \widetilde{v}_{H\mathbf{k}}^{cv} + \widetilde{v}_{xc\mathbf{k}}^{cv} \right] \rho_{\mathbf{k}}^{vc}(t) \right\} , \quad (12.51)$$

$$i\frac{\partial}{\partial t} \rho_{\mathbf{k}}^{vc}(t) = [\varepsilon_{\mathbf{k}}^v - \varepsilon_{\mathbf{k}}^c + \widetilde{v}_{H\mathbf{k}}^{vv}(t) + \widetilde{v}_{xc\mathbf{k}}^{vv}(t) - \widetilde{v}_{H\mathbf{k}}^{cc}(t) - \widetilde{v}_{xc\mathbf{k}}^{cc}(t)]\rho_{\mathbf{k}}^{vc}(t)$$
$$+ [\mathbf{E}(t) \cdot \mathbf{d}_{\mathbf{k}}^{vc} + \widetilde{v}_{H\mathbf{k}}^{vc}(t) + \widetilde{v}_{xc\mathbf{k}}^{vc}(t)][\rho_{\mathbf{k}}^{cc}(t) - \rho_{\mathbf{k}}^{vv}(t)] . \quad (12.52)$$

Notice that $\rho_{\mathbf{k}}^{vv} + \rho_{\mathbf{k}}^{cc} = 1$ and $\rho_{\mathbf{k}}^{vc} = \rho_{\mathbf{k}}^{cv*}$. Equations (12.51) and (12.52) are the TDDFT versions of the so-called *semiconductor Bloch equations* (Turkowski and Ullrich, 2008), which can be used to study the ultrafast carrier dynamics of semiconductors following pulsed excitations (Schäfer and Wegener, 2002; Haug and Koch, 2004).

To calculate excitonic binding energies, we drop the time-dependent external-field term and look for the eigenmodes of the system. In analogy with Section 7.4, we linearize eqn (12.52) (see Exercise 12.8), which gives

$$i\frac{\partial}{\partial t} \rho_{\mathbf{k}}^{vc}(t) = -\omega_{\mathbf{k}}^{cv} \rho_{\mathbf{k}}^{vc}(t) - \delta\widetilde{v}_{H\mathbf{k}}^{vc}(t) - \delta\widetilde{v}_{xc\mathbf{k}}^{vc}(t) . \quad (12.53)$$

Here, the $\omega_{\mathbf{k}}^{cv} = \varepsilon_{\mathbf{k}}^c - \varepsilon_{\mathbf{k}}^v$ are vertical single-particle interband transitions, which are indicated by bold arrows in Fig. 12.11. The linearized dynamical Hartree and xc potentials are denoted by $\delta\widetilde{v}_{H\mathbf{k}}^{vc}$ and $\delta\widetilde{v}_{xc\mathbf{k}}^{vc}$. The Hartree term causes only minor local-field corrections and does not lead to any excitonic binding.[10] We will therefore keep only the xc contribution.

Fourier transforming eqn (12.53) and the corresponding equation for $\rho_{\mathbf{k}}^{cv}(t)$ yields

$$\sum_{\mathbf{q}} \left[F_{\mathbf{kq}}^{vccv}(\omega)\rho_{\mathbf{q}}^{vc}(\omega) + F_{\mathbf{kq}}^{vcvc}(\omega)\rho_{\mathbf{q}}^{cv}(\omega) \right] = -(\omega + \omega_{\mathbf{k}}^{cv})\rho_{\mathbf{k}}^{vc}(\omega) , \quad (12.54)$$

$$\sum_{\mathbf{q}} \left[F_{\mathbf{kq}}^{cvcv}(\omega)\rho_{\mathbf{q}}^{vc}(\omega) + F_{\mathbf{kq}}^{cvvc}(\omega)\rho_{\mathbf{q}}^{cv}(\omega) \right] = (\omega - \omega_{\mathbf{k}}^{cv})\rho_{\mathbf{k}}^{cv}(\omega) , \quad (12.55)$$

where the matrix elements of the xc kernel are given by

$$F_{\mathbf{kq}}^{ijmn}(\omega) = \frac{2}{\Omega^2} \int_{\Omega} d^3r \int_{\Omega} d^3r' \, \psi_{i\mathbf{k}}^*(\mathbf{r})\psi_{j\mathbf{k}}(\mathbf{r}) f_{xc}(\mathbf{r}, \mathbf{r}', \omega)\psi_{m\mathbf{q}}^*(\mathbf{r}')\psi_{n\mathbf{q}}(\mathbf{r}') . \quad (12.56)$$

The $\mathbf{q}$-summation runs over the first BZ. Equations (12.54) and (12.55) represent an eigenvalue problem whose solutions are the exact exciton binding energies within the two-band model.

---

[10]Evidence for this is given in Fig. 12.8, where the RPA spectrum lacks any excitonic features.
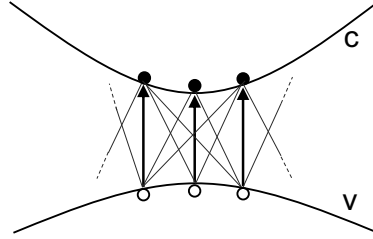
Fig. 12.11 Schematic representation of interband transitions in a two-band model. Vertical single-particle transitions with different wave vectors are coupled [see eqn (12.57)], which illustrates the collective nature of excitonic effects.

Typical exciton binding energies are much smaller than the band gap, i.e., $\omega + \omega_{\mathbf{k}}^{cv} \gg \omega - \omega_{\mathbf{k}}^{cv}$. We can therefore ignore the pole at negative ω, which is equivalent to the TDA. The result is the following eigenvalue equation:

$$\sum_{\mathbf{q}} \left[\omega_{\mathbf{q}}^{cv} \delta_{\mathbf{k}\mathbf{q}} + F_{\mathbf{k}\mathbf{q}}^{cvvc}(\omega) \right] \rho_{\mathbf{q}}^{cv}(\omega) = \omega \rho_{\mathbf{k}}^{cv}(\omega) . \tag{12.57}$$

The negative solutions of eqn (12.57), if they exist, can be interpreted as exciton binding energies relative to the conduction band edge (Turkowski *et al.*, 2009).

Equation (12.57) is the equivalent of the SPA for extended systems. For finite atomic or molecular systems, the SPA (7.159) involves only two discrete levels, as we saw in Chapter 7. Here, on the other hand, it involves two entire bands: solving eqn (12.57) requires diagonalization of a matrix in $\mathbf{k}$-space.[11] In other words, vertical single-particle excitations with different wave vectors are coupled, which clearly shows the collective nature of excitonic effects. This mixing in $\mathbf{k}$-space, caused by the matrix elements $F_{\mathbf{k}\mathbf{q}}^{cvvc}$ of the xc kernel, is represented by the thin lines in Fig. 12.11.

Table 12.1 shows some numbers for the simple bulk semiconductors GaAs and β-GaN, with a zincblende structure, and α-GaN, CdS, and CdSe, with a wurtzite structure. The experimental values[12] of the lowest exciton binding energies are all in the range of a few meV, which indicates weakly bound Mott–Wannier excitons.

The TDDFT calculations were carried out using the PGG x-only kernel (11.67), which has the required long spatial range and should therefore produce bound excitons. Indeed, solving eqn (12.57) with this xc kernel produces a single negative eigenvalue (except for CdSe, where no exciton is found). However, no excitonic Rydberg series is produced, and the binding energies are somewhat too small compared with experiment.[13] Some improvement is achieved by extending the calculation to a three-band model, except for CdS and CdSe, where the exciton remains significantly underbound.

These results provide a proof of concept that TDDFT, even with relatively simple xc kernels, is capable of producing bound excitons. Later, in Section 13.3, we will discuss xc kernels from many-body theory which give more accurate results.

---

[11]The dimension of this matrix depends on the number of $\mathbf{k}$-points one chooses in practice.

[12]See Turkowski *et al.* (2009) for references.

[13]The results in Table 12.1 (courtesy of A. Leonardo) were obtained using LDA band structures calculated with ABINIT, and carefully checking convergence with the number of $\mathbf{k}$-points.

Table 12.1 Lowest exciton binding energies (in meV) for III–V and II–VI bulk semiconductors, comparing experiment and TDDFT calculations with results obtained using the PGG x-only kernel (11.67).

	PGG (2-band)	PGG (3-band)	experiment
GaAs	2.4	7.1	3.27
β-GaN	7.6	24.0	26.0
α-GaN	9.6	18.5	20.4
CdS	5.5	6.6	28.0
CdSe	—	1.1	15.0

To conclude this section, let us return to the Wannier equation (12.39) and ask whether there is a TDDFT counterpart for it. This means that we need to transform eqn (12.57) from reciprocal into real space. Since $\rho_{\mathbf{k}}^{cv}$ is periodic in reciprocal space, its Fourier transform is $\rho(\mathbf{R}, \omega) = \sum_{\mathbf{k}} e^{-i\mathbf{k}\cdot\mathbf{R}} \rho_{\mathbf{k}}^{cv}(\omega)$, where $\mathbf{R}$ is a direct-lattice vector. Similarly, we define the nonlocal effective electron–hole interaction as the Fourier transform of the matrix elements of the xc kernel:

$$V_{eh}(\mathbf{R}, \mathbf{R}', \omega) = \sum_{\mathbf{k},\mathbf{q}} e^{-i\mathbf{k}\cdot\mathbf{R}} F_{\mathbf{k}\mathbf{q}}^{cvvc}(\omega) e^{i\mathbf{q}\cdot\mathbf{R}'}. \tag{12.58}$$

From the point of view of a Wannier exciton, which extends over many lattice constants, $\mathbf{R}$ can be approximated as a continuous variable. We assume a direct-band-gap material with a reduced effective electron–hole mass m_{eh}. After a few steps (see Exercise 12.9), one ends up with the TDDFT version of the Wannier equation (12.39),

$$\left[-\frac{\nabla^2}{2m_{eh}} - E_i \right] \rho_i(\mathbf{r}) + \int_{\substack{\text{all} \\ \text{space}}} d^3r' \, V_{eh}(\mathbf{r}, \mathbf{r}', \omega) \rho_i(\mathbf{r}') = 0 \,, \tag{12.59}$$

where $\omega = E_{g,s} + E_i$, and $E_{g,s}$ is the Kohn–Sham band gap. The ith exciton binding energy E_i is measured with respect to the conduction band edge, and $\rho_i(\mathbf{r})$ is analogous to the excitonic wave functions $\phi(\mathbf{r})$ of eqn (12.39). We thus see that in the TDDFT Wannier equation the screened Coulomb interaction $-e^2/\epsilon_r r$ is replaced by the nonlocal, frequency-dependent electron–hole interaction $V_{eh}(\mathbf{r}, \mathbf{r}', \omega)$.

> Exciton binding in TDDFT is caused by dynamical xc effects, which lead to a coupling of independent single-particle interband transitions. Out of these coupled transitions, the excitons emerge as collective excitations whose energies are lower than the single-particle gap.
>
> The traditional Wannier exciton picture consists of an electron–hole pair bound by a dielectrically screened Coulomb interaction. In TDDFT, the latter is replaced by a nonlocal, frequency-dependent effective electron–hole interaction. For this interaction to be attractive, the xc kernel must have a long spatial range. Semilocal xc kernels (obtained from the ALDA or GGAs) do not give any exciton binding.

12.4   TDCDFT in periodic systems

12.4.1   Existence theorems

Let us now address an important fundamental question: is TDDFT at all applicable to the response in periodic solids? Our presentation of the Runge–Gross and van Leeuwen existence theorems in Chapter 3 was limited to finite systems such as isolated atoms or molecules. Therefore, it is not clear a priori whether these basic existence theorems continue to hold if the system is periodic in space.

Recall that the Runge–Gross theorem establishes a one-to-one correspondence between time-dependent scalar potentials and time-dependent densities, for given initial states. A key step in the proof, where the size of the system comes in, is eqn (3.43), in which a surface integral needs to vanish. As we discussed, this is the case if the potential arises from finite, normalizable external charge distributions. Does this automatically preclude periodic solids? Fortunately not: the Runge–Gross theorem does apply to periodic solids, too (Maitra *et al.*, 2003; Botti *et al.*, 2007).

To see this, consider a one-dimensional extended system for simplicity, and let the external potential be periodic with a wavelength λ. The surface can then be chosen to be two points whose separation is given by the lattice constant of the (unperturbed) periodic system, multiplied by the wavelength λ of the time-dependent perturbation. The integrand of the surface integral is the same at the two points, and the integral vanishes. This argument can be readily generalized to two and three dimensions.

However, there are situations where this doesn't work, and the unique potential–density mapping breaks down. Following Maitra *et al.* (2003), let us consider an example with a special geometry which allows us to study the effect of uniform electric fields. Figure 12.12 shows a ring-shaped system which is threaded by a time-dependent magnetic field along the axis of the ring. The associated time-varying vector potential is in the azimuthal direction (along the circumference of the ring). It induces a uniform time-dependent electric field that is also in the azimuthal direction.

Assume that the electrons in the ring are initially in the ground state, and that their density is homogeneous along the azimuthal direction of the ring. Turning on a time-dependent electric field which has no radial component will set the electrons collectively in motion *without changing their density*. See Exercise 12.10 for an explicit one-electron example.

In general, turning on a uniform electric field in a (1D) system with a periodic potential produces a density and current response that is also periodic. All components of the current density at a reciprocal-lattice vector $G \neq 0$ are determined by

$$j_G(\omega) = \omega n_G(\omega)/G \,, \tag{12.60}$$

thanks to the continuity equation. But the uniform ($G = 0$) component of the current response, i.e., the macroscopic current, is undetermined by the time-dependent periodic density. This means that the proof of the Runge–Gross theorem does not apply to the case of uniform electric fields in periodic systems.[14]

---

[14]There is a static analog to this statement, whereby ground-state DFT is not sufficient to describe the macroscopic polarization in insulating periodic solids (Gonze *et al.*, 1995). From the point of
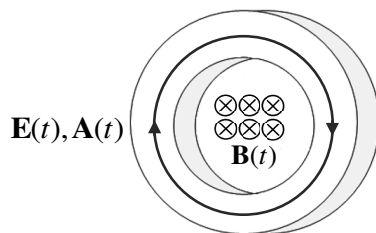
Fig. 12.12 A time-dependent magnetic field along the axis of a ring causes a time-dependent vector potential along the circumference of the ring. This, in turn, induces a uniform time-dependent azimuthal electric field.

If, however, the currents are used as basic variables, the existence theorems of TDCDFT (Section 10.3.2) guarantee the desired correspondence between electric fields (vector potentials) and currents. At variance with the proofs of the Runge–Gross and van Leeuwen theorems, the basic existence proof of TDCDFT does not require the currents to vanish at infinity, and thus immediately carries over to extended systems, including systems with uniform fields and currents (Vignale, 2004).

> The Runge–Gross theorem of TDDFT holds for extended systems and guarantees a one-to-one correspondence between periodic densities and potentials. However, the response to a uniform electric field cannot be treated with TDDFT, since it involves a uniform current which is left undetermined by the time-dependent periodic density. In this case, TDCDFT is required.

12.4.2 Performance of the VK functional for bulk metals and insulators

As we discussed in Chapter 10, the VK functional of TDCDFT represents a local nonadiabatic approximation to the tensor xc kernel. Because of the ultranonlocality of nonadiabatic xc effects, this means that the corresponding scalar xc kernel has a long spatial range. We show this explicitly in Appendix J.

The implicit long-rangedness of the VK functional immediately suggests that it could be useful for those problems in extended systems where local functionals fail. Indeed, we saw in Section 10.5 that it gives very good results for the static polarizability of polymers and for the stopping power in metals. Results were also good for the linewidths of plasmon excitations, but not so good for atomic and molecular excitation energies. This raises the question of how the VK functional performs for response properties of bulk metals and insulators: does it produce excitons?

Earlier work (de Boeij *et al.*, 2001) seemed to indicate that the VK functional does indeed give good agreement with experimental optical absorption spectra of insulators and semiconductors—though at the cost of using an empirical prefactor in the functional. However, the initial optimism waned when subsequent studies revealed

---

view of TDCDFT, such a polarization can be understood as an infinite memory effect, because it originated in the distant past owing to the flow of currents when the field was switched on (Maitra *et al.*, 2003).
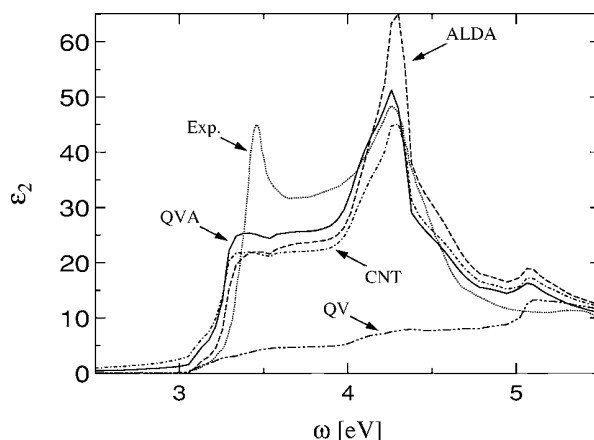
Fig. 12.13 Imaginary part of the dielectric function of bulk Si. [Adapted with permission from APS from Berger *et al.* (2007), ©2007.]

that the performance of the VK functional for solids can at best be called inconsistent (Romaniello and de Boeij, 2005; Berger *et al.*, 2005, 2006, 2007). Let us illustrate this with two examples.

Figure 12.13 shows the imaginary part of the dielectric function for bulk Si, comparing experiment with calculations (see also Figs. 12.8 and 12.10). The spectra have been shifted so that the optical gap agrees with experiment. As we already saw in Fig. 12.8, the ALDA underestimates the first peak, since it does not include excitonic effects.

The VK functional was implemented in three different flavors, using the NCT and QV parametrizations for the xc kernels $f_{xc}^L(\omega)$ and $f_{xc}^T(\omega)$ (see Section 8.3.3), as well as a modification of the QV parametrization (QVA) in which the xc shear modulus μ_{xc} is set to zero. The NCT (implemented here with $\mu_{xc} = 0$; see footnote 3 in Chapter 8) and QVA parametrizations thus both reduce to the ALDA in the static limit.

The NCT and QVA spectra for Si are close to one another, and show only a marginal improvement over the ALDA. The excitonic peak, however, is still absent. On the other hand, the QV spectrum has completely collapsed. The transverse xc kernel apparently has a disastrous effect on the spectral shape.

The reasons for this disappointing performance are similar to those in the case of the excitation energies of atoms and molecules (see Section 10.5.2), where the VK functional didn't do too well, either:

- The criteria (10.58)–(10.60) for the validity of the VK functional are strongly violated. In other words, the assumption that the ground-state density and the current response are slowly varying cannot be upheld.

- The approximations used for the xc kernels are appropriate for a weakly homogeneous electron liquid above the particle–hole continuum. But this is not the right regime for optical excitations in insulators or semiconductors, which involve the particle–hole continuum itself.
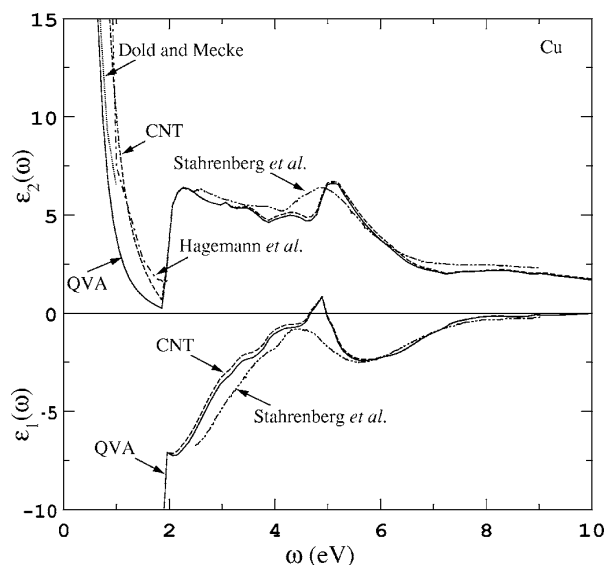
Fig. 12.14 Real and imaginary parts of the dielectric function of copper, calculated using the VK functional, and compared with experiment (Dold and Mecke, 1965; Hagemann *et al.*, 1975; Stahrenberg *et al.*, 2001). [Adapted with permission from APS from Berger *et al.* (2006), ©2006.]

Things look slightly better for metallic systems. Figure 12.14 shows the real and imaginary parts of the dielectric function for copper, comparing VK calculations with experimental results. To avoid the trouble with the transverse xc kernel, only NCT and QVA results are shown (where the xc shear modulus μ_{xc} is set to zero).

The NCT and QVA results are almost identical to the ALDA results (which are not shown), with one important difference: in contrast to the ALDA, they produce a Drude-like tail in the absorption spectrum. This means that the imaginary part of the dielectric function increases strongly for low frequencies. This is due to dissipation processes which are beyond the ALDA, but which are included in the VK functional.

Exercise 12.1 Derive the low-q expansion (12.36) of the Lindhard function $\chi_0(q,\omega)$, and from that the plasmon dispersion relation (12.37).

Exercise 12.2 Derive the classical plasma frequency $\omega_{pl} = \sqrt{4\pi n}$ by considering a slab of uniform negative charge density moving with respect to a fixed slab of uniform positive background charge.

Exercise 12.3 Show that the continuum of single particle–hole excitations for the Lindhard function is defined by the condition (12.34).

Exercise 12.4 Derive the expression (12.25) for the inverse dielectric function.

Exercise 12.5 Go through the derivation of the macroscopic dielectric constant (12.27) given in Appendix M. In particular, verify the relations (M.13) and (M.14) using matrix algebra.

Exercise 12.6 As a numerical exercise, write a computer program to obtain the plasmon dispersion in the RPA (setting $f_{xc} = 0$) by solving eqn (12.35). Use the explicit expressions for the Lindhard functions from the literature (Giuliani and Vignale, 2005), and find the zero of eqn (12.35) by iteration.

To keep things simple, limit yourself to those values of q for which the plasmon is undamped. If you want more challenge, consider the Landau-damped plasmon, where you need to find a zero in the complex frequency plane. As a check, you can compare your results with the results shown in Fig. 12.2.

Exercise 12.7 The normal-incidence reflectance is given by

$$R = \left| \frac{\widetilde{n} - 1}{\widetilde{n} + 1} \right| , \tag{12.61}$$

where $\widetilde{n}$ is defined in eqn (12.29). Show that the reflectance can also be expressed as

$$R = \left| \frac{(n-1)^2 + \kappa^2}{(n+1)^2 + \kappa^2} \right| , \tag{12.62}$$

where $n = \Re\widetilde{n}$ and $\kappa = \Im\widetilde{n}$.

Exercise 12.8 (a) Fill in the steps leading from the equation of motion (12.48) to the TDDFT semiconductor Bloch equations (12.51) and (12.52). (b) Linearize the TDDFT semiconductor Bloch equations and derive eqns (12.54) and (12.55).

Exercise 12.9 Derive the TDDFT Wannier equation (12.59), starting from eqn (12.57).

Exercise 12.10 Consider a single electron living on a ring, such as in Fig. 12.12. Assuming that the ring is infinitesimally thin, the electronic eigenstates can be written as

$$\varphi_m^0(x) = L^{-1/2} e^{2\pi i m x/L} ,$$

where the x-coordinate is along the azimuthal direction, L is the circumference of the ring, and m is an integer. The associated ground-state density is uniform, $n_0 = 1/L$.

Now turn on a magnetic field along the axis which increases linearly with time, such that the associated azimuthal vector potential is $A(t) = -\mathcal{E}t$ (what does the **B**-field look like?). This corresponds to a constant uniform azimuthal electric field $\mathcal{E}$, turned on at the initial time. Show that the time-dependent wave function of the electron is

$$\varphi_m(x,t) = L^{-1/2} \exp\left[-i \left(\frac{k_m^2 t}{2} - \frac{k_m \mathcal{E} t^2}{2} + \frac{\mathcal{E}^2 t^3}{6} \right) \right] e^{2\pi i m x/L} ,$$

where $k_m = 2\pi m/L$.

As you can see, the time dependence is only in the phase, and the density is unchanged. What is the current around the ring? What does this example tell you about TDDFT versus TDCDFT for periodic systems?

13
TDDFT and many-body theory

TDDFT is an exact approach to the time-dependent many-body problem. In practice, success or failure depends on the quality of the approximation to the xc potential when one solves the full TDKS equation, or the quality of the xc kernel when a linear-response treatment is carried out to determine excitation spectra. In the preceding chapters, we have encountered many such approximate schemes, starting from the ALDA and other adiabatic approximations, the TDOEP, and nonadiabatic xc functionals via TDCDFT. We have also assembled a long list of exact properties of the xc potential, and found ways to compare our approximations with numerically exact benchmark calculations and, of course, with experimental data.

In this chapter, we go a bit more deeply into the formal and technical aspects of TDDFT and discuss exact representations of $v_{\mathrm{xc}}(\mathbf{r}, t)$ and $f_{\mathrm{xc}}(\mathbf{r}, \mathbf{r}', \omega)$ which provide explicit avenues for the construction of approximations and for their systematic improvement. To do this we need to introduce several new concepts, such as nonequilibrium Green's functions, perturbation theory along an adiabatic connection, and diagrammatic expansion of response functions and related quantities. While the various methodologies differ in their technical details, they have much in common: each approach yields the xc potential or the xc kernel as an expansion in terms of some parameter. We will soon find out that in lowest order, the exact-exchange TDOEP is recovered, while the treatment of higher-order correlation contributions differs from method to method. The point is that each method allows successive and systematic improvement—although it becomes increasingly difficult beyond the x-only approximation.

Diagrammatic many-body theory is a wide field, and it is beyond the scope of this book to give it the thorough treatment it deserves. Appendix N lists some of the most popular review literature in many-body theory, where the interested reader can learn about technical details such as Feynman rules. In this chapter, we will limit ourselves to a minimalist but hopefully sufficiently intuitive presentation of many-body theory, to the extent that we will be able to establish a connection to TDDFT.

13.1 Perturbation theory along the adiabatic connection

13.1.1 The adiabatic connection

The *adiabatic connection* has been an extremely important and fruitful concept in ground-state DFT. The idea is the following: we define a modified many-body Hamiltonian, which differs from the original $\hat{H}$ [eqn (2.2)] by the presence of a scaling factor λ, where $0 \leq \lambda \leq 1$:

$$\hat{H}^{\lambda} = \hat{T} + \hat{V}^{\lambda} + \lambda \hat{W} . \tag{13.1}$$

Here, the particle–particle interaction $\hat{W}$ is multiplied by λ, which means that we have fully interacting electrons at $\lambda = 1$ and noninteracting particles at $\lambda = 0$; but nonintegral values of λ, all the way from 0 to 1, are also considered. The scaling factor λ is also known as the *coupling constant*.

The potential term $\hat{V}^\lambda = \sum_{j=1}^N v^\lambda(\mathbf{r}_j)$ is related to the original $\hat{V}$ as follows: for each λ, the single-particle potential $v^\lambda(\mathbf{r})$ is chosen in such a way that the ground-state many-body wave function Ψ_0^λ associated with $\hat{H}^\lambda$ reproduces the exact ground-state density of the fully interacting system:

$$\langle \Psi_0^\lambda | \hat{n}(\mathbf{r}) | \Psi_0^\lambda \rangle = n_0(\mathbf{r}) \,. \tag{13.2}$$

This particular choice for $v^\lambda(\mathbf{r})$ is always uniquely possible, thanks to the Hohenberg–Kohn theorem. At $\lambda = 1$, $v^\lambda(\mathbf{r})$ is the given external potential, $v^{\lambda=1}(\mathbf{r}) = v(\mathbf{r})$; at $\lambda = 0$, it is the Kohn–Sham effective potential, $v^{\lambda=0}(\mathbf{r}) = v_s(\mathbf{r})$. This means that $\Psi_0^{\lambda=0} = \Phi_0$ is the Kohn–Sham ground-state Slater determinant.

The reason for the name "adiabatic connection" now becomes clear: the parameter λ allows us to go smoothly back and forth between the interacting and the noninteracting system, but keeping the density fixed at $n_0(\mathbf{r})$ along the path. In Section 14.1, we will take advantage of the adiabatic connection and show that it provides a way of expressing the ground-state xc energy via the so-called coupling-constant integration.

13.1.2 Perturbative expansion of the xc potential

For now, however, we have a different goal, namely, we want to derive a perturbative expansion of the time-dependent xc potential $v_{xc}(\mathbf{r}, t)$ (Görling, 1997, 2006). To do this, let us consider the time-dependent analog of the adiabatic connection and define a modified time-dependent Schrödinger equation as follows:

$$i\frac{\partial}{\partial t}\Psi^\lambda(t) = \left[\hat{T} + \hat{V}^\lambda(t) + \lambda\hat{W}\right]\Psi^\lambda(t) \,, \tag{13.3}$$

with the initial condition $\Psi^\lambda(t_0) = \Psi_0^\lambda$. Let us limit the discussion here to the special case where we start from a system in the ground state at time t_0.[1]

The basic idea of the adiabatic connection remains the same: we choose the time-dependent single-particle potential $v^\lambda(\mathbf{r}, t)$ in such a way that the resulting time-dependent density remains unchanged:

$$\langle \Psi^\lambda(t) | \hat{n}(\mathbf{r}) | \Psi^\lambda(t) \rangle = n(\mathbf{r}, t) \,, \tag{13.4}$$

where $v^{\lambda=1}(\mathbf{r}, t) = v(\mathbf{r}, t)$ is the given external potential, and $v^{\lambda=0}(\mathbf{r}, t) = v_s(\mathbf{r}, t)$ is the time-dependent Kohn–Sham potential. For each value of λ, the Runge–Gross and van Leeuwen theorems guarantee the existence and uniqueness of $v^\lambda(\mathbf{r}, t)$, up to a purely time-dependent function.

---

[1]This restriction is by no means required. When we discussed the Runge–Gross and van Leeuwen theorems in Chapter 3 we made it clear that the initial state of the system does not have to be the ground state. Similarly, the perturbative expansion of $v_{xc}(\mathbf{r}, t)$ can be developed for the general case of systems that do not necessarily start from the ground state; the initial-state dependence then requires a more careful treatment (Görling, 1997, 2006).

In the next step, we take a closer look at $v^\lambda(\mathbf{r}, t)$ and expand it in a Taylor series:[2]

$$v^\lambda(\mathbf{r}, t) = \sum_{p=0}^{\infty} \lambda^p v^{(p)}(\mathbf{r}, t)$$
$$= v_s(\mathbf{r}, t) + \lambda v^{(1)}(\mathbf{r}, t) + \lambda^2 v^{(2)}(\mathbf{r}, t) + \dots . \tag{13.5}$$

Setting $\lambda = 0$, it is easy to see that the first term on the right-hand side of eqn (13.5) is given by the Kohn–Sham effective potential. Since $v^{\lambda=1}(\mathbf{r}, t)$ must be the bare external potential, it immediately follows from eqn (13.5) and from the definition (4.9) of the time-dependent Kohn–Sham potential that

$$v_{\mathrm{H}}(\mathbf{r}, t) + v_{\mathrm{xc}}(\mathbf{r}, t) = -v^{(1)}(\mathbf{r}, t) - v^{(2)}(\mathbf{r}, t) - \dots . \tag{13.6}$$

The first-order term can be identified as the sum of the negative Hartree and local exchange potentials:

$$v^{(1)}(\mathbf{r}, t) = -v_{\mathrm{H}}(\mathbf{r}, t) - v_{\mathrm{x}}(\mathbf{r}, t) . \tag{13.7}$$

All higher-order terms taken together yield the negative correlation potential:

$$\sum_{p=2}^{\infty} v^{(p)}(\mathbf{r}, t) = -v_{\mathrm{c}}(\mathbf{r}, t) . \tag{13.8}$$

We can consider this to be a *definition* of the exchange potential and the correlation potential in TDDFT. What remains to be done is to derive explicit expressions; as we will see, this is straightforward for the first-order (exchange) term, but becomes increasingly cumbersome in higher orders.

The λ-dependent Hamiltonian can be written as

$$\hat{H}^\lambda(t) = \hat{T} + \hat{V}^\lambda(t) + \lambda \hat{W}$$
$$= \hat{T} + \hat{V}_s(t) + \lambda \left[\hat{W} - \hat{V}_{\mathrm{H}}(t) - \hat{V}_{\mathrm{x}}(t) \right] + \lambda^2 \hat{V}^{(2)}(t) + \dots . \tag{13.9}$$

The key idea is now to regard the time-dependent Kohn–Sham system, described by the Hamiltonian

$$\hat{H}_s(t) = \hat{T} + \hat{V}_s(t) , \tag{13.10}$$

as the *unperturbed* system, and treat all λ-dependent terms in the Hamiltonian (13.9) as perturbations using standard time-dependent perturbation theory, writing

$$\Psi^\lambda(t) = \sum_{p=0}^{\infty} \lambda^p \Psi^{(p)}(t) . \tag{13.11}$$

To zeroth order in λ, the time-dependent many-body wave function is the Kohn–Sham wave function, $\Psi^{(0)}(t) = \Phi(t)$, with the initial condition $\Phi(t_0) = \Phi_0$. The first-order term in eqn (13.11) is found to be given by the following expression:

---

[2]There are mathematical subtleties associated with a series expansion like this, such as the question of its convergence, and of the existence of the derivatives with respect to λ implied in the definition of $v^{(p)}(\mathbf{r}, t)$. However, we will sweep these general concerns under the rug, since they do not create any trouble for the lowest-order terms of the expansion, which is where our main interest lies.

$$\Psi^{(1)}(t) = \frac{1}{i} \sum_{k=0}^{\infty} \int_{t_0}^{t} dt' \, \Phi_k(t') \langle \Phi_k(t') | \hat{W} - \hat{V}_{\mathrm{H}}(t') - \hat{V}_{\mathrm{x}}(t') | \Phi_0(t') \rangle$$

$$+ \sum_{k=1}^{\infty} \Phi_k(t) \frac{\langle \Phi_k(t_0) | \hat{W} - \hat{V}_{\mathrm{H}}(t_0) - \hat{V}_{\mathrm{x}}(t_0) | \Phi_0(t_0) \rangle}{E_{s,0} - E_{s,k}} \, . \qquad (13.12)$$

Here, the $\Phi_k(t_0)$ are simply the solutions of the static Kohn–Sham equation at the initial time:

$$\hat{H}_s(t_0) \Phi_k(t_0) = E_{s,k} \Phi_k(t_0) \, , \qquad (13.13)$$

where $\Phi_0(t_0)$ is the ground-state Kohn–Sham Slater determinant, and all other $\Phi_k(t_0)$ are excited-state Slater determinants, with associated energies $E_{s,k}$. The $\Phi_k(t)$ are the time-dependent Slater determinants that arise from the initial $\Phi_k(t_0)$ by time propagation under the influence of the time-dependent Kohn–Sham Hamiltonian $\hat{H}_s(t)$.

Equation (13.12) for $\Psi^{(1)}(t)$ has two contributions. The first one can be derived using a time-dependent perturbation approach similar to that which we used to derive the TDOEP equation in Section 11.2.2. The second term accounts for the fact that there is already a static perturbation present at the initial time, which simply gets propagated forward; this term therefore arises from static first-order perturbation theory.

Let us now carry out a Taylor series expansion of the time-dependent density, similarly to what we did for the potential v^λ:

$$n(\mathbf{r}, t) = \sum_{p=0}^{\infty} \lambda^p n^{(p)}(\mathbf{r}, t) \, . \qquad (13.14)$$

However, since the density is independent of λ, all terms of this Taylor expansion vanish except for the zero-order term, i.e., $n^{(p)} = 0$ for $p > 0$. In particular, this means that the first-order correction $\Psi^{(1)}(t)$ to the wave function does not cause any density changes to first order. Setting the first-order density change to zero, we obtain

$$0 = \frac{1}{i} \sum_{k=1}^{\infty} \int_{t_0}^{t} dt' \langle \Phi_0(t') | \hat{n}(\mathbf{r}) | \Phi_k(t') \rangle \langle \Phi_k(t') | \hat{W} - \hat{V}_{\mathrm{H}}(t') - \hat{V}_{\mathrm{x}}(t') | \Phi_0(t') \rangle + \mathrm{c.c.}$$

$$+ \sum_{k=1}^{\infty} \langle \Phi_0(t) | \hat{n}(\mathbf{r}) | \Phi_k(t) \rangle \frac{\langle \Phi_k(t_0) | \hat{W} - \hat{V}_{\mathrm{H}}(t_0) - \hat{V}_{\mathrm{x}}(t_0) | \Phi_0(t_0) \rangle}{E_{s,0} - E_{s,k}} + \mathrm{c.c.} \qquad (13.15)$$

In the next step we use the explicit form of the $\Phi_k(t)$ as Slater determinants made up of time-dependent Kohn–Sham single-particle orbitals $\varphi_j(\mathbf{r}, t)$, and the total energies $E_{s,k}$ are written as sums of Kohn–Sham single-particle energies ε_j. In this manner, we arrive at the following integral equation for the exact time-dependent Kohn–Sham exchange potential:

$$\sum_{j=1}^{N} \sum_{\substack{k=1 \\ k \neq j}}^{\infty} \left\{ i \int_{t_0}^{t} dt' \int d^3 r' \left[v_{\mathrm{x}}(\mathbf{r}', t') - \mathcal{V}_{\mathrm{x}j}(\mathbf{r}', t') \right] \varphi_j(\mathbf{r}, t) \varphi_j^*(\mathbf{r}', t') \varphi_k^*(\mathbf{r}, t) \varphi_k(\mathbf{r}', t') \right.$$

$$\left. + \int d^3 r' \left[v_{\mathrm{x}}^0(\mathbf{r}') - \mathcal{V}_{\mathrm{x}j}^0(\mathbf{r}') \right] \varphi_j(\mathbf{r}, t) \varphi_k^*(\mathbf{r}, t) \frac{\varphi_j^{0*}(\mathbf{r}') \varphi_k^0(\mathbf{r}')}{\varepsilon_j - \varepsilon_k} \right\} + \mathrm{c.c.} = 0 \, . \ (13.16)$$

This expression is formally identical to the x-only TDOEP equation (11.56), which was derived variationally in Chapter 11. Notice that the Kohn–Sham single-particle orbitals and energy eigenvalues entering the definition of $v_x(\mathbf{r}, t)$ in eqn (13.16) must be those that are obtained self-consistently by solving the Kohn–Sham equation with the same time-dependent exchange potential $v_x(\mathbf{r}, t)$. Furthermore, the initial ground-state condition at time t_0 is obtained by solving the static x-only OEP equation.

We thus see that the exact Kohn–Sham exchange potential emerges as the first-order term in a perturbative expansion along the adiabatic connection. $v_x(\mathbf{r}, t)$ is defined as a functional of the time-dependent Kohn–Sham orbitals as well as of the initial static Kohn–Sham orbitals and orbital eigenvalues (both occupied and unoccupied). As we discussed in Section 11.2.4, so far there exists one application in the time domain where the full x-only TDOEP equation was solved for the intersubband electron dynamics in a quantum well; approximate solutions such as the TDKLI functional have been used routinely for many years.

Higher orders of the perturbative expansion define the time-dependent correlation potential $v_c(\mathbf{r}, t)$, and can in principle used to construct better and better approximations. However, the formalism quickly becomes more and more complicated beyond the first order; as a matter of fact, currently there exist no applications beyond the first order (x-only) in the time domain.

In the static case, on the other hand, perturbation theory along the adiabatic connection (Görling and Levy, 1994; Görling, 1996) has been successfully pushed beyond first order; second-order correlation functionals have been derived and tested for molecules. The resulting expressions bear some formal similarity to the second-order Møller–Plesset (MP2) perturbation theory of quantum chemistry, with numerical results of comparable quality. An overview of orbital-dependent correlation energies and potentials has been given by Engel (2003); see also Kümmel and Kronik (2008). We should also mention a beautiful application of the second-order correlation potential to the subband structure in semiconductor quantum wells by Rigamonti and Proetto (2006, 2007).

13.2   Nonequilibrium Green's functions and the Keldysh action

In this section, we will discuss some basic concepts of nonequilibrium many-body theory using Keldysh Green's functions, and establish a connection to TDDFT via an action principle and via the so-called Sham–Schlüter equation. This has several benefits:

- The new action functional provides a variational definition of the xc potential which preserves causality just like the action principle discussed in Section 6.6.2, and therefore constitutes an alternative to it.
- The possibility of a diagrammatic expansion leads to systematic avenues for constructing xc functionals, and gives new approximations that respect important conservation laws.
- Later, in Chapter 15, we will see that nonequilibrium Green's functions (NEGFs) are very useful for describing transport through nanoscale junctions.

Green's function approaches and many-body theory are governed by a catalog of prescriptions and rules which are relatively straightforward in and by themselves, but

require some time and effort to master. Here, we will skip most of these technical details. There is a sizable body of literature on the subject of Keldysh NEGFs and many-body theory (Kadanoff and Baym, 1989; Haug and Jauho, 2009). A concise introduction can be found in Di Ventra (2008). The connection to TDDFT, which we will discuss in this section, was pioneered by van Leeuwen (1996, 1998, 2001) and coworkers (von Barth *et al.*, 2005; van Leeuwen *et al.*, 2006). We refer the interested reader to these original references for a thorough treatment.

13.2.1   The Keldysh contour

As we discussed in Section 3.1.2, the time evolution of a many-body wave function $\Psi(t)$ from t_0 to t is determined by the time evolution operator $\hat{U}(t, t_0)$. The expectation value of any observable $\hat{O}$ then follows from $O(t) = \langle \Psi(t)|\hat{O}|\Psi(t)\rangle$ (here, we assume $\hat{O}$ to be independent of time).

However, this way of determining the expectation value of an observable holds only for pure states. In general, quantum mechanical systems are described by a statistical density operator $\hat{\rho}$, and quantum mechanical expectation values are then written as

$$
\begin{aligned}
O(t) &= \mathrm{Tr}\left\{\hat{\rho}\hat{O}_{\mathrm{H}}(t)\right\} \\
&= \mathrm{Tr}\left\{\hat{\rho}\hat{U}(t_0, t)\hat{O}\hat{U}(t, t_0)\right\} .
\end{aligned}
\tag{13.17}
$$

Here, $\hat{O}_{\mathrm{H}}(t) = \hat{U}(t_0, t)\hat{O}\hat{U}(t, t_0)$ is the operator $\hat{O}$ in the Heisenberg picture.

Let us now be specific about the physical situation that we wish to describe. We assume that the system is in thermal equilibrium at the initial time t_0 (this can be viewed as generalizing our usual assumption that the system is initially in the ground state), with an initial Hamiltonian $\hat{H}_0$. At time t_0, an explicitly time-dependent external potential is switched on, which perturbs the equilibrium and makes the Hamiltonian $\hat{H}(t)$ time-dependent.

The density operator corresponding to thermal equilibrium at time t_0 is given by

$$
\hat{\rho} = \frac{e^{-\beta(\hat{H}_0 - \mu\hat{N})}}{\mathrm{Tr}\left\{e^{-\beta(\hat{H}_0 - \mu\hat{N})}\right\}} ,
\tag{13.18}
$$

where $\beta = 1/k_B T$ (k_B is the Boltzmann constant and T is the temperature), μ is the chemical potential, and $\hat{N}$ is the particle number operator. The density operator can be rewritten as

$$
\hat{\rho} = \frac{e^{\beta\mu\hat{N}}\hat{U}(t_0 - i\beta, t_0)}{\mathrm{Tr}\left\{e^{\beta\mu\hat{N}}\hat{U}(t_0 - i\beta, t_0)\right\}} ,
\tag{13.19}
$$

and it is easy to see why: comparing this with eqn (3.11), one immediately realizes that $\hat{U}(t_0 - i\beta, t_0) = e^{-\beta\hat{H}_0}$ describes the time evolution of the system along the imaginary time argument $t = -i\beta$ under the influence of the stationary Hamiltonian $\hat{H}_0$. Putting everything together, we obtain

$$
O(t) = \frac{\mathrm{Tr}\left\{e^{\beta\mu\hat{N}}\hat{U}(t_0 - i\beta, t_0)\hat{U}(t_0, t)\hat{O}\hat{U}(t, t_0)\right\}}{\mathrm{Tr}\left\{e^{\beta\mu\hat{N}}\hat{U}(t_0 - i\beta, t_0)\right\}} .
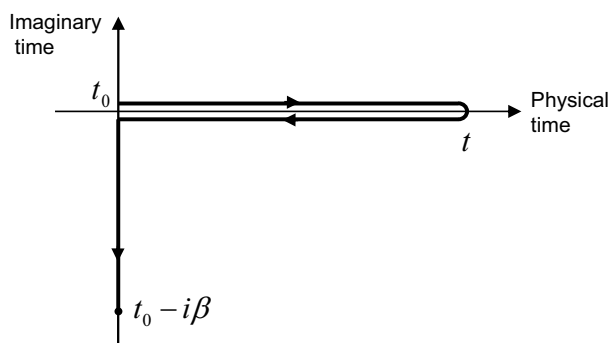\tag{13.20}
$$

Fig. 13.1 The Keldysh time contour $\mathcal{C}$.

A graphical representation of the whole time evolution process implied in this definition of $O(t)$ is given in Fig. 13.1. Reading the argument of the trace in the numerator in eqn (13.20) from right to left, we first have a time evolution from the initial time t_0 until some final time t, then back again from t to t_0, and finally down along the imaginary time axis until $t_0 - i\beta$. The contour so defined in the complex time plane is called the *Keldysh contour* (Keldysh, 1965).

Although the Keldysh contour seems very complicated at first sight (it certainly is more complicated than the usual forward time propagation we've been dealing with so far), it has many formal and practical advantages. There exists a well-documented set of rules for how to treat objects such as Green's functions on the contour, and with a bit of practice one can soon get used to them.

13.2.2   The Keldysh action principle

In static DFT, the ground-state xc potential is defined as the functional derivative of the xc energy, $v_{\mathrm{xc}}^0(\mathbf{r}) = \delta E_{\mathrm{xc}}/\delta n(\mathbf{r})$. Finding a TDDFT counterpart of this relation has not been so straightforward. In Sections 6.6 and 8.1.3 we discussed time-dependent variational principles, and we concluded that a naive definition of the time-dependent xc potential as a functional derivative of the xc action functional [eqn (8.18)], violates causality. A modified stationary-action principle, which pays attention to the boundary condition at the final time of the propagation interval, then led to the correct expression (6.78): the time-dependent xc potential is given as a functional derivative of the xc action functional plus some extra boundary terms.

The Keldysh contour, as we shall now discuss, offers an alternative way of defining the time-dependent xc potential via an action principle.[3] We begin by introducing the following object:

$$\widetilde{\mathcal{K}} = i \ln \mathrm{Tr} \left\{ e^{\beta \mu \hat{N}} \hat{U}(t_0 - i\beta, t_0) \right\}. \tag{13.21}$$

---

[3]The idea of using the Keldysh formalism for a TDDFT action principle had already appeared in earlier work by Peuckert (1978), but was fully formulated only by van Leeuwen (1998, 2001) and van Leeuwen *et al.* (2006).

By comparison with the definition of the statistical density operator (13.19), we see that $\widetilde{\mathcal{K}} = i \ln Z$, where Z is the thermodynamic partition function. Notice that in the zero-temperature limit one has $\lim_{T \to 0}(ik_B T \widetilde{\mathcal{K}}) = E_0 - \mu N$.

$\widetilde{\mathcal{K}}$ has an important property:

$$\frac{\delta \widetilde{\mathcal{K}}[v]}{\delta v(\mathbf{r}, z)} = n(\mathbf{r}, z) \, . \tag{13.22}$$

In other words, its functional derivative with respect to the potential, taken on the Keldysh contour, gives the density. To see this, we rewrite eqn (13.21) as

$$\widetilde{\mathcal{K}}[v] = i \ln \mathrm{Tr} \left\{ e^{\beta \mu \hat{N}} \hat{U}(t_0 - i\beta, t_0) \hat{U}(t_0, t) \hat{U}(t, t_0) \right\} \, . \tag{13.23}$$

This is a functional of the potential, because the time evolution operators satisfy the equation of motion

$$i \frac{d}{dz} \hat{U}(z, z') = \hat{H}(z) \hat{U}(z, z') \, . \tag{13.24}$$

The potential can be varied independently on any branch of the Keldysh contour. Let us, for instance, vary the potential on the forward branch from t_0 to t, so that

$$\begin{aligned}
\frac{\delta \widetilde{\mathcal{K}}[v]}{\delta v(\mathbf{r}, z)} &= \frac{i}{\mathrm{Tr} \left\{ e^{\beta \mu \hat{N}} \hat{U}(t_0 - i\beta, t_0) \right\}} \mathrm{Tr} \left\{ e^{\beta \mu \hat{N}} \hat{U}(t_0 - i\beta, t_0) \hat{U}(t_0, t) \frac{\delta \hat{U}(t, t_0)}{\delta v(\mathbf{r}, z)} \right\} \\
&= \frac{\mathrm{Tr} \left\{ e^{\beta \mu \hat{N}} \hat{U}(t_0 - i\beta, t_0) \hat{U}(t_0, t) \hat{n}(\mathbf{r}) \hat{U}(t, t_0) \right\}}{\mathrm{Tr} \left\{ e^{\beta \mu \hat{N}} \hat{U}(t_0 - i\beta, t_0) \right\}} \, .
\end{aligned} \tag{13.25}$$

Showing that $\delta \hat{U}(t, t_0) / \delta v(\mathbf{r}, z) = \hat{n}(\mathbf{r}) \hat{U}(t, t_0)$ will be the subject of Exercise 13.4. Comparison with eqn (13.20) finally proves eqn (13.22).

From this point onwards, things are quite straightforward. We first define a new functional,

$$\mathcal{K}[n] = -\widetilde{\mathcal{K}}[v] + \int d^3 r \int_{\mathcal{C}} dz \, n(\mathbf{r}, z) v(\mathbf{r}, z) \, . \tag{13.26}$$

This means that we switch from the potential functional $\widetilde{\mathcal{K}}[v]$ to the density functional $\mathcal{K}[n]$ via a so-called *Legendre transformation*. This change of independent variables is possible because the potential is a functional of the density, thanks to the Runge–Gross theorem. We call $\mathcal{K}[n]$ the *Keldysh action functional*.

An important difference between $\mathcal{K}[n]$ and the action functional $\mathcal{A}[n]$ defined earlier (Section 6.6.2)—apart from the time contour—is that the Keldysh action does not contain a time derivative; therefore, there are no extra boundary terms. Another difference is that the numerical value of $\mathcal{A}[n]$ is zero, whereas the Keldysh action reduces to the grand canonical potential in the equilibrium limit. But these values are not so interesting by themselves: the main purpose of action functionals is to generate equations of motions with certain desirable properties or conservation laws built in.

In our case, the main purpose of introducing the Keldysh action principle is to obtain a variational definition of $v_{\mathrm{xc}}(\mathbf{r}, t)$ which respects causality.

From eqn (13.26), one sees immediately that

$$\frac{\delta \mathcal{K}[n]}{\delta n(\mathbf{r}, z)} = v(\mathbf{r}, z) \,. \tag{13.27}$$

Likewise, we can define the Keldysh action functional for the Kohn–Sham system as

$$\mathcal{K}_s[n] = -\widetilde{\mathcal{K}}_s[v_s] + \int d^3r \int_{\mathcal{C}} dz \, n(\mathbf{r}, z) v_s(\mathbf{r}, z) \,, \tag{13.28}$$

so that

$$\frac{\delta \mathcal{K}_s[n]}{\delta n(\mathbf{r}, z)} = v_s(\mathbf{r}, z) \,. \tag{13.29}$$

The xc action functional can be defined as

$$\mathcal{K}_{\mathrm{xc}}[n] = \mathcal{K}_s[n] - \mathcal{K}[n] - \frac{1}{2} \int_{\mathcal{C}} dz \int d^3r \int d^3r' \, \frac{n(\mathbf{r}, z) n(\mathbf{r}', z)}{|\mathbf{r} - \mathbf{r}'|} \,, \tag{13.30}$$

which yields the xc potential as

$$v_{\mathrm{xc}}(\mathbf{r}, z) = \frac{\delta \mathcal{K}_{\mathrm{xc}}[n]}{\delta n(\mathbf{r}, z)} \,. \tag{13.31}$$

If the time argument is on the real axis, then it doesn't matter whether we are on the forward or the backward branch of the time contour; one can simply replace z with the time variable t.

So far, so good; but don't we run into problems similar to those for eqn (8.19), where the second derivative of the xc action functional was found to be symmetric, thus violating causality? In Section 8.1.3, the problem was solved by an appropriate inclusion of boundary terms. How does this work for the Keldysh action? The answer turns out to be quite simple. We can define a response function on the Keldysh contour as

$$\chi(\mathbf{r}, z, \mathbf{r}', z') = \frac{\delta^2 \widetilde{K}}{\delta v(\mathbf{r}, z) \delta v(\mathbf{r}', z')} \,, \tag{13.32}$$

which is manifestly symmetric under interchange of $(\mathbf{r}, z)$ and $(\mathbf{r}', z')$. This is perfectly fine for calculating the response on the Keldysh contour, because forward and backward time propagation have an equal status there. But when the response to an actual physical perturbing potential is considered, the contributions of the forward and backward time branches combine in such a way that the resulting response is retarded, as it should be (van Leeuwen *et al.*, 2006). The causality principle is thus obeyed.

The Keldysh action can be used in a variational derivation of the TDOEP equation for $v_{\mathrm{xc}}(\mathbf{r}, t)$, similarly to what we did in Section 11.2.1. We shall not pursue this any further here; the x-only case was worked out by van Leeuwen (1998, 2001) and van Leeuwen *et al.* (2006).

13.2.3   Nonequilibrium Green's functions

Second quantization in a nutshell, and definition of NEGFs.   In many-body theory, the central quantities are the Green's functions associated with a quantum mechanical state (or an ensemble of states) describing the system. To define a Green's function it is most convenient to work in second quantization (which we've been avoiding so far), and use the *field operators* $\hat{\psi}(\mathbf{r})$ and $\hat{\psi}^\dagger(\mathbf{r})$.

In the second-quantization formalism, one works in the so-called *Fock space*, which essentially means that one considers Hilbert spaces with different total particle numbers and goes freely back and forth between them. The physical interpretation of the field operators is that $\hat{\psi}(\mathbf{r})$ destroys a particle at position $\mathbf{r}$, and $\hat{\psi}^\dagger(\mathbf{r})$ creates a particle at $\mathbf{r}$. The words "creation" and "destruction" may appear somewhat overly dramatic; what this simply means is that one goes from a state with N particles to an $(N+1)$-particle state (creation) or from N to $N-1$ (destruction).

The precise rules which govern the action of field operators (or creation and destruction operators) on many-body wave functions are well explained in the textbooks on many-body theory listed in Appendix N, but these technical details are not so important for what we want to do in this chapter. A nice thing about field operators is that one can use them to express quantum mechanical operators, and then discuss them in very intuitive terms. To give an example, the density operator $\hat{n}(\mathbf{r})$, which is given in first quantization in eqn (3.20), is written as follows in second quantization:

$$\hat{n}(\mathbf{r}) = \hat{\psi}^\dagger(\mathbf{r})\hat{\psi}(\mathbf{r}) \; ; \tag{13.33}$$

the particle density is then obtained as

$$n(\mathbf{r}, t) = \langle \Psi(t)|\hat{\psi}^\dagger(\mathbf{r})\hat{\psi}(\mathbf{r})|\Psi(t)\rangle. \tag{13.34}$$

In other words, the density operator $\hat{\psi}^\dagger(\mathbf{r})\hat{\psi}(\mathbf{r})$ probes the state $\Psi(t)$ by destroying and immediately recreating a particle at the same position $\mathbf{r}$. If no electron is present at that position, then the result is 0; if we know for sure that there is an electron, then the result is 1. In all other cases, the result is between zero and one.

The Green's function is in principle very similar to this, in the sense that the state of the system is probed by destroying and then recreating a particle (or the other way round); the main difference is that this is now done at different times and places! This gives us much more than just the probability of finding a particle: it tells us something about the dynamics of the system, and allows us to extract information such as energies and excitation spectra, and much more. We thus define the NEGF as

$$\mathcal{G}(\mathbf{r}, z, \mathbf{r}', z') = -i \left\langle \hat{\mathcal{T}}_\mathcal{C} \hat{\psi}_{\mathrm{H}}(\mathbf{r}, z)\hat{\psi}_{\mathrm{H}}^\dagger(\mathbf{r}', z') \right\rangle. \tag{13.35}$$

This definition is made with respect to the Keldysh time contour $\mathcal{C}$ of Fig. 13.1, and we use z and z' to denote a position on this contour; this can be a real physical time on the forward or backward branch of $\mathcal{C}$, or an imaginary time along the downward branch. The definition (13.35) uses the field operators in the Heisenberg representation, i.e., $\hat{\psi}(\mathbf{r}, z) = \hat{U}(0, z)\hat{\psi}(\mathbf{r})\hat{U}(z, 0)$, and the expectation value is taken over a statistical ensemble with density operator $\hat{\rho}$ (see Section 13.2.1).

$\hat{\mathcal{T}}_{\mathcal{C}}$ is a time-ordering operator with respect to $\mathcal{C}$, which ensures that all operators to the right of it are arranged in such a way that the "earliest" operator is the rightmost one (here, "earlier" and "later" refer to the variable z along the contour $\mathcal{C}$, not to the physical time t). Instead of using the compact notation of $\hat{\mathcal{T}}_{\mathcal{C}}$, we can also write eqn (13.35) as follows:

$$\mathcal{G}(\mathbf{r}, z, \mathbf{r}', z') = \theta(z, z')\mathcal{G}^>(\mathbf{r}, z, \mathbf{r}', z') + \theta(z', z)\mathcal{G}^<(\mathbf{r}, z, \mathbf{r}', z') , \tag{13.36}$$

where $\theta(z_1, z_2)$ is 1 or 0 if z_1 is later or earlier, respectively, on the contour than z_2. This defines the "greater" and "lesser" Green's functions as

$$\mathcal{G}^>(\mathbf{r}, z, \mathbf{r}', z') = -i \left\langle \hat{\psi}_{\mathrm{H}}(\mathbf{r}, z)\hat{\psi}_{\mathrm{H}}^\dagger(\mathbf{r}', z') \right\rangle , \tag{13.37}$$

$$\mathcal{G}^<(\mathbf{r}, z, \mathbf{r}', z') = i \left\langle \hat{\psi}_{\mathrm{H}}^\dagger(\mathbf{r}', z')\hat{\psi}_{\mathrm{H}}(\mathbf{r}, z) \right\rangle . \tag{13.38}$$

The physical interpretation is that $\mathcal{G}^>$ adds a particle at $(\mathbf{r}', z')$, propagates it forward along $\mathcal{C}$ until $(\mathbf{r}, z)$, and then destroys it. $\mathcal{G}^<$ does the opposite: it destroys a particle at $(\mathbf{r}, z)$ and then recreates it at $(\mathbf{r}', z')$; one can also say that it adds a hole at $(\mathbf{r}', z')$, propagates it backward along $\mathcal{C}$ until $(\mathbf{r}, z)$, and then destroys it. For these reasons, Green's functions are also called particle and hole *propagators*.

Equation of motion for the NEGFs.   Under the influence of a many-body Hamiltonian of the form (3.1), the NEGFs satisfy the following equation of motion:

$$\left(i\frac{\partial}{\partial z} + \frac{\nabla^2}{2} - v(\mathbf{r}, z) \right) \mathcal{G}(\mathbf{r}, z, \mathbf{r}', z') = \delta(\mathbf{r} - \mathbf{r}')\delta(z - z')$$
$$- i \int d^3\widetilde{r} \int_{\mathcal{C}} d\widetilde{z}\, w(\mathbf{r} - \widetilde{\mathbf{r}})\mathcal{G}_2(\mathbf{r}, z, \widetilde{\mathbf{r}}, \widetilde{z}, \widetilde{\mathbf{r}}, \widetilde{z}^+, \mathbf{r}', z') . \tag{13.39}$$

Here, $\mathcal{G}_2$ is the two-particle NEGF, which can be defined in an analogous manner to $\mathcal{G}$, involving time-ordered combinations of four field operators (which correspond to propagating pairs of particles and/or holes). We thus see that the equation of motion (13.39) for the NEGF is not closed but involves higher-order Green's functions. In turn, the equation of motion for $\mathcal{G}_2$ contains yet higher-order Green's functions, leading to a hierarchy of coupled equations of motion for the n-particle NEGFs.[4]

At first sight, it seems that not much has been gained compared with the full N-particle Schrödinger equation, and this is of course true when it comes to solving the many-body problem exactly. However, the whole point of introducing Green's functions is that they open up new avenues towards finding approximate solutions that allow systematic improvement. Let us rewrite eqn (13.39) in the following way:

$$\left(i\frac{\partial}{\partial z} + \frac{\nabla^2}{2} - v(\mathbf{r}, z) \right) \mathcal{G}(\mathbf{r}, z, \mathbf{r}', z') = \delta(\mathbf{r} - \mathbf{r}')\delta(z - z')$$
$$+ \int d^3\widetilde{r} \int_{\mathcal{C}} d\widetilde{z}\, \Sigma(\mathbf{r}, z, \widetilde{\mathbf{r}}, \widetilde{z})\mathcal{G}(\widetilde{\mathbf{r}}, \widetilde{z}, \mathbf{r}', z') . \tag{13.40}$$

---

[4]In general, the equation of motion for $\mathcal{G}_n$ is coupled to $\mathcal{G}_{n-1}$ and $\mathcal{G}_{n+1}$. The extent of the hierarchy of equations of motion is limited by the total number of particles N in the system.

Imposing the condition that eqns (13.39) and (13.40) give identical results for $\mathcal{G}$ formally defines the *irreducible self-energy* Σ as a functional of $\mathcal{G}$. The problem of $\mathcal{G}_2$ and the hierarchy of equations of motions, inherent in eqn (13.39), has thus been converted into the problem of finding an expression for the self-energy.

Assuming that we have an explicit expression for Σ, the equation of motion (13.40) can be solved and $\mathcal{G}$ can be determined. To do this, one needs to specify the correct boundary conditions at the initial time, corresponding to thermal equilibrium (as we saw above, this implies a propagation along the imaginary time axis). Taking these together, one arrives at a set of equations of motion for $\mathcal{G}^<$ and $\mathcal{G}^>$ known as the Kadanoff–Baym equations. These equations can be numerically solved to various levels of approximation for Σ to obtain the time evolution of the NEGFs under the influence of a time-dependent perturbation (Dahlen and van Leeuwen, 2007; Stan *et al.*, 2009).

The Dyson equation.   Let us now consider a noninteracting system, whose NEGF is given by the following equation of motion:

$$\left(i\frac{\partial}{\partial z} + \frac{\nabla^2}{2} - v(\mathbf{r}, z) \right) \mathcal{G}_0(\mathbf{r}, z, \mathbf{r}', z') = \delta(\mathbf{r} - \mathbf{r}')\delta(z - z') \, . \qquad (13.41)$$

Comparing this with the equation of motion of $\mathcal{G}$ for the interacting system, eqn (13.40), we find (see Exercise 13.5)

$$\mathcal{G}(\mathbf{r}, z, \mathbf{r}', z') = \mathcal{G}_0(\mathbf{r}, z, \mathbf{r}', z') + \int d^3r_1 \int_\mathcal{C} dz_1 \int d^3r_2 \int_\mathcal{C} dz_2 \, \mathcal{G}_0(\mathbf{r}, z, \mathbf{r}_1, z_1)$$
$$\times \, \Sigma(\mathbf{r}_1, z_1, \mathbf{r}_2, z_2)\mathcal{G}(\mathbf{r}_2, z_2, \mathbf{r}', z') \, . \qquad (13.42)$$

This is the so-called *Dyson equation*: it is an integral equation relating the interacting and noninteracting NEGFs via the irreducible self-energy Σ.

In general, Dyson-type equations can be derived to express any type of Green's function (or, even more generally, any type of two-point function) for an interacting system in terms of its noninteracting counterpart and the appropriate self-energy, which implicitly contains all correlation effects of the many-body system. To give a simple and perhaps more familiar example, we consider the "usual" Green's function for equilibrium systems,[5]

$$G(\mathbf{r}, t, \mathbf{r}', t) = -i \left\langle \hat{\mathcal{T}}\hat{\psi}_\mathrm{H}(\mathbf{r}, t)\hat{\psi}_\mathrm{H}^\dagger(\mathbf{r}', t') \right\rangle , \qquad (13.43)$$

where $\mathcal{T}$ is the time-ordering operator on the real-time axis. Since the Hamiltonian is assumed to be time-independent, G can be Fourier transformed and expressed in terms of the frequency. The associated Dyson equation looks like this:

$$G(\mathbf{r}, \mathbf{r}', \omega) = G_0(\mathbf{r}, \mathbf{r}', \omega) + \int d^3r_1 \int d^3r_2 \, G_0(\mathbf{r}, \mathbf{r}_1, \omega)\Sigma(\mathbf{r}_1, \mathbf{r}_2, \omega)G(\mathbf{r}_2, \mathbf{r}', \omega) \, . \quad (13.44)$$

---

[5]$G(\mathbf{r}, t, \mathbf{r}', t')$ is just a special case of a Keldysh NEGF in which the time contour is chosen to be the real time axis. The main derivations in NEGF theory are independent of the choice of contour.
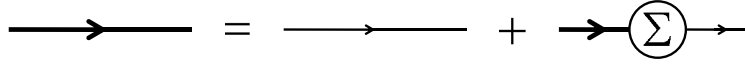
Fig. 13.2 Graphical representation of the Dyson equation. Thick lines correspond to interacting Green's functions, and thin lines to noninteracting Green's functions.

A nice way of representing the Dyson equation, as well as many other relations in many-body theory, is via Feynman diagrams, as shown in Fig. 13.2. The Green's functions of the interacting system are represented as thick lines, and thin lines stand for noninteracting Green's functions.[6] At each vertex (where Green's functions connect with other objects, such as the self-energy insertion Σ), integrations are to be performed, which then leads to eqn (13.44).

There exist very precise rules for how to translate many-body equations into diagrams (see the literature in Appendix N); however, the detailed rules are not important for our purposes, and we limit ourselves here to simply pointing out the correspondence between equations and diagrams.

The Sham–Schlüter equation. In the next step, we now wish to make contact with TDDFT. We proceed in close analogy to the above derivation of the Dyson equation. We define the Kohn–Sham NEGF $\mathcal{G}_s$ by its equation of motion,

$$\left(i\frac{\partial}{\partial z} + \frac{\nabla^2}{2} - v_s(\mathbf{r}, z) \right) \mathcal{G}_s(\mathbf{r}, z, \mathbf{r}', z') = \delta(\mathbf{r} - \mathbf{r}')\delta(z - z') \,. \tag{13.45}$$

Comparing this with the equation of motion of $\mathcal{G}$ for the interacting system, we find

$$\mathcal{G}(\mathbf{r}, z, \mathbf{r}', z') = \mathcal{G}_s(\mathbf{r}, z, \mathbf{r}', z') + \int d^3 r_1 \int_{\mathcal{C}} dz_1 \int d^3 r_2 \int_{\mathcal{C}} dz_2 \, \mathcal{G}_s(\mathbf{r}, z, \mathbf{r}_1, z_1) \tag{13.46}$$
$$\times \left\{ \Sigma(\mathbf{r}_1, z_1, \mathbf{r}_2, z_2) - [v_{\mathrm{H}}(\mathbf{r}_1, z_1) + v_{\mathrm{xc}}(\mathbf{r}_1, z_1)] \delta(\mathbf{r}_1 - \mathbf{r}_2)\delta(z_1 - z_2) \right\} \mathcal{G}(\mathbf{r}_2, z_2, \mathbf{r}', z') \,.$$

The derivation of eqn (13.46) is similar to that for the Dyson equation (13.42). We can make this a bit more compact by defining the xc part of the self-energy as

$$\Sigma_{\mathrm{xc}}(\mathbf{r}, z, \mathbf{r}', z') = \Sigma(\mathbf{r}, z, \mathbf{r}', z') - v_{\mathrm{H}}(\mathbf{r}, z)\delta(\mathbf{r} - \mathbf{r}')\delta(z - z') \,, \tag{13.47}$$

so that

$$\mathcal{G}(\mathbf{r}, z, \mathbf{r}', z') = \mathcal{G}_s(\mathbf{r}, z, \mathbf{r}', z') + \int d^3 r_1 \int_{\mathcal{C}} dz_1 \int d^3 r_2 \int_{\mathcal{C}} dz_2 \, \mathcal{G}_s(\mathbf{r}, z, \mathbf{r}_1, z_1)$$
$$\times \left\{ \Sigma_{\mathrm{xc}}(\mathbf{r}_1, z_1, \mathbf{r}_2, z_2) - v_{\mathrm{xc}}(\mathbf{r}_1, z_1)\delta(\mathbf{r}_1 - \mathbf{r}_2)\delta(z_1 - z_2) \right\} \mathcal{G}(\mathbf{r}_2, z_2, \mathbf{r}', z') \,. \tag{13.48}$$

Now let us make use of the following important property of the Green's function:

$$n(\mathbf{r}, z) = -i\mathcal{G}(\mathbf{r}, z, \mathbf{r}, z^+) = -i\mathcal{G}_s(\mathbf{r}, z, \mathbf{r}, z^+) \,, \tag{13.49}$$

---

[6]The arrows on the Green's function lines indicate the propagation direction from a creation to an annihilation operator, if G is represented as a function of t and t'; this directionality of G is preserved after Fourier transformation.
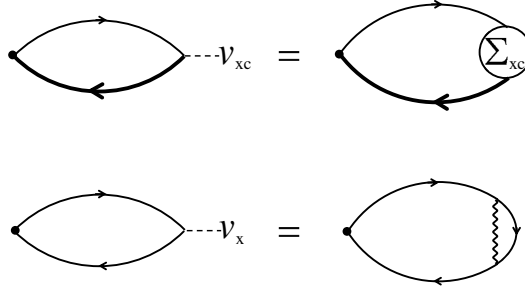
Fig. 13.3 Graphical representation of the full Sham–Schlüter equation (top), and the Sham–Schlüter equation in the x-only limit (bottom). The thin lines denote Kohn–Sham Green's functions. The x-only self-energy diagram is shown in eqn (13.58).

where z^+ is a time argument infinitesimally later than z on the Keldysh contour. The second equality accounts for the fact that the Kohn–Sham system is designed to deliver the same density as the interacting system. Equation (13.48) therefore becomes

$$\int d^3 r_1 \int_{\mathcal{C}} dz_1 \, \mathcal{G}_s(\mathbf{r}, z, \mathbf{r}_1, z_1) v_{\text{xc}}(\mathbf{r}_1, z_1) \mathcal{G}(\mathbf{r}_1, z_1, \mathbf{r}, z^+)$$
$$= \int d^3 r_1 \int_{\mathcal{C}} dz_1 \int d^3 r_2 \int_{\mathcal{C}} dz_2 \, \mathcal{G}_s(\mathbf{r}, z, \mathbf{r}_1, z_1) \Sigma_{\text{xc}}(\mathbf{r}_1, z_1, \mathbf{r}_2, z_2) \mathcal{G}(\mathbf{r}_2, z_2, \mathbf{r}, z^+) \, . \quad (13.50)$$

This integral equation is called the Sham–Schlüter equation of TDDFT (van Leeuwen, 1996). It is formally important because it connects TDDFT to many-body theory, by expressing the xc potential v_{xc} in terms of the xc self-energy Σ_{xc}.

The name "Sham–Schlüter equation" dates back to work in the mid 1980s (Sham and Schlüter, 1983; Sham, 1985), in which the xc potential of ground-state DFT was expressed via a similar integral equation,

$$\int d^3 r_1 \int d^3 r_2 \int d\omega \, G_s(\mathbf{r}, \mathbf{r}_1, \omega) \left[v_{\text{xc}}^0(\mathbf{r}_1) \delta(\mathbf{r}_1 - \mathbf{r}_2) - \Sigma_{\text{xc}}(\mathbf{r}_1, \mathbf{r}_2, \omega) \right] G(\mathbf{r}_2, \mathbf{r}, \omega) = 0 \, .$$
$$(13.51)$$

involving the frequency-dependent equilibrium Green's functions of eqn (13.44).

From a formal perspective, the Sham–Schlüter equation doesn't really make life much simpler. All the many-body complications are hidden in the xc self-energy, which now becomes the quantity that needs to be approximated. However, the xc self-energy lends itself to a diagrammatic expansion, which is a powerful technique for systematically including successive orders of many-body correlations. To keep things simple, we will now illustrate this for the equilibrium case.

From eqn (13.36), we obtain the following expression for the Green's function on the forward branch of the Keldysh contour, which is our familiar time axis:

$$G(\mathbf{r}, t, \mathbf{r}', t') = \theta(t - t') G^>(\mathbf{r}, t, \mathbf{r}', t') + \theta(t' - t) G^<(\mathbf{r}, t, \mathbf{r}', t') \, . \quad (13.52)$$

Let us now consider a noninteracting Kohn–Sham system at zero temperature. The associated Green's functions can then be expressed in terms of the Kohn–Sham orbitals in the following simple form:

$$iG_s^>(\mathbf{r}, t, \mathbf{r}', t') = \sum_j \theta(\varepsilon_j - \varepsilon_F)\varphi_j(\mathbf{r}, t)\varphi_j^*(\mathbf{r}', t') \,, \tag{13.53}$$

$$iG_s^<(\mathbf{r}, t, \mathbf{r}', t') = -\sum_j \theta(\varepsilon_F - \varepsilon_j)\varphi_j(\mathbf{r}, t)\varphi_j^*(\mathbf{r}', t') \,. \tag{13.54}$$

Clearly, the time-dependent density is obtained as $-iG_s^<(\mathbf{r}, t, \mathbf{r}, t) = n(\mathbf{r}, t)$.

Now assume the system is in equilibrium, where $\varphi_j(\mathbf{r}, t) = \varphi_j^0 e^{-i\varepsilon_j t}$. Thus,

$$iG_s(\mathbf{r}, \mathbf{r}', t-t') = \sum_j \varphi_j^0(\mathbf{r})\varphi_j^{0*}(\mathbf{r}')e^{-i\varepsilon_j(t-t')}[\theta(t-t')\theta(\varepsilon_j - \varepsilon_F) - \theta(t'-t)\theta(\varepsilon_F - \varepsilon_j)].$$

$$\tag{13.55}$$

This can be Fourier transformed into

$$G_s(\mathbf{r}, \mathbf{r}', \omega) = \sum_j \varphi_j^0(\mathbf{r})\varphi_j^{0*}(\mathbf{r}') \left[\frac{\theta(\varepsilon_j - \varepsilon_F)}{\omega - \varepsilon_j + i\eta} + \frac{\theta(\varepsilon_F - \varepsilon_j)}{\omega - \varepsilon_j - i\eta} \right], \tag{13.56}$$

where η is a positive infinitesimal, and use has been made of eqn (7.16).

Let us now solve the Sham–Schlüter equation (13.51) to lowest order in the Coulomb interactions, which, following reasoning similar to that in Section 13.1, defines the x-only limit. Thus, we replace the full Green's functions with the Kohn–Sham Green's functions and obtain the following integral equation for the local exchange potential:

$$\int d^3r_1 \int d^3r_2 \int d\omega \, G_s(\mathbf{r}, \mathbf{r}_1, \omega) \left[v_x^0(\mathbf{r}_1)\delta(\mathbf{r}_1 - \mathbf{r}_2) - \Sigma_x(\mathbf{r}_1, \mathbf{r}_2, \omega) \right] G_s(\mathbf{r}_2, \mathbf{r}, \omega) = 0 \,.$$

$$\tag{13.57}$$

We know from Chapter 11 that the exact exchange potential in DFT is given by the OEP integral equation (11.12) [together with eqn (11.28)]. And, indeed, one can show that eqn (13.57) reduces to the x-only OEP equation (see Exercise 13.7), using the following form of the exchange part of the self-energy:

$$\Sigma_x(\mathbf{r}_1, \mathbf{r}_2) = \quad\overparen{\wwww}\quad = -\frac{1}{|\mathbf{r} - \mathbf{r}'|} \sum_j \theta(\varepsilon_F - \varepsilon_j)\varphi_j^0(\mathbf{r})\varphi_j^{0*}(\mathbf{r}') \,. \tag{13.58}$$

This pictorial representation shows Σ_x as a combination of a (wavy) interaction line and a Kohn–Sham Green's function line. Both the full and the x-only Sham–Schlüter equations are represented in diagrammatic form in Fig. 13.3.

In a similar manner, the x-only TDOEP equation can be derived from the nonequilibrium Sham–Schlüter equation (13.50). However, this involves some bookkeeping rules for NEGFs on the Keldysh contour which we have not covered here; we refer to van Leeuwen *et al.* (2006) for further details.

13.3   xc kernels from many-body theory

13.3.1   Diagrammatic expansion of the xc kernel

Formalism.   Let us now derive a formal expression for the xc kernel which is suitable for a diagrammatic expansion (Tokatly and Pankratov, 2001; Tokatly *et al.*, 2002). Recall from Chapter 7 that the frequency-dependent xc kernel is defined as

$$\chi(\omega) = \chi_s(\omega) + \chi_s(\omega)[w + f_{xc}(\omega)]\chi(\omega) \,, \tag{13.59}$$

where we have used a symbolic notation in which the spatial arguments of the functions are suppressed and integration is implied in the appropriate places. w is the bare Coulomb interaction. Defining the *proper response function* $\widetilde{\chi}(\omega)$ as

$$\chi(\omega) = \widetilde{\chi}(\omega) + \widetilde{\chi}(\omega)w\chi(\omega) \,, \tag{13.60}$$

we find the following expression for the xc kernel (omitting the ω-dependence):

$$f_{xc} = \chi_s^{-1} - \widetilde{\chi}^{-1} \,. \tag{13.61}$$

It is convenient to recast the proper response function in a form where the xc contributions are separated out:

$$\widetilde{\chi} \equiv \chi_s + \pi_{xc} \,. \tag{13.62}$$

Inserting this into eqn (13.61) yields

$$\chi_s f_{xc} \chi_s = \pi_{xc} - \pi_{xc} f_{xc} \chi_s \,. \tag{13.63}$$

The solution for f_{xc} can be written as a series expansion in terms of π_{xc}:

$$\chi_s f_{xc} \chi_s = \pi_{xc} - \pi_{xc} \chi_s^{-1} \pi_{xc} + \pi_{xc} \chi_s^{-1} \pi_{xc} \chi_s^{-1} \pi_{xc} - \dots \,. \tag{13.64}$$

What we now need is a systematic way to construct π_{xc}.

In many-body theory, diagrammatic representations of perturbation expansions are a very powerful tool. In standard many-body perturbation theory, the expansion is in orders of the Coulomb interaction, where the zeroth order refers to a system without any interactions, subject to an external potential only. This gives the representation of the proper response function illustrated in Fig. 13.4(a). The filled bubble on the left-hand side is $\widetilde{\chi}$. The first term on the right-hand side (the empty bubble) is the response function of a noninteracting system, χ_0. The next five terms are the first-order contributions, indicated by the presence of one wavy interaction line. The second and higher orders of the perturbation expansion will contain many more topologically distinct diagrams.[7]

An alternative diagrammatic representation of the proper response function is shown in Fig. 13.4(b). Here, the zeroth-order term is the response function of the Kohn–Sham system, χ_s. In other words, the "unperturbed" system is noninteracting, but subject to the effective Kohn–Sham potential. Thus, to avoid double counting of interaction effects, the perturbation is the bare Coulomb interaction w minus the Hartree and xc potentials. Another important feature of Kohn–Sham perturbation theory is that the zeroth order already gives the correct density. The density change in higher orders must therefore vanish. To summarize:

---

[7] For technical reasons, the causal response function cannot be directly constructed via the standard perturbation expansion; instead, one considers a closely related object called the time-ordered response function (also known as the polarization propagator). The causal response function $\chi(\omega)$ is related to the time-ordered response function $\chi^T(\omega)$ as follows: $\Re\chi(\omega) = \Re\chi^T(\omega)$ and $\Im\chi(\omega) = \text{sign}(\omega)\Im\chi^T(\omega)$. In the following, this distinction will not be important, but it should be kept in mind.
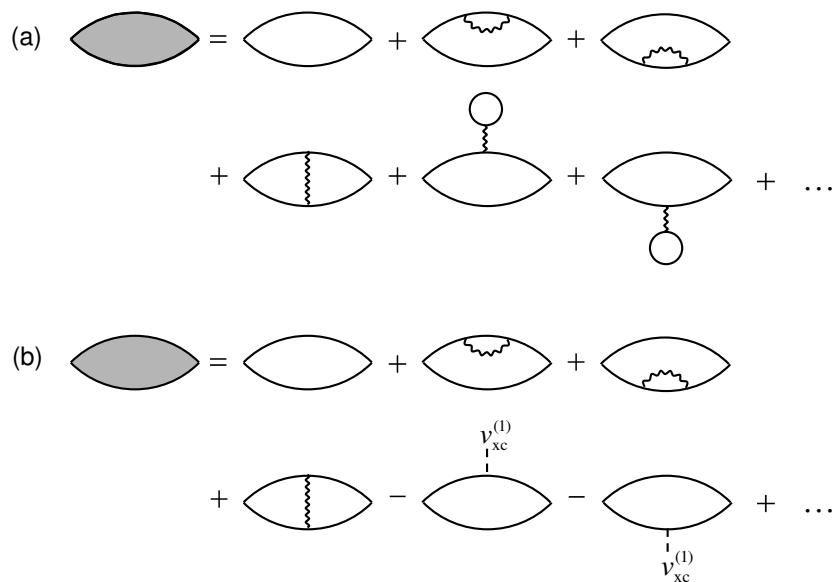
Fig. 13.4 Diagrammatic expansion of the proper response function, up to first order. (a) Standard many-body perturbation theory. Here, the unperturbed system is noninteracting, and the perturbation is the bare Coulomb interaction w. (b) Kohn–Sham perturbation theory. Here, the unperturbed system is the Kohn–Sham system, and the perturbation is the bare Coulomb interaction minus the Hartree and xc potentials.

Standard many-body perturbation theory for $\widetilde{\chi}$:
     zeroth order, $\chi_0(\omega)$;   perturbation, $\hat{V}' = \hat{W}$.

Kohn–Sham many-body perturbation theory for $\widetilde{\chi}$:
     zeroth order, $\chi_s(\omega)$;   perturbation, $\hat{V}' = \hat{W} - \hat{V}_{\mathrm{H}} - \hat{V}_{\mathrm{xc}}$.

We now return to our original problem, namely, constructing the xc part π_{xc} of the proper response function. From Fig. 13.4(b), we see that it consists of all diagrams beyond the zero-order bubble. We can therefore write

$$\pi_{\mathrm{xc}} = \pi_{\mathrm{xc}}^{(1)} + \pi_{\mathrm{xc}}^{(2)} + \pi_{\mathrm{xc}}^{(3)} + \dots \ . \tag{13.65}$$

There is a subtle point, however. The xc potential itself, which is part of the perturbation, implicitly contains all orders of the Coulomb interaction. Via the Sham–Schlüter equation (see Fig. 13.3), we could construct a diagrammatic expansion of it, $v_{\mathrm{xc}} = v_{\mathrm{xc}}^{(1)} + v_{\mathrm{xc}}^{(2)} + v_{\mathrm{xc}}^{(3)} + \dots$. In the first order we have $v_{\mathrm{xc}}^{(1)} = v_{\mathrm{x}}$, given by the x-only OEP. Therefore, if you look closely at Fig. 13.4(b), you will see that the last two diagrams contain only $v_{\mathrm{xc}}^{(1)}$ and not the full xc potential. Higher orders of v_{xc} will appear in second- and higher-order diagrams of π_{xc}.

Inserting the expansion (13.65) into eqn (13.64) and collecting terms of the same order in the Coulomb interaction finally gives the desired expansion of the xc kernel:
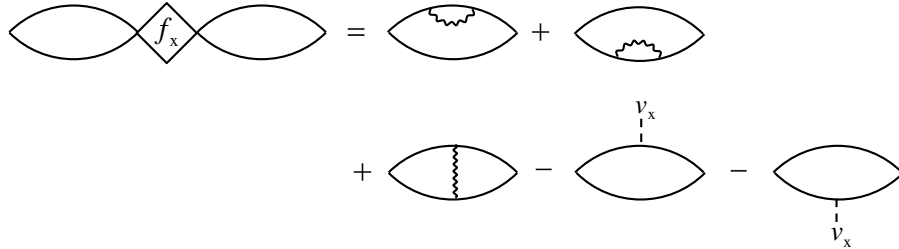
Fig. 13.5 Diagrammatic representation of the exact x-only kernel f_{x}.

$$f_{\mathrm{xc}} = f_{\mathrm{xc}}^{(1)} + f_{\mathrm{xc}}^{(2)} + \dots . \tag{13.66}$$

This establishes an exact connection between TDDFT and many-body perturbation theory, and allows (at least in principle) a systematic improvement of $f_{\mathrm{xc}}(\omega)$ by including higher-order diagrammatic contributions.

The exact exchange limit. The first-order term of the perturbative expansion of the xc kernel is given by

$$\chi_s f_{\mathrm{xc}}^{(1)} \chi_s = \pi_{\mathrm{xc}}^{(1)} . \tag{13.67}$$

This defines the exact x-only kernel, i.e., $f_{\mathrm{xc}}^{(1)} = f_{\mathrm{x}}$. Figure 13.5 shows a diagrammatic representation, consisting of five first-order diagrams. We quote here the explicit expression given by Hellgren and von Barth (2008, 2009):[8]

$$\int d^3 r_1 \int d^3 r_2 \chi_s(\mathbf{r}, \mathbf{r}_1, \omega) f_{\mathrm{x}}(\mathbf{r}_1, \mathbf{r}_2, \omega) \chi_s(\mathbf{r}_2, \mathbf{r}', \omega) = R_V(\mathbf{r}, \mathbf{r}', \omega) + R_\Sigma(\mathbf{r}, \mathbf{r}', \omega). \tag{13.68}$$

R_V is the first-order vertex diagram (the third one on the right-hand side in Fig. 13.5),

$$R_V(\mathbf{r}, \mathbf{r}', \omega) = -2 \sum_{ijkl} \varphi_i^0(\mathbf{r}) \varphi_j^{0*}(\mathbf{r}) \varphi_k^{0*}(\mathbf{r}') \varphi_l^0(\mathbf{r}') \langle il|w|jk \rangle \frac{(f_i - f_j)(f_k - f_l)}{(z - \omega_{ij})(z - \omega_{lk})} , \tag{13.69}$$

where $z = \omega + i0^+$, and the f_j are the usual occupation factors. R_Σ denotes the sum of all the remaining four diagrams (the self-energy diagrams):

$$R_\Sigma(\mathbf{r}, \mathbf{r}', \omega) = 4 \sum_{ijk} \frac{\varphi_i^0(\mathbf{r}) \varphi_i^{0*}(\mathbf{r}') \varphi_j^0(\mathbf{r}) \varphi_k^{0*}(\mathbf{r}') \langle j|\Delta|k \rangle}{\omega_{kj}} \left\{ \frac{(f_k - f_i)\omega_{ik}}{z^2 - \omega_{ik}^2} - \frac{(f_j - f_i)\omega_{ij}}{z^2 - \omega_{ij}^2} \right\} , \tag{13.70}$$

where $\Delta(\mathbf{r}_1, \mathbf{r}_2) = \Sigma_{\mathrm{x}}(\mathbf{r}_1, \mathbf{r}_2) - v_{\mathrm{x}}(\mathbf{r}_1)\delta(\mathbf{r}_1 - \mathbf{r}_2)$.

Exact-exchange TDDFT has been tested and applied for a variety of systems:

- Low-lying excitation energies of atomic and small molecular systems are found to be close to TDHF results (Hirata *et al.*, 2002).

---

[8]The exact $f_{\mathrm{x}}(\omega)$ was first explicitly derived by Görling (1998*a*, 1998*b*, 2006), using a direct evaluation of the functional derivative $f_{\mathrm{x}}(\omega) = \delta v_{\mathrm{x}}(\omega)/\delta n(\omega)$. Specific matrix elements of f_{x} at Kohn–Sham resonances were considered by Gonze and Scheffler (1999); see Exercise 13.9.

- Charge-transfer excitations are obtained with the qualitatively correct behavior at large distances (Heßelmann and Görling, 2009; Ipatov *et al.*, 2010).
- Static and dynamical polarizabilities, as well as van der Waals coefficients (see Chapter 14), are found to be in close agreement with TDHF results (Hirata, 2005; Hirata *et al.*, 2005; Shigeta *et al.*, 2006; Hellgren and von Barth, 2008).
- In periodic insulators, the exact-exchange kernel has the long-range behavior that is necessary for the formation of excitons (Kim and Görling, 2002*b*, 2002*a*). However, just as in the case of the TDHF approximation, the resulting unscreened electron–hole interaction leads to a dramatic overbinding of the excitons that causes a collapse of the optical spectra. This collapse can be prevented by a cutoff of the Coulomb singularity, which is equivalent to an evaluation of the xc kernel with a screened interaction (Bruneval *et al.*, 2006; Botti *et al.*, 2007).

Overall, there is not much of a surprise: exact-exchange TDDFT behaves a lot like TDHF theory. But we need to clarify some important points related to the frequency dependence of $f_{\mathrm{x}}(\mathbf{r}, \mathbf{r}', \omega)$. As we discussed in Section 9.3, a frequency-dependent xc kernel means that the Casida equation becomes nonlinear, and this opens up the possibility of additional solutions which are not present when an adiabatic xc kernel is used. So, could it be that we can get double excitations with $f_{\mathrm{x}}(\omega)$? Unfortunately, this is not the case. The xc kernel would need a strong frequency dependence in the vicinity of a double excitation [we showed this explicitly in eqn (9.10)], but there is nothing in $f_{\mathrm{x}}(\omega)$ which can do that: R_V and R_Σ both have their poles at the Kohn–Sham single-particle excitations. Multiple excitations in TDDFT are due to correlation beyond f_{x}.

On the other hand, the frequency dependence of $f_{\mathrm{x}}(\omega)$ can give rise to some rather unpleasant effects owing to the fact that $f_{\mathrm{x}} = \chi_s^{-1} \pi_{\mathrm{xc}}^{(1)} \chi_s^{-1}$, i.e., the inverse Kohn–Sham response function is required. We discussed the question of invertibility in Section 7.3.1, and we saw there that it can happen that response functions are not invertible for isolated frequencies above the first resonance. This should put us on high alert.

Indeed, Hellgren and von Barth (2009) studied the case of isolated Be and Ne atoms and found that χ_s has vanishing eigenvalues close to every inner-shell transition. As a result, $f_{\mathrm{x}}(\omega)$ has a weak frequency dependence for small ω, but starts to diverge at higher frequencies when χ_s becomes noninvertible; $R_V + R_\Sigma$ cannot compensate for this. As a result, inner-shell excitations disappear in the optical absorption spectrum, which renders the full frequency-dependent $f_{\mathrm{x}}(\omega)$ practically useless in this region. These difficulties can of course be avoided using the adiabatic limit, $f_{\mathrm{x}}^{\mathrm{A}} = f_{\mathrm{x}}(\omega = 0)$.

Beyond exchange. From the above discussion, it is clear that it is necessary to go beyond the x-only limit and include correlation effects of second and higher order. This poses numerous technical and conceptual difficulties. First of all, the diagrams become very complicated and their number rapidly increases. On top of this one encounters divergences, and summations must in principle be carried out to infinite order, which is well known from diagrammatic many-body perturbation theory. But even then, there is no guarantee that the resulting approximations will have the desired physical properties.

Fortunately, there are ways out of this dilemma. Below, in Section 13.3.2, we will

introduce the Bethe–Salpeter equation, and show how it can be used to introduce physically well-motivated approximations for f_{xc}.

On a somewhat more formal level, it is possible to construct xc functionals from many-body theory using so-called *conserving approximations*, which satisfy important sum rules and conservation laws. This requires a judicious choice of diagrams, which can be accomplished through a variational approach. More details can be found in Almbladh *et al.* (1999) and von Barth *et al.* (2005).

13.3.2 xc kernels from the Bethe–Salpeter equation

Two-particle Green's functions and scattering amplitudes. In Section 13.2.3 we defined the equilibrium one-particle Green's function $G(\mathbf{r}, t, \mathbf{r}', t')$ [see eqn (13.43)]. In a similar manner, we define the two-particle Green's function,

$$G_2(\mathbf{r}_1, t_1, \mathbf{r}_2, t_2, \mathbf{r}_3, t_3, \mathbf{r}_4, t_4) = -\left\langle \hat{\mathcal{T}} \hat{\psi}_{\mathrm{H}}(\mathbf{r}_1, t_1) \hat{\psi}_{\mathrm{H}}(\mathbf{r}_2, t_2) \hat{\psi}_{\mathrm{H}}^{\dagger}(\mathbf{r}_4, t_4) \hat{\psi}_{\mathrm{H}}^{\dagger}(\mathbf{r}_3, t_3) \right\rangle, \tag{13.71}$$

which describes the propagation of two particles, two holes, or a particle–hole pair, depending on the time arguments. Since we are interested in absorption, we will focus on the particle–hole case. G_2 clearly contains more physical information than G, and in the following we will discuss how we can use this to our advantage in the construction of approximations to f_{xc}.

For the following diagrammatic analysis, it will be more convenient not to work directly with the two-particle Green's function but instead with the following object, which we call the four-point polarization:

$$L(1, 2, 3, 4) = G_2(1, 2, 3, 4) - G(1, 3)G(2, 4), \tag{13.72}$$

where the numbers represent space–time arguments [e.g., $1 = (\mathbf{r}_1, t_1)$]. In the equal-time limit, one finds that L reduces to the time-ordered response function (see footnote 7):

$$L(1, 2, 1, 2) = i\chi^T(1, 2). \tag{13.73}$$

For a noninteracting system, this simply becomes the product of two one-particle Green's functions:

$$L_0(1, 2, 3, 4) = G_0(1, 4)G_0(2, 3). \tag{13.74}$$

A similar relation holds for the four-point polarization L_s of the Kohn–Sham system. We choose the following intuitive diagrammatic representations of the interacting and noninteracting four-point polarizations:

$$L(1, 2, 3, 4) = \begin{array}{c} 1 \leftarrow \quad \leftarrow 4 \\ \rule{0pt}{1.5em} \\ 3 \rightarrow \quad \rightarrow 2 \end{array} \quad , \qquad L_0(1, 2, 3, 4) = \begin{array}{c} 1 \longleftarrow 4 \\ \rule{0pt}{1.5em} \\ 3 \longrightarrow 2 \end{array} . \tag{13.75}$$

The orientation and the labeling of the incoming and outgoing arrows corresponds to the creation and annihilation operators in the definition of G_2 in eqn (13.71).

In Section 13.3.1, we saw that the one-particle Green's function satisfies the Dyson equation (13.44). In general, Dyson equations are integral equations for two-point functions, and can be viewed as resummations of diagrammatic perturbation expansions.
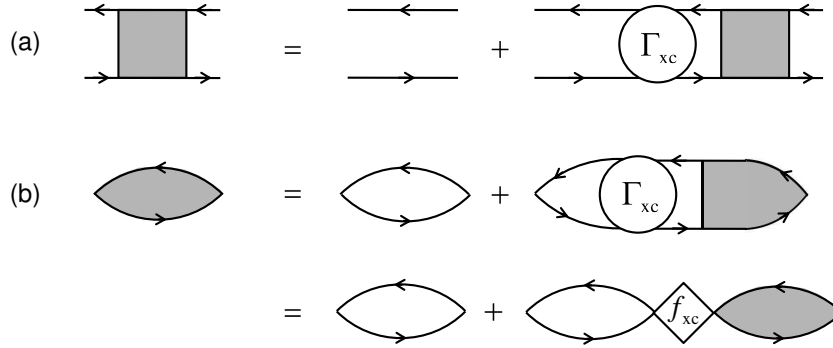
Fig. 13.6 (a) Diagrammatic representation of the Bethe–Salpeter equation for the proper four-point polarization $\widetilde{L}$ [see eqn (13.78)]. (b) The proper response function $\widetilde{\chi}$ can be represented in two ways.

For four-point functions (which depend on four sets of space-time arguments), one can use a similar approach. For instance, L can be formally expressed as

$$L(1,2,3,4) = L_0(1,2,3,4) + \int d5d6d7d8 \, L_0(1,7,3,5)\Gamma(5,6,7,8)L(8,2,6,4), \quad (13.76)$$

where Γ is a two-particle scattering amplitude—a quantity that corresponds to the self-energy Σ. Equation (13.76) is called the *Bethe–Salpeter equation* (BSE).[9] Needless to say, solving the full BSE is numerically complicated, since it involves four sets of space–time integrations.

But let us go a little further on this formal level and establish a connection to TDDFT. First of all, we define the proper four-point polarization $\widetilde{L}$ as[10]

$$L = \widetilde{L} + \widetilde{L}\,^4 wL\,, \quad (13.77)$$

$$\widetilde{L} = L_s + L_s\Gamma_{\mathrm{xc}}\widetilde{L}\,, \quad (13.78)$$

where L_s is the four-point polarization of the Kohn–Sham system, and Γ_{xc} is the xc scattering amplitude. The diagrammatic form of eqn (13.78) for the proper four-point polarizability is represented in Fig. 13.6(a).

We can now take the limit (13.73) on both sides of eqn (13.78), and end up with an equation for the proper response function, which is represented in Fig. 13.6(b). Comparison with

$$\widetilde{\chi} = \chi_s + \chi_s f_{\mathrm{xc}}\widetilde{\chi} \quad (13.79)$$

gives the following formally exact representation of the xc kernel:

$$\int d3d4 \, \chi_s(1,3)f_{\mathrm{xc}}(3,4)\widetilde{\chi}(4,2) = \int d3d4d5d6 \, L_s(1,5,1,3)\Gamma_{\mathrm{xc}}(3,4,5,6)\widetilde{L}(6,2,4,2). \quad (13.80)$$

---

[9]There are other forms of the BSE for L which are more widely used in practice (Onida *et al.*, 2002), but eqn (13.76) corresponds most directly to the Dyson equation (13.44).

[10]The four-point extension of the bare Coulomb interaction is defined as $^4 w(1,2,3,4) = \delta(1,3)\delta(2,4)w(1,2)$.

As it is, this representation appears to be not very useful, since we have merely replaced one set of unknown quantities, $f_{\rm xc}$ and $\widetilde{\chi}$, by another set, $\Gamma_{\rm xc}$ and $\widetilde{L}$. However, expressing the two-point function $f_{\rm xc}$ in terms of a contraction of four-point functions has some very important advantages. As we will see in the following, it allows us to construct physically and practically well-motivated approximations.

Quasiparticles and the excitonic xc kernel. In our discussion of the optical response of insulators in Section 12.3, we pointed out that there are two key requirements which TDDFT has to fulfill:

- The Kohn–Sham system suffers from the band-gap problem. As we have seen before, the optical gap is usually significantly underestimated, and spectra tend to be redshifted. The xc kernel has to "open up" the gap.
- The xc kernel also has to introduce the electron–hole interaction which is needed to reproduce excitonic effects.

Both requirements pose a severe challenge for standard xc functionals, but a significant breakthrough was achieved about a decade ago in a merger of TDDFT and many-body theory. We will go over the key ideas in the following, and mention a few applications. A detailed account can be found in several review articles (Onida *et al.*, 2002; Marini *et al.*, 2006; Botti *et al.*, 2007) and original references (Reining *et al.*, 2002; Marini *et al.*, 2003; Adragna *et al.*, 2003, Sottile *et al.*, 2003, 2007; Bruneval *et al.*, 2005, 2006; Gatti *et al.*, 2007; Gatti, 2011).

In many-body theory, *quasiparticles* constitute a noninteracting system whose one-particle Green's function is the same as that of the real interacting system. The simplest quasiparticle system is the HF system, with the single-particle equation (D.9). In general, quasiparticles satisfy the following nonlinear equation:

$$\left[-\frac{\nabla^2}{2} + v(\mathbf{r}) \right] \varphi_j^{\rm qp}(\mathbf{r}) + \int d^3r'\, \Sigma(\mathbf{r}, \mathbf{r}', \varepsilon_j^{\rm qp})\, \varphi_j^{\rm qp}(\mathbf{r}') = \varepsilon_j^{\rm qp} \varphi_j^{\rm qp}(\mathbf{r}) , \qquad (13.81)$$

which gives the Green's function $G_{\rm qp}(\mathbf{r}, \mathbf{r}', \omega) = \sum_k^N \varphi_k^{\rm qp}(\mathbf{r})\varphi_k^{\rm qp}(\mathbf{r}')/(\omega - \varepsilon_k^{\rm qp})$. If the exact self-energy Σ were known, then this recipe would yield the exact Green's function of the interacting system.

The so-called GW approximation (Hedin, 1965; Ariasetiawan and Gunnarsson, 1998) is an approximation to the self-energy to lowest order in the screened interaction:

$$\Sigma_{GW}(1, 2) = iG(1, 2)W(1, 2) , \qquad (13.82)$$

where W is the screened interaction, defined as

$$W(1, 2) = w(1, 2) + \int d3d4\, w(1, 3)\widetilde{\chi}(3, 4)W(4, 2) . \qquad (13.83)$$

This Dyson-type equation is diagrammatically represented in Fig. 13.7(b). The screened interaction W is shown as a thick wavy line, and the bare Coulomb interaction w as a thin wavy line. The irreducible response function $\widetilde{\chi}$ in eqn (13.83) is approximated by the response function of noninteracting quasiparticles,
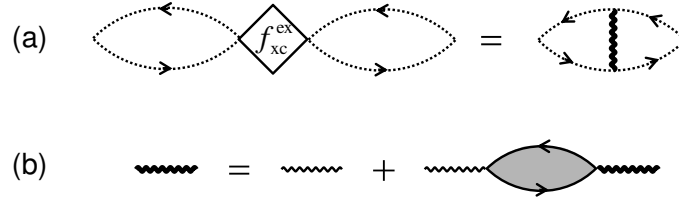
Fig. 13.7 (a) Diagrammatic representation of the excitonic xc kernel [eqn (13.90)]. The dotted lines indicate quasiparticle Green's functions. (b) Definition of the screened interaction.

$$\chi_{\text{qp}}(1,2) = -iG_{\text{qp}}(1,2)G_{\text{qp}}(2,1^+) \,. \tag{13.84}$$

The GW scheme (13.81)–(13.84) is now complete. It requires, in principle, a self-consistent solution. In practice, however, one usually stops after the first iteration step, which constitutes the so-called G_0W_0 scheme. To summarize:

> The GW method constitutes a (computationally quite expensive) state-of-the-art approach to electronic structure calculation. The resulting quasiparticle energy spectra give an accurate description of one-particle excitations such as electron addition and removal energies, and give band structures that agree well with experiment. In particular, band gaps are accurately reproduced.

For the following development, it will be convenient to write the xc kernel as

$$f_{\text{xc}} = f_{\text{xc}}^{\text{qp}} + f_{\text{xc}}^{\text{ex}} \,, \tag{13.85}$$

i.e., we introduce a *quasiparticle* and an *excitonic* part of the xc kernel, which are meant to capture different physical aspects and will be handled in different ways [see also eqn (12.41)]. The two kernels satisfy the following relations (Stubner *et al.*, 2004):

$$\chi_{\text{qp}} = \chi_s + \chi_s f_{\text{xc}}^{\text{qp}} \chi_{\text{qp}} \,, \tag{13.86}$$

$$\widetilde{\chi} = \chi_{\text{qp}} + \chi_{\text{qp}} f_{\text{xc}}^{\text{ex}} \widetilde{\chi} \,. \tag{13.87}$$

So far, no approximation has been made.

Now let us assume, for the moment, that we have been able to obtain the quasiparticle response function χ_{qp} (e.g., using the GW approach), and let us focus on the excitonic kernel of eqn (13.87). We can carry out a formal analysis similar to what led us to eqn (13.80), and write $f_{\text{xc}}^{\text{ex}}$ in terms of four-point functions:

$$\int d3d4 \, \chi_{\text{qp}}(1,3) f_{\text{xc}}^{\text{ex}}(3,4)\widetilde{\chi}(4,2) = \int d3d4d5d6 \, L_{\text{qp}}(1,5,1,3)\Gamma_{\text{qp}}(3,4,5,6)\widetilde{L}(6,2,4,2). \tag{13.88}$$

Here, L_{qp} is the four-point polarization of the quasiparticle system. The quasiparticle scattering amplitude Γ_{qp} now needs to be approximated. We use

$$\Gamma_{\text{qp}}(3,4,5,6) = \quad \Gamma_{\text{qp}} \quad \approx \quad . \tag{13.89}$$

This means that the particle–hole interaction is approximated by a single screened interaction line. In general, W is a frequency-dependent interaction, but one often approximates it by the static limit $W(\mathbf{r}, \mathbf{r}', \omega = 0)$.

To arrive at the final expression for the excitonic xc kernel, we replace $\widetilde{\chi}$ and $\widetilde{L}$ in eqn (13.88) with the corresponding quasiparticle expressions. This gives

$$\int d3d4 \chi_{\text{qp}}(1,3) f_{\text{xc}}^{\text{ex}}(3,4) \chi_{\text{qp}}(4,2) = \int d3d4 G_{\text{qp}}(1,3) G_{\text{qp}}(4,1) W(3,4) G_{\text{qp}}(3,2) G_{\text{qp}}(2,4).$$

(13.90)

This is the xc kernel of Reining *et al.* (2002) and many others.[11] Figure 13.7(a) shows its diagrammatic representation.

We conclude this somewhat formal section by recapitulating what makes the diagrammatic approach so attractive to work with. First of all, the complicated technical aspects of many-body perturbation theory are hidden away behind very simple diagrammatic rules. This makes many-body theory very intuitive, and manipulating abstract objects such as Green's functions or self-energies becomes almost trivial. Secondly, diagrammatic theory allows one to sum certain classes of diagrams to infinite order, which often gives rise to new physical properties. For instance, using the quasiparticle scattering amplitude (13.89) in the Bethe–Salpeter equation results in an expansion of the four-point polarization function in terms of so-called ladder diagrams (Exercise 13.11). As we shall now see, this is the crucial ingredient for a description of excitonic effects in insulators.

Applications. The many-body xc kernel $f_{\text{xc}}^{\text{ex}}$ has been applied (in conjunction with the GW scheme for the ground state) to describe the optical properties of various bulk semiconductors and insulators. We will now discuss two representative examples.

The first example is bulk silicon. Earlier, in Section 12.3.2, we saw that TDDFT with local or semilocal approximations can account neither for the correct optical gap nor for the excitonic features of the absorption spectrum. Figure 13.8 compares the experimental optical spectrum of Si (Lautenschlager *et al.*, 1987) with various calculations. Results obtained with the RPA and ALDA were shown previously in Fig. 12.8. The GW-RPA curve was obtained using the GW quasiparticle response function, but then setting f_{xc} to zero. Therefore, the optical gap is correctly reproduced (i.e., the onset of absorption occurs at about 3.1 eV, as in the experiment), but instead of a strong excitonic feature we observe just the same weak shoulder as was found in the RPA and ALDA results.

By contrast, excellent agreement with experimental data was achieved both by using the full BSE and by using TDDFT with the $f_{\text{xc}}^{\text{ex}}$ of eqn (13.90). Figure 13.9 shows the absorption spectrum of solid argon, which is an insulator with a wide band gap. The experimental data shows a very pronounced series of strongly bound excitons (Saile *et al.*, 1976). As a matter of fact, the first ($n = 1$) exciton has a binding energy of around 2 eV and should therefore be viewed as a localized Frenkel exciton. Closer to the onset of the continuum (at 14.2 eV), the excitons are of the more delocalized

---

[11] This xc kernel is also sometimes referred to as the "nanoquanta kernel," named after a European scientific network that operated from 2004 to 2008.
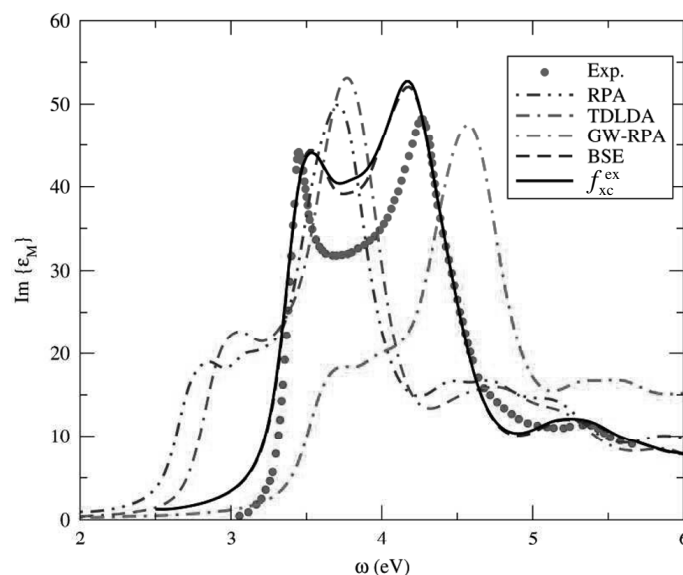
Fig. 13.8 Imaginary part of the dielectric function of bulk Si. [Adapted with permission from IOP from Botti *et al.* (2007), ©2007.].

Mott–Wannier type. Notice that the experiment shows a splitting of the excitonic peaks due to spin–orbit interactions, which are not included in the calculations.

As expected, the ALDA does not reproduce any of the excitonic features, and just gives a diffuse absorption background. Again, the full BSE and TDDFT results with the excitonic f_{xc}^{ex} kernel are very close to each other, and agree very well with the experimental data. There is some remaining discrepancy, which can be explained by the neglect of spin–orbit interactions, the use of pseudopotentials, and the approximation of the static screened interaction $W(\mathbf{r}, \mathbf{r}', 0)$.

The many-body xc kernel has been applied to other bulk materials (Marini *et al.*, 2003; Marini and Rubio, 2004; Sagmeister and Ambrosch-Draxl, 2009), lower-dimensional systems such as surfaces (Pulci *et al.*, 2010), and conjugated polymers and other molecular chains (Varsano *et al.*, 2008). In all cases it gives practically the same results as the BSE, and tends to describe the experimental data very well.

Other current efforts are focused on applying frequency-dependent many-body xc kernels to describe double excitations (Casida, 2005; Romaniello *et al.*, 2009; Sangalli *et al.*, 2011). The first tests for model molecular systems have been encouraging and indeed produce extra peaks in the spectra. This indicates that practical TDDFT schemes to handle double excitations may soon be within reach.

Let us conclude this section with a few words about computational cost. At present, finding a direct solution of the BSE still seems to be the method of choice in a large number of applications, and more and more efficient implementations are becoming available (e.g., Fuchs *et al.*, 2008; Olovsson *et al.*, 2009). Nevertheless, many-body calculations involving four-point functions such as the *GW*-BSE approach, are expensive,
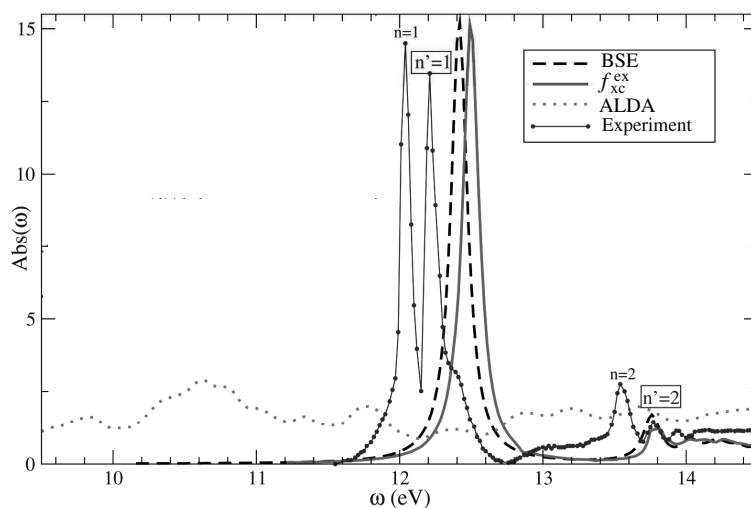
Fig. 13.9 Absorption spectrum of solid argon. [Adapted with permission from APS from Sottile *et al.* (2007), ©2007.].

which severely limits the size and complexity of the systems that can be treated—hence the motivation to develop TDDFT approaches that can do similar things but more cheaply.

Using the state-of-the-art many-body xc kernel which we have discussed in this section, TDDFT is basically as expensive as the BSE when only the optical spectrum is desired. On the other hand, when the full dielectric matrix is to be calculated, TDDFT is favorable. In addition, TDDFT has some numerical advantages when it comes to storage and memory requirements.

The bottom line is the following: we now have a proof of concept that TDDFT linear-response methods exist which are capable of describing excitonic effects at a level of accuracy comparable to the most sophisticated many-body theories. This can be taken as a starting point from which simpler xc functionals can be developed (we've already seen some of them in Section 12.3). Future progress will likely come about from joint efforts of the "many-body" and TDDFT communities.

Exercise 13.1 Derive the expression (13.12) for the first-order contribution $\Psi^{(1)}(t)$ to the perturbation expansion of the many-body wave function. Use a time-dependent perturbation approach similar to what we used to derive the TDOEP equation in Section 11.2.2.

Exercise 13.2 Fill in the steps between eqns (13.15) and (13.16).

Exercise 13.3 In Section 13.1.2 we discussed a perturbative expansion of the time-dependent xc potential, using the adiabatic-connection approach. Carry out a similar expansion for the ground-state xc potential of static DFT; this is known as the static Görling–Levy perturbation theory (Görling and Levy, 1994; Görling, 1996). Show that in lowest order, the static x-only OEP equation is obtained.

Exercise 13.4 A key step in the proof of eqn (13.22) is the relation $\delta\hat{U}(t,t_0)/\delta v(\mathbf{r},z) = \hat{n}(\mathbf{r})\hat{U}(t,t_0)$. To show this, make a perturbation $\delta\hat{V}(z) = \int d^3r\,\delta v(\mathbf{r},z)\hat{n}(\mathbf{r})$ in the Hamiltonian, which changes the time evolution operator to $\hat{U} + \delta\hat{U}$. From eqn (13.24), convince yourself that

$$i\frac{d}{dz}\delta\hat{U}(z,z') = \delta\hat{V}(z)\hat{U}(z,z') + \hat{H}(z)\delta\hat{U}(z,z')\,.$$

Show that this has the solution

$$\delta\hat{U}(z,z') = -i\int_{z'}^{z}dz_1\,\hat{U}(z,z')\delta\hat{V}(z_1)\hat{U}(z_1,z')\,,$$

and proceed from there.

Exercise 13.5 Derive the Dyson equation (13.42). The easiest way to do this is to write the equations of motion of the interacting system and of the noninteracting system, eqns (13.40) and (13.41), in a symbolic manner,

$$h\mathcal{G} = 1 + \Sigma\mathcal{G}\,,$$
$$h\mathcal{G}_0 = 1\,,$$

where $h = i\partial/\partial t + \nabla^2/2 + v$, and manipulate the two equations algebraically, treating operators as if they were numbers.

Exercise 13.6 Convince yourself that the real-time Kohn–Sham Green's function (13.52) satisfies the equation of motion (13.45).

Exercise 13.7 Show that the x-only Sham–Schlüter equation, eqn (13.57), reduces to the x-only OEP equation.

Exercise 13.8 Show that f_x reduces to $-(1/2)w$ for a two-electron system.

Exercise 13.9 Starting from eqn (13.68), show that the exact x-only kernel has the following matrix elements for frequencies that are resonant with a Kohn–Sham excitation ω_{jk}:

$$\langle\varphi_j^0\varphi_k^0|f_x(\omega_{jk})|\varphi_j^0\varphi_k^0\rangle = \langle\varphi_j^0|\hat{v}_x^{\mathrm{HF}} - v_x|\varphi_j^0\rangle - \langle\varphi_k^0|\hat{v}_x^{\mathrm{HF}} - v_x|\varphi_k^0\rangle - \langle\varphi_k^0\varphi_k^0|w|\varphi_j^0\varphi_j^0\rangle\,,$$

where $\hat{v}_x^{\mathrm{HF}}$ is the nonlocal HF potential operator evaluated with Kohn–Sham orbitals. This result defines the x-only SPA.

It will be instructive to go over the original derivation of this result (Gonze and Scheffler, 1999), which was done in a different manner.

Exercise 13.10 Check the translation of the Bethe–Salpeter-type equation (13.78) for $\widetilde{L}$ into diagrammatic form in Fig. 13.6(a). Do this by comparing the definitions (13.75) of the four-point diagrams and the full form (13.76) of the integral equation. Assign labels to all incoming and outgoing arrows in the diagram, including variables that are integrated over.

Do a similar analysis for the diagrammatic representations in Figs. 13.6(b) and 13.7 and check how they correspond to eqns (13.80) and (13.90).

Exercise 13.11 Convince yourself that the Bethe–Salpeter equation for the four-point polarization L can be rewritten as an infinite sum of ladder diagrams if you use eqn (13.89) to approximate the quasiparticle scattering amplitude.

Likewise, show that the RPA response function χ_{RPA}, which is obtained from eqn (12.3) with $f_{xc} = 0$, can be written as an infinite sum of bubble diagrams. As we saw in Chapter 12, the RPA produces plasmons in metals.